FUNCTIONALIZATION OF GLASS FIBER WOVEN FABRICS BY ITO COATINGS AND CHARACTERIZATION OF THEIR ELECTROMAGNETIC PROPERTIES

A THESIS SUBMITTED TO
THE GRADUATE SCHOOL OF NATURAL AND APPLIED SCIENCES
OF
MIDDLE EAST TECHNICAL UNIVERSITY

BY

MERVE ÖZDİL DARICIOĞLU

IN PARTIAL FULFILLMENT OF THE REQUIREMENTS
FOR
THE DEGREE OF MASTER OF SCIENCE
IN
METALLURGICAL AND MATERIALS ENGINEERING

JANUARY 2022

Approval of the thesis:

FUNCTIONALIZATION OF GLASS FIBER WOVEN FABRICS BY ITO COATINGS AND CHARACTERIZATION OF THEIR ELECTROMAGNETIC PROPERTIES

submitted by **MERVE ÖZDİL DARICIOĞLU** in partial fulfillment of the requirements for the degree of **Master of Science** in **Metallurgical and Materials Engineering, Middle East Technical University** by,

Prof. Dr. Halil Kalıpçılar
Dean, Graduate School of **Natural and Applied Sciences** _____

Prof. Dr. C. Hakan Gür
Head of the Department, **Met. And Mat. Eng., METU** _____

Prof. Dr. Arcan Fehmi Dericioğlu
Supervisor, **Met. And Mat. Eng., METU** _____

Examining Committee Members:

Prof. Dr. Caner Durucan
Metallurgical and Materials Eng, METU _____

Prof. Dr. Arcan Fehmi Dericioğlu
Metallurgical and Materials Eng, METU _____

Assist. Prof. Dr. Simge Çınar Aygün
Metallurgical and Materials Eng, METU _____

Prof. Dr. Özlem Aydın Çivi
Electrical Electronics Eng, METU _____

Prof. Dr. Ziya Esen
Department of Inter-Curricular Courses, Çankaya University _____

Date: 14.01.2022

I hereby declare that all information in this document has been obtained and presented in accordance with academic rules and ethical conduct. I also declare that, as required by these rules and conduct, I have fully cited and referenced all material and results that are not original to this work.

Name Last name : Merve Özdil Darıcıoğlu

Signature :

ABSTRACT

FUNCTIONALIZATION OF GLASS FIBER WOVEN FABRICS BY ITO COATINGS AND CHARACTERIZATION OF THEIR ELECTROMAGNETIC PROPERTIES

Özdil Darıcıoğlu, Merve
Master of Science, Metallurgical and Materials Engineering
Supervisor: Prof. Dr. Arcan Fehmi Dericioğlu

January 2022, 103 pages

ITO sols were deposited on glass fiber woven fabrics by spray pyrolysis technique and electrical conductivity of these layers was controlled to incorporate electromagnetic (EM) wave absorbing characteristics to glass fabrics. The surface functionalized fabrics were used as reinforcement in a hybrid type multilayer EM wave absorbing composite which is a combination of Jaumann and graded type absorbers effective in 8-12 GHz frequency range (X-band).

The effects of the conductivity and the cascading order for ITO coated layers on the electromagnetic behavior of the hybrid type multilayered composite were investigated. The main objective was to create a guideline for the design of multilayer EM wave absorbing composite according to the needs of a specific application.

The highest composite design has been formed by cascading six ITO coated fabrics both with and without metal sheet placed at the back of the composite. This composite has ~-11 dB reflection loss and ~-9 dB transmission loss which corresponds to ~85% average absorption without metallic sheet, while its reflection loss and average absorption values are ~-10.5 dB and ~93%, respectively, in the X-band with metallic backing. The front layer of multilayered structure with the lowest

surface conductivity provided impedance matching between air and the receiving surface of the composite minimizing reflection, where the gradual increase in surface conductivity of the layers towards the back provided balanced internal reflection and transmission leading to high overall EM wave absorption. Consequently, by controlling the grading of the surface conductivity of the layers the reflection and transmission response of the multilayered composites can be adjusted to provide tailored characteristics for the required EM wave absorption levels.

Keywords: Indium tin oxide, Spray pyrolysis technique, Electromagnetic wave absorber, Reflection loss, Transmission loss

ÖZ

CAM ELYAF DOKUMA KUMAŞLARIN ITO KAPLAMALARI İLE İŞLEVSELLEŞTİRİLMESİ VE ELEKTROMANYETİK ÖZELLİKLERİNİN KARAKTERİZASYONU

Özdil Darıcıoğlu, Merve
Yüksek Lisans, Metalurji ve Malzeme Mühendisliği
Tez Yöneticisi: Prof. Dr. Arcan Fehmi Dericioğlu

Ocak 2022, 103 sayfa

Bu tez çalışmasında, sprey piroliz tekniği ile cam elyaf dokuma kumaşlar üzerine indiyum kalay oksit (İTO) filmler biriktirilmiş ve bu iletken oksit tabakalarının elektrik iletkenliği kontrol edilerek elektromanyetik (EM) dalga soğurma özellikleri incelenmiştir. Daha sonra bu yüzeyleri fonksiyonelleştirilmiş kumaşlar, 8-12 GHz arasındaki X bant frekanslarında elektromanyetik dalgaları soğurabilen Jaumann ve kademeli tip soğurucunun bir kombinasyonu olan hibrit tip EM dalga soğurucu kompozite takviye olarak kullanılmıştır.

Çalışmanın temel amacı, ITO kaplı cam elyaf dokuma kumaşların iletkenliğinin, basamaklı düzeninin ve kompozitin arkasına yerleştirilen metal levhanın kompozitlerin elektromanyetik davranışı üzerindeki etkisini gözlemlemektir. Bu kapsamda, çalışma, spesifik uygulama ihtiyaçlarına göre EM dalga soğurucu tasarımına rehberlik etmeyi amaçlamıştır.

Kompozit tasarım aşamasında, kompozit hazırlamanın zaman alıcı adımlarından kaçınmak için simülasyon çalışmaları yapılmış ve simülasyon çalışmaları deneysel çalışmalarla desteklenmiştir. Çalışmanın sonunda, en iyi kompozit tasarımı hem

metalik arkalığın olduğu hem olmadığı durumlar için, 6 iletken levhanın kademeli olarak artan sırayla basamaklandırılmasıyla elde edilmiştir. Bu kompozit X bant frekans aralığında, metal levha olmadan ~%85 ortalama soğurma yüzdesine karşılık gelen ~-11 dB yansıma kaybına ve ~-9 dB iletim kaybına sahipken, metal arkalığın varlığında sırasıyla ~-10.5 dB yansıma kaybı ve ortalama ~%93 soğurma yüzdesine sahiptir. Bu tasarımdaki ön katman hava ile empedans uyumu sağlayarak, iki yüzey arasındaki yansımayı en aza indirmiştir. Katmanların arkaya doğru yüzey iletkenliğindeki kademeli artışı, kompozitlerin yansıma ve geçirme davranışlarını dengede tutarak yüksek soğurma yüzdesi sağlamıştır. Sonuç olarak, katmanların yüzey iletkenliğinin derecelendirilmesini kontrol edilerek, çok katmanlı kompozitlerin yansıtma, geçirme ve soğurma davranışları kontrol edilebilmiştir.

Anahtar Kelimeler: İndiyum kalay oksit, Sprey piroliz tekniği, Elektromanyetik dalga soğurucu, yansıma kaybı, İletim kaybı

To my family

ACKNOWLEDGMENTS

I would like to express my deepest gratitude and greatest thanks to my advisor Prof. Dr. Arcan F. Dericioğlu for his guidance, support, advice, patience, tolerance and encouragement throughout the research. I feel so lucky and grateful to find a possibility to work with such a successful, experienced and insightful person.

I would also like to extend my sincere thanks to Prof. Dr. Caner Durucan for his suggestions and comments from beginning to end of the study.

I would like to thank Prof. Dr. Özlem Aydın Çivi, Assist. Prof. Dr. Simge Çınar Aygün, Assoc. Prof. Dr. Ziya Esen for being on my thesis committee.

I would like to thank Prof. Dr. Emrah Ünalan and the lab members of METE Nanolab for their help through 4-point probe measurements. I would like to express my special thanks to Doğa Doğanay for his help and advice.

I would like to thank Seren Özer and all the other members of the Electromagnetic Materials Laboratory and my lab mates for their support throughout the thesis.

I specially thank my labmate and my good friend Başar Süer for his support, friendship and endless patience. I am grateful to him for sharing all his experiences with me and for all his help.

I owe a great depth to my precious mom, dad and my beloved sister for their caring, support, endless and unconditional love not only throughout this thesis but my whole life.

Finally, but most importantly, I would like to thank my husband, love of my life Özgür Darıcıoğlu for everything. I am so grateful for his support, care, selfless love and understanding all my stressful days.

I want to dedicate this thesis to my husband, family and also my dog for their endless love.

TABLE OF CONTENTS

LIST OF TABLES

TABLES

LIST OF FIGURES

FIGURES

LIST OF ABBREVIATIONS

ABBREVIATIONS	
EMI	Electromagnetic Interference
ITO	Indium Tin Oxide
IR	Infrared Radiation
AZO	Aluminum Doped Zinc Oxide
FTO	Fluorine Doped Tin Oxide
ATO	Aluminum Doped Titanium Oxide
TCO	Transparent Conductive Oxide
VNA	Vector Network Analyzer
SOLT	Short Open Load Thru
LRL	Line Reflected Line
TRM	Thru Reflect Match
SEM	Scanning Electron Microscopy
XRD	X-Ray Diffraction
EDS	Energy-Dispersive X-Ray Spectroscopy

CHAPTER 1

INTRODUCTION

1.1 Electromagnetic Shielding History and Developments

Advancements in the technology increase the demand for electronic devices which are more developed and complex, can work in hard conditions with higher performance, can react and respond rapidly with higher packing density [1]. The usage of electromagnetic waves with a wide frequency range in various systems shows an increasing trend with the technological improvements to speed up the data transferring between electronic devices. The electromagnetic wave-assisted technology is not only limited to military applications but is also expanded to civilian, industrial, commercial applications. Wireless communication systems, radars, medical treatment and diagnostic systems, air defense and military systems, telecommunication systems, portable consumer devices can be given as examples to electromagnetic applications which can work in a wide frequency range [2].

The growth in application areas of electromagnetic devices results in the pollution of unwanted radiation or electromagnetic interference (EMI). The pollution caused by unwanted radiation can bring on some negative effects such as deviation or misconstruction of the data that is transferred between devices, degradation or damage on the device, and in the end, decrease the performance of the device. It has not only negative effects on the device but also has a negative effect on the environment. In addition to that, research about the electromagnetic field on human health proves that electromagnetic fields have negative effects on human health, such as headaches, insomnia, nervousness etc. [3,4]. An increase in the usage of electronic devices and the harmful effects of electromagnetic radiation have created the need for electromagnetic shielding of unwanted radiations [5].

Electromagnetic shielding can be defined as the absorption and the reflection of the incident electromagnetic wave via shielding material to avoid penetration of the unwanted radiation through the protected material. With the scope of this aim, electromagnetic wave absorbers are used as a shielding material. Research about electromagnetic wave absorber materials begins with the invention of the radar and according to various papers in the literature. It occurs at the same time as the beginning of World War 2 which corresponds to an early stage of the 1930s. The first patent of electromagnetic wave absorber material was taken in the Netherlands in 1936 by Naamloze Vennootschap Machinerieen. The first absorber, a quarter-wave resonant type absorber, was built by using carbon black as a lossy resistive material and titanium dioxide as high permittivity material. The aim of using these two materials was to achieve good dissipation and a high dielectric constant [6, 7].

After the first successful achievement of electromagnetic wave absorber, radar absorbing materials gained more attention in the 1950s in both Germany and US. Two new types of absorbers were enhanced in Germany to use them in submarines. The first one of the absorbers was called as Wesh. In this structure, a flexible rubber sheet thickness of about 7.6 mm was stacked with carbonyl iron. The second one was called Jaumann type absorber, and it consists of multilayer structures. The reflection loss was lower than the -20 dB between 2-15 GHz in this structure. At the same time interval as Germany, the US also developed two types of absorbers which both called with general name as HARP (Halper Anti Radar Paint). Reflection reduction was 15-20 dB at resonance in both absorbers. The first one is called MX-410, and it was formed by suspending oriented disc-shaped aluminum flakes into a rubber matrix. The permittivity value of the MX-410 absorber was 150. The second one is called shipborne absorber, and it contains iron particles in neoprene binder. The permittivity value of the 1.77 mm thick shipborne absorber was 20 [8, 9].

Developments on electromagnetic wave absorbers continuous with getting patent of Salisbury screen absorbers. Although the invention of this simple absorber type goes back to the 1940s, it was patented in the 1950s. Salisbury screen is a type of absorber invented by engineer Winfield Salisbury. It was constructed by placing a resistive

sheet on a perfect electrical conductor at a quarter wavelength distance of a specific frequency. It can be categorized as a resonant type absorber. Another resonant type of absorber that was invented in the 1970s is the Dallenbach layer. It is comprised of a homogeneous lossy layer backed by a metal plate, and the thickness of the lossy layer is selected in such a way that its input impedance should match with the intrinsic impedance of the free space [10, 11, 12].

EMI absorbers which were explained so far works fine at narrowband. However, they have some disadvantages resulting from their high weight structures and over thicknesses besides narrowband working conditions. For these reasons, optimization studies gain more and more interest nowadays. From the 1990s to today, optimization techniques have been expanded with the enhancement of the technology, and absorbers which can shield a wide frequency of waves with lighter weight and thickness are produced. The aim of the studies is not only limited to the optimizations on the design of the absorber but also related to finding a new and better classes of EMI absorber materials [13].

1.2 Structure of the Thesis

In this thesis study, glass fiber woven fabrics were functionalized with ITO coatings by spray pyrolysis technique. The study was carried on with the development of multilayered absorber design, which combines Jaumann and graded type absorber approaches by cascading these surface functionalized glass fiber woven fabrics both using experiment and simulation. Then electromagnetic properties (reflection loss, transmission loss, absorption percentage) were characterized by using the free space method at the X-band frequency range (8-12 GHz).

The thesis study was divided into five chapters and Chapter 1 covers the general introduction, history, and the developments along with the aim and the structure of the thesis study.

The first part of Chapter 2 covers the theoretical background and technical knowledge about electromagnetic theory, wave matter interactions, microwaves and applications. In addition to these, history, general knowledge and technical information about electromagnetic shielding theory, electromagnetic wave absorber structures, and their characterization technique have been explained. Later parts of Chapter 2 cover the brief information and essential properties of indium tin oxide (ITO), which belongs to the class of transparent conductive oxide as an EM wave absorbing material. After that, important process parameters and their effect on the properties and quality of ITO coatings are discussed. At the end of the chapter, literature studies using ITO as an EM wave absorber are discussed.

Chapter 3 covers the experimental procedure of preparing ITO sols and deposition on glass fiber woven fabrics by spray pyrolysis. After that, characterization techniques and simulation approaches are explained.

The first part of Chapter 4 covers the microstructural, electrical, and electromagnetic characterization of ITO coated glass fiber woven fabrics. Later parts of Chapter 4 cover the electromagnetic characterization of single and multilayered absorber structures and simulation studies in order to correlate these two. Finally, all of the results are discussed and compared to prepare a guideline for EM wave absorber design.

The final chapter of the thesis summarizes the conclusion of the study.

CHAPTER 2

LITERATURE RESEARCH

2.1 Electromagnetic Theory

In this chapter of the thesis, in order to get familiar with the concept of electromagnetic theory, literature review will be presented. The basics of electromagnetic theory, electromagnetic spectrum, microwave frequencies, and their applications, electromagnetic waves, and their interactions with the matters will be covered. After the brief introduction, the mechanism of electromagnetic shielding theory and electromagnetic loss mechanism will be discussed. Additionally, in line with the purpose of the thesis, an introduction to electromagnetic wave absorber material, the types, working principles, and the application areas of these materials will be presented. Finally, electromagnetic characterization techniques and the free space method will be covered extensively.

2.1.1 Electromagnetic Spectrum and Electromagnetic Waves

In classical physics, electromagnetic radiation can be defined as an electromagnetic wave formed by the oscillation of electric and magnetic fields and propagates through in a medium or free space at a speed of light by carrying electromagnetic radiant energy.

Discoveries about electromagnetic radiation started with the studies of the German physicist Heinrich Rudolf Hertz. He is the scientist who demonstrated the radiation of electromagnetic waves. The set-up to create and to detect electromagnetic waves is shown in Figure 2.1. In this setup, he used a transmitter and receiver, which both contain two electrodes, and with the help of an induction coin, he created oscillation between electrodes. He also found that the speed of the electromagnetic wave is

equal to the speed of light, and he suggested that electromagnetic waves are also reflected, diffracted and transmitted just like light waves [14].

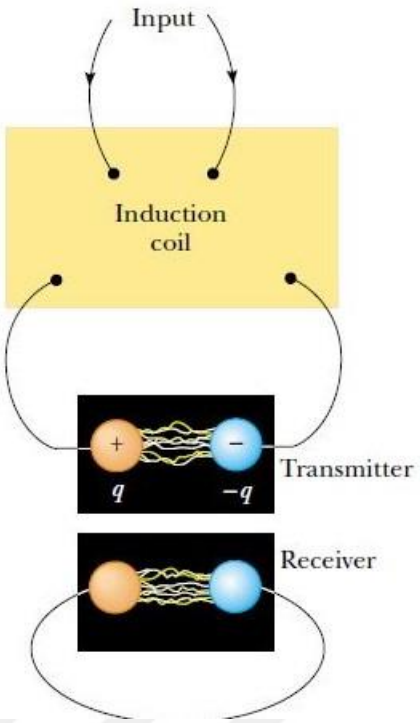

Figure 2.1. Schematic image of Hertz's set-up for detection of electromagnetic waves [14].

Another important discovery related to the electromagnetic theory was put forward by British chemist and physicist Michael Faraday. Faraday's law simply says that changing the magnetic field produces an electric field.

The best way to get the fundamental knowledge about electromagnetism and electromagnetic theory is to look at the Maxwell's equations. Maxwell's equations are the unification of all the phenomena about electricity and magnetism by combining the mathematical expressions of Faraday's laws, Gauss's law and Ampere's law [15].

As it is mentioned earlier, in most of the engineering applications electromagnetic radiation acts as a sinusoidal wave form and it forms oscillations of the electric and magnetic field at any point where they need to be perpendicular to each other and the direction of wave propagates. The phenomenon that the wave is moved to the

single plane along the direction of propagation is called linear polarization. Figure 2.2 shows the linearly polarized electromagnetic wave propagating along the +y direction.

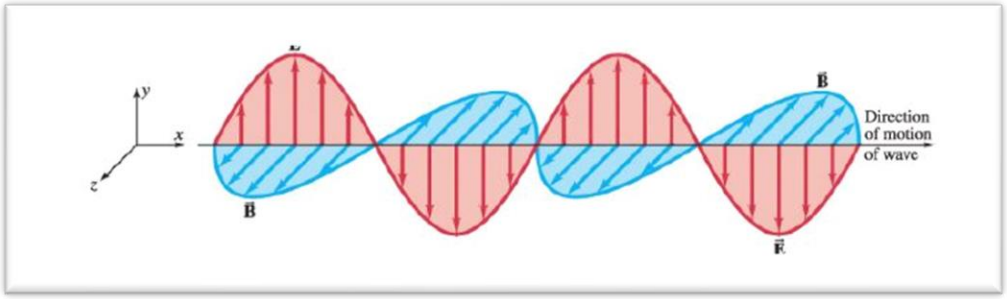

Figure 2.2. Linearly polarized EM wave propagates in +y direction. $\vec{E}$ and $\vec{B}$ are perpendicular to each other and direction of propagation [15].

Maxwell's equations suggest that any change in time in the magnetic field, **B**, (electric field, **E**) causes spatial changes in the electric field, **E** (magnetic field **B**). Electromagnetic waves travel not only in free space but also in a medium. In addition, EM waves behave as light in free space, it moves with a known velocity of 3.00 x 10^8 m/s which is a speed of light (c). The speed of light could be expressed by the magnetic permeability (μ_o) and electrical permittivity (ϵ_o) of a vacuum which is shown in Equation 2.1:

$$c = \frac{E}{B} = \frac{1}{\sqrt{\epsilon_o \mu_o}} = 3.00\ x\ 10^8\ m/s \qquad \text{(Equation 2.1)}$$

Speed of light (c) can also be expressed by the frequency (f) and wavelength (λ) of the EM wave and it is shown in Equation 2.2:

$$c = \lambda . f \qquad \text{(Equation 2.2)}$$

When EM wave propagates through free space, it moves with the electromagnetic radiant energy, and this energy is carried with the help of photons. The photon energy (E) can be expressed by the speed of light in free space, wavelength, and Planck's

constant [16]. The equation that formulates the photon energy is shown in Equation 2.3:

$$E = \frac{h.c}{\lambda} \qquad \text{(Equation 2 3)}$$

Since each electromagnetic wave carries a certain amount of photon energy, its wavelength can be calculated with the help of Equation 2.3. Then each electromagnetic wave can be classified into one of the several regions of the electromagnetic spectrum based on its frequency or wavelength. The demonstration of the electromagnetic spectrum is shown in Figure 2.3.

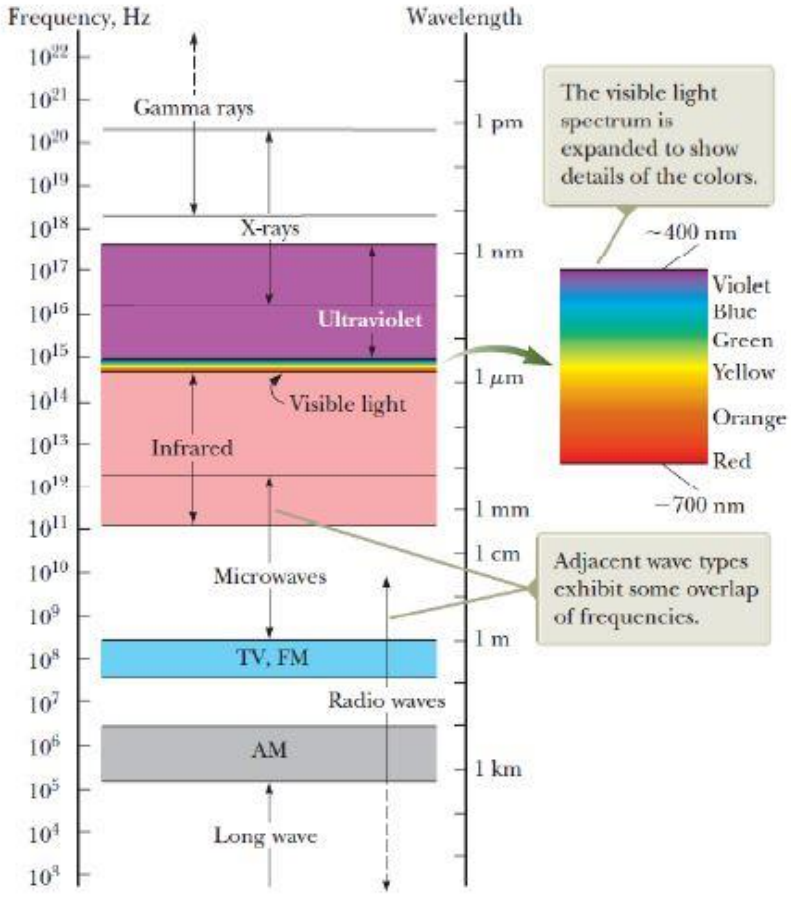

Figure 2.3. Electromagnetic (EM) spectrum [15].

Since the speed of light is constant, frequency and the wavelength of the wave are inversely proportional to each other according to Equation 2.2. This means that increase in frequency results in a decrease in wavelength. In addition to that, Equation 2.3 suggests that wave with a lower wavelength has higher photon energy [17]. These relations between photon energy, wavelength and the frequency of the wave can also be seen by looking at the electromagnetic spectrum, which is given in Figure 3.

Electromagnetic waves can be ordered as radio waves, microwaves, infrared, visible light, ultraviolet, X-rays, and gamma rays according to their increasing frequency. There are no sharp points to separate one region from another. Generally, regions overlap at some frequencies.

Radio waves have the lowest frequency and highest wavelength, such that their range of wavelength is between 0.1 m and 1 km. Radio waves are produced by the acceleration of charged particles, and they can be obtained using laboratory equipment. The primary application areas of radio waves are communication and broadcasting systems such as tv, radio, cell phones.

Among the electromagnetic spectrum, microwaves have the second lowest wavelength value, and the value ranges between 0.3 m and 10^{-4} m. They can be produced in a laboratory environment just like radio waves. Since the usage area of microwaves covers radar applications, detailed information will be given in the following parts of the thesis.

EM radiation with a greater wavelength than visible light is known as an infrared wave, and its wavelengths range from 1 mm to 700 n. The heating effect of the Sun is the primary source caused by infrared radiation. Another thing that results in the generation of infrared radiation (IR) is the movement of molecules and objects at room temperature. Since the wavelength of the IR resonates with the skin molecules of humans, they are readily absorbed by the skin. Even though human eyes can’t detect them, they can be felt as heat.

Electromagnetic radiations with wavelength between 350 to 700 nm are called as visible light. Since human eyes are only sensitive to the certain wavelengths, visible light is the only EM wave that can be detected by the humans. The visible light spectrum consists of different regions according to wavelength and photon energy. Therefore, each region in this spectrum corresponds to different color. Violet color has the shortest wavelength with 400 nm and red has the longest wavelength with 700 nm. The other colors line up between these two.

Ultraviolet waves have shorter wavelength and higher energy than visible light. The wavelength of these radiation ranges between 10^{-7} to 10^{-10} m. The Sun can be thought as a primary source resulting in generation of ultraviolet radiation. Even though it can't be detected with eyes, it may cause disturbance on the skin when the light comes from the sun. Some of the applications areas of ultraviolet waves are sterilization, neon lights, security, etc.

X-ray is another type of radiation that has wavelength between 10^{-8} and 10^{-12} m. The common source for the production of X-rays is free electrons. X-rays are generated by speeding free electrons with the help of electrical voltage and then stopping them in a target. Since the wavelength of the X-ray matches with the atoms, it is used to determine the crystal structure of materials. In addition to that, it is also used in the medical industry to diagnose some diseases like cancer.

The last type of EM radiation is gamma rays, and they have very high energy compared to the other waves. Their wavelengths change between 10^{-10} and 10^{-14} m. The source of the gamma rays comes from four nuclear reactions, which are nuclear fusion, fission, gamma and alpha decay. They are readily filtered from the earth's atmosphere, but if they can reach the human body, they are very harmful to human beings and their tissues. The gamma rays are used in medicine to detect and treat tumors, to find microscopic and tiny cracks in aircraft components etc. [14],[18].

EM waves can be generated from different sources like electronic devices, nuclear phenomena, natural events, radiations from the Sun, or they can be created by laboratory equipment. Therefore, these radiations travel in space in order to transfer

information between devices and to provide wireless communication. In free space, all EM waves can travel from one point to another with the speed of light without any blocking. However, in the atmosphere, these radiations interact with the atmospheric gases, and they encounter the absorption of some wavelengths. The atmosphere is opaque to many radiations in the EM spectrum, and it has different absorption behavior for different wavelengths. In this way, it prevents people from the negative effects of these radiations. The electronic devices and the electronic systems on the Earth are adjusted according to the opacity of the atmosphere. Figure 2.4 shows the percent of atmospheric opacity with respect to wavelength and the waves blocked by the atmosphere [19].

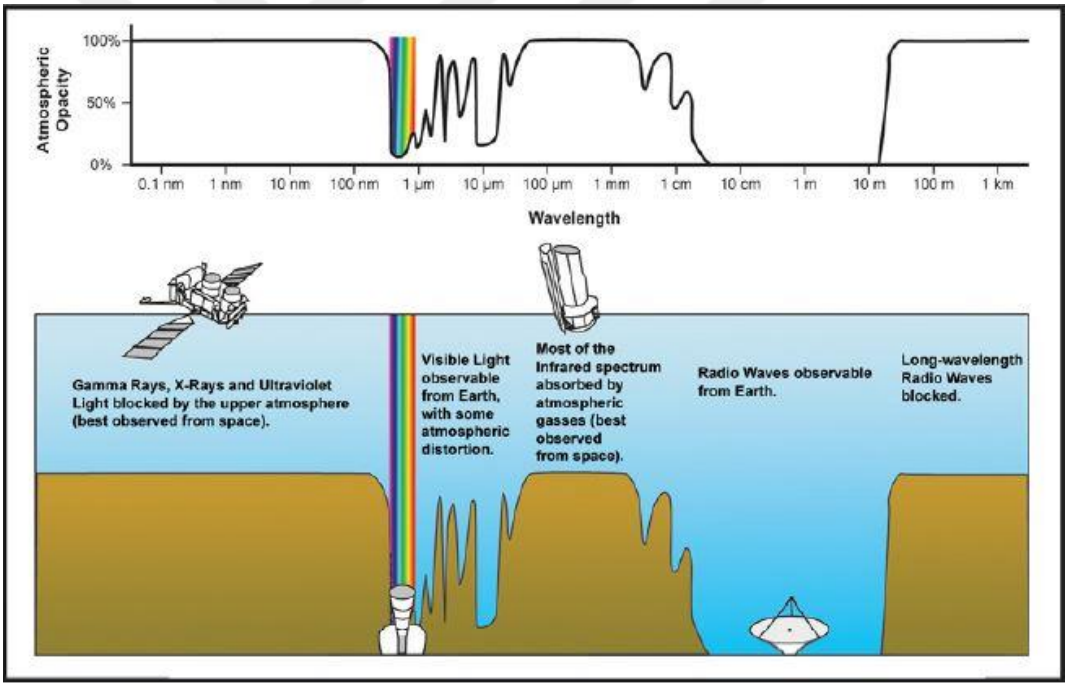

Figure 2.4. The graph of atmospheric opacity vs wavelength and the blocked radiations [19].

2.2 Microwave Frequencies and Applications

Microwave frequencies fall into the frequency range from 300 MHz to 300 GHz, corresponding to the region between radio waves and infrared waves. The wavelengths of the microwave radiations range between 1 mm and 1 m.

Since objects with the same wavelength as microwave frequencies resonant with each other, microwave frequencies include many molecular and atomic resonance frequencies. Wireless devices, radars, medical applications, navigation systems, mobile phones, military applications, satellites, cooking, and processing applications can be given as an example of applications that work in the microwave frequency range. Figure 2.5 shows the main application areas of microwaves which correspond to radar applications in a certain frequency and band ranges [20].

Increase in the usage of electronic devices that work in the microwave frequency range increases the pollution of unwanted radiations. This situation creates need for EM wave shielding and/or absorbing. In this thesis study, electromagnetic properties and absorbing characteristic of indium tin oxide (ITO) modified glass fiber woven fabric were studied within the 8-12 GHz frequency range.

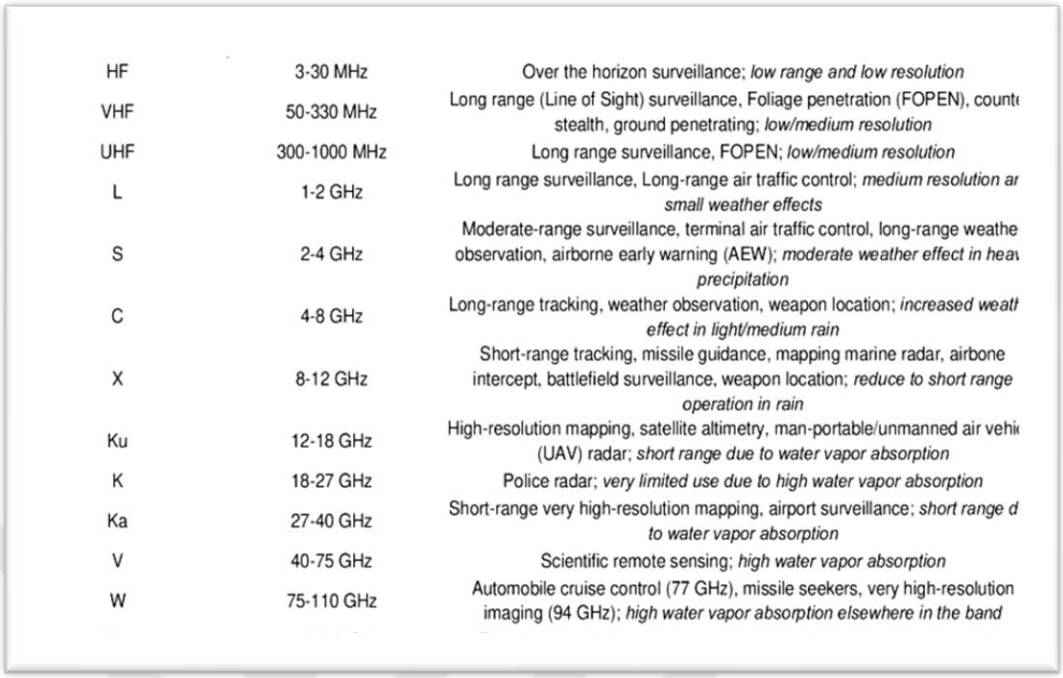

HF	3-30 MHz	Over the horizon surveillance; *low range and low resolution*
VHF	50-330 MHz	Long range (Line of Sight) surveillance, Foliage penetration (FOPEN), counte stealth, ground penetrating; *low/medium resolution*
UHF	300-1000 MHz	Long range surveillance, FOPEN; *low/medium resolution*
L	1-2 GHz	Long range surveillance, Long-range air traffic control; *medium resolution ar small weather effects*
S	2-4 GHz	Moderate-range surveillance, terminal air traffic control, long-range weathe observation, airborne early warning (AEW); *moderate weather effect in hea precipitation*
C	4-8 GHz	Long-range tracking, weather observation, weapon location; *increased weatl effect in light/medium rain*
X	8-12 GHz	Short-range tracking, missile guidance, mapping marine radar, airbone intercept, battlefield surveillance, weapon location; *reduce to short range operation in rain*
Ku	12-18 GHz	High-resolution mapping, satellite altimetry, man-portable/unmanned air vehi (UAV) radar; *short range due to water vapor absorption*
K	18-27 GHz	Police radar; *very limited use due to high water vapor absorption*
Ka	27-40 GHz	Short-range very high-resolution mapping, airport surveillance; *short range d to water vapor absorption*
V	40-75 GHz	Scientific remote sensing; *high water vapor absorption*
W	75-110 GHz	Automobile cruise control (77 GHz), missile seekers, very high-resolution imaging (94 GHz); *high water vapor absorption elsewhere in the band*

Figure 2.5. Microwave frequency ranges in radar applications [20].

2.3 Electromagnetic Wave - Material Interactions

Electromagnetic radiation can be defined as the energy formed due to the relationship between the electrical and magnetic fields, and it travels through free space or in a medium. During this propagation, it may come across with another wave in a constructive or destructive manner, it may have resonance with the object that's size matches with the wavelength of the radiation, or it may be encountered with elementary particles like electrons.

EM waves behave in three different ways when they interact with the matter which are reflection (R), transmission (T), or absorption (A). As a result of these interactions, the energy of the wave decreases and this energy loss transfers to the reflected, transmitted, or absorbed waves. According to the energy conservation law, the initial energy of the system must be equal to the final energy of the system. So,

it can be seen from Equation 2.3, power fraction of reflected (P_R), absorbed (P_A), transmitted (P_T) waves with respect to the power of the incident wave (P_0) must be equal to one [21].

$$1 = \frac{P_R}{P_0} + \frac{P_A}{P_0} + \frac{P_T}{P_0} \qquad \text{(Equation 2.4)}$$

Materials can be classified according to their behavior when they encountered with the electromagnetic wave:

The first class covers opaque materials. If an EM wave is reflected from the surface of the material, the material is opaque to the EM wave. These materials are typically conductors because reflection occurs when the material has mobile charge carriers like electrons.

The second class of materials is transparent materials. As can be understood from the name, they are transparent to EM waves and allow the wave to pass through them. They are generally insulators or low dielectric loss material.

The third class of materials is absorbing material. These materials should be able to absorb incident EM power and produce both magnetic and electric dipoles for absorption. Polarization of dipoles (dielectric loss), rotation of magnetic domains (magnetic loss), and free electron flow (conductance loss) can all be used to absorb energy. Since the main objective of the thesis is related with the EM wave absorbing materials, these concepts will be explained in detail in the following chapter [18]. Figure 2.6 shows the interaction of EM waves with these three classes of materials.

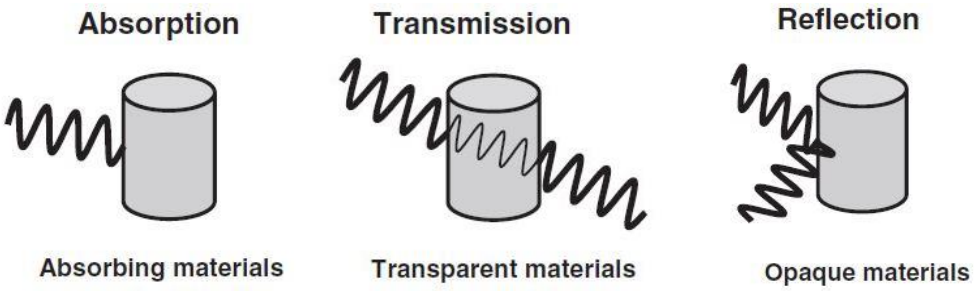

Figure 2.6. Classification of materials according to their interaction between the EM waves [18].

2.4 Electromagnetic Shielding Theory

With the advancement of technology, the variety and the use of electronic devices are increased to a considerable extent day by day. As explained earlier, most of these devices operate at microwave frequencies, and they generate electromagnetic fields which may be spread into the environment. Such EM fields can interfere with other electronic devices, causing damage and failures in their use. This situation brings the need for electromagnetic shielding of harmful and unwanted radiation from electronic devices. So, the purpose of electromagnetic (EM) shielding is to protect electronic and electrical components and systems from external EM fields or to avoid EM fields from being emitted by the components and systems [22].

EM wave can behave in three different manner when it interacts with the matter which are reflection, transmission and absorption. Reflection and absorption are the main mechanisms responsible for shielding of EM wave. Figure 2.7 shows the mechanisms caused by the interaction between EM wave and shielding material [23].

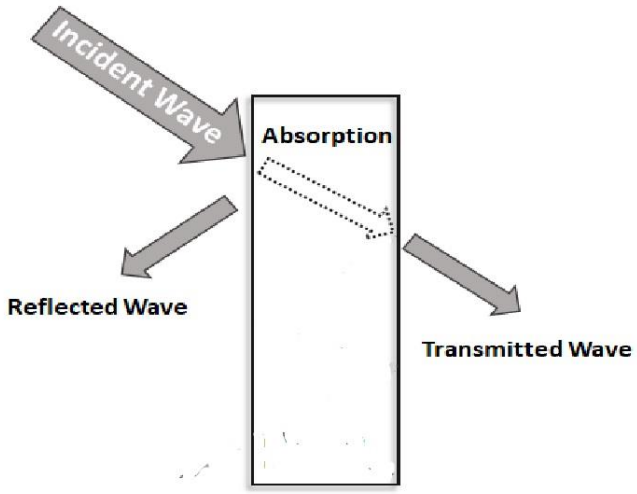

Figure 2.7. EM wave-material interaction [23].

Reflection is the first mechanism for EM shielding and this phenomenon results from the interaction between electromagnetic waves with the mobile charge carriers, electrons, and holes. Even though conductivity is not the only requirement for shielding, high conductivity materials enhance the amount of reflection for electromagnetic shielding. This is why the most suitable and common choice for high reflection to occur is metals.

Absorption is the second mechanism for EM shielding. To absorption occur, either electrical or magnetic field components of the EM wave should interact with electrical or magnetic dipoles of shield material. This means that shielding materials should have magnetic or electrical dipoles to decrease the energy of incoming radiation by locking this loss of energy inside their structure [24].

Another thing that should have been considered is shielding effectiveness (SE). Shielding effectiveness can be defined as the ability of the material to act as a shield against external and internal electromagnetic fields in order to avoid the harmful effect of these radiations. There are a lot of parameters that affect the shielding effectiveness, and they are tabulated in Figure 2.8.

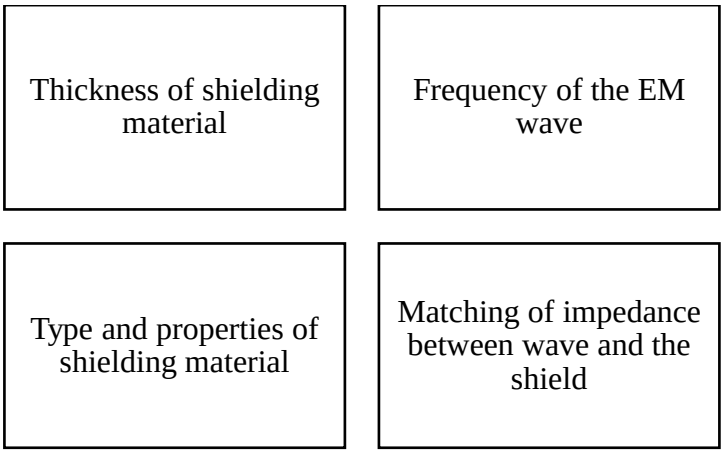

Figure 2.8. Parameters for shielding effectiveness [25].

Shielding effectiveness is stated in decibels (dB) and can be related to the EM shielding mechanisms that were explained before. The absorbed part of the incident wave is called absorption loss (A_{loss}), the reflected part of the incident wave is called reflection loss (R_{loss}) and shielding effectiveness can be found by adding up these terms.

$$SE(dB) = A_{loss} + R_{loss} \quad \text{(Equation 2.5)}$$

Another way to express shielding effectiveness is to take logarithm of the ratio of the initial and final electrical and magnetic field and equation 2.6 and 2.7 show the relationship between SE and electrical and magnetic fields.

$$SE = 20\,log\left(\frac{E_f}{E_i}\right) \quad \text{(Equation 2.6)}$$

$$SE = 20\,log\left(\frac{H_f}{H_i}\right) \quad \text{(Equation 2.7)}$$

2.5 Electromagnetic (EM) Wave Absorbers

At the beginning of the thesis study, the definition and history of electromagnetic shielding and the reason of the need for these materials are briefly explained. In addition to these, theoretical knowledge about electromagnetic theory and loss

mechanisms for electromagnetic shielding was explained. In this section of the study, the classification of electromagnetic wave absorbers and the material used for this purpose will be discussed.

2.5.1 Classification of Electromagnetic Wave Absorbers

2.5.1.1 Graded Dielectric Absorbers: Impedance Matching

In the impedance matching absorbers, the amount of reflection depends on the impedance matching between incident wave and the transmitting media. When a propagating wave hits an interface, it would be reflected to a degree equal to the magnitude of the impedance difference between the incident and transmission medium. With the scope of this aim, impedance matching absorbers can be divided into three classes: pyramidal, tapered, and matched absorbers.

2.5.1.1.1 Pyramidal Absorbers

These absorbers are produced for broadband impedance matching that reduces reflections at interfaces within the appropriate frequency band. They are generally fabricated in pyramidal or cone form with the desired thickness depending on the property requirements. Pyramids are typically constructed to be on the order of one wavelength in height and periodicity [26].

Pyramidal absorbers provide good absorption over a broad frequency spectrum. Absorption values greater than 50 dB can be achieved by using pyramidal absorbers. On the other hand, the thickness may be a disadvantage for some applications, and they tend to be fragile when a comparison is made between other absorbers. The schematic drawing of pyramidal absorber is shown in Figure 2.9.

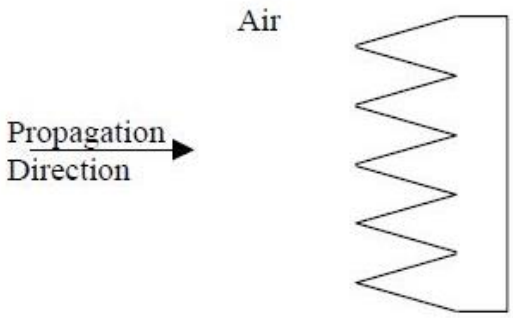

Figure 2.9. Pyramidal absorber [26].

2.5.1.1.2 Tapered Absorbers

The tapered type absorber can be thought of as a slab be formed by the combination of low loss and lossy materials. The lossy material is uniformly distributed parallel to the surface so that the gradient should rise perpendicular to the surface and into the material. The thickness of the tapered absorber is lower than the pyramidal absorber, so this creates an advantage over the pyramidal absorber. However, their absorber characteristics are lower than the pyramidal type, so their performance is poor when they are compared. Figure 2.10 shows the schematic drawing of tapered type absorbers [27].

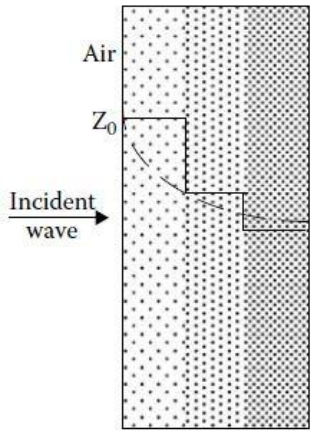

Figure 2.10. Schematic tapered absorber structure [27].

2.5.1.1.3 Matching Layer Absorbers

The main objective of using matching layer absorbers is to eliminate the absorption film thickness problem by creating gradual transition. The whole absorber can be produced by placing a transition matching layer between the incident wave and the absorbing media. The thickness and the impedance of the of the matching layer are important for effective absorption. The impedance of the matching layer (Z_1) should between the impedance of the absorbing layer (Z_2) and the incident media (Z_0). When the thickness of this layer is equal to the quarter wavelength of the incident wave in the layer, matching occurs, and absorption takes place. The schematic view of the matching layer absorber is shown in Figure 2.11.

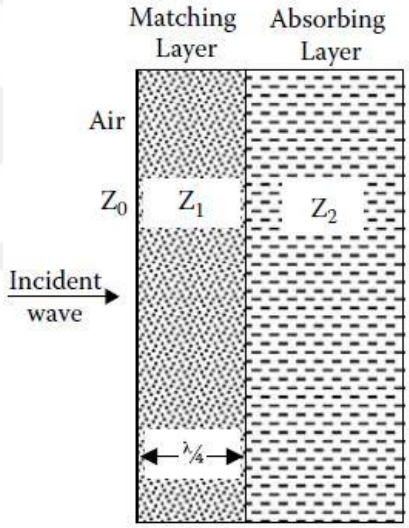

Figure 2.11. Matching layer absorber structure [27].

2.5.1.2 Resonant Absorbers

The second class of EM wave absorbers is resonant absorbers. They can also be named as tuned or quarter wavelength absorbers. In the first type of absorbers, primary absorption mechanism is to create impedance matching between the incident wave and the absorbing media. Unlike the first type of absorbers, not all EM energy

is absorbed since there is no impedance matching between the incident and absorbing medium.

When the incident wave encounters the system, transmission and reflection of the wave takes place at the first interface. Then the transmitted wave passes through the absorbing medium and is reflected from a metal backing put behind the absorber. If first reflected wave undergoes a phase reversal with an amount of π, and if the optical distance traveled by the transmitted wave is an even multiple of half wavelengths, then the two reflected waves will be out of phase and destructively interfere. Furthermore, if the intensities of both waves match, then the total reflected intensity is zero [28].

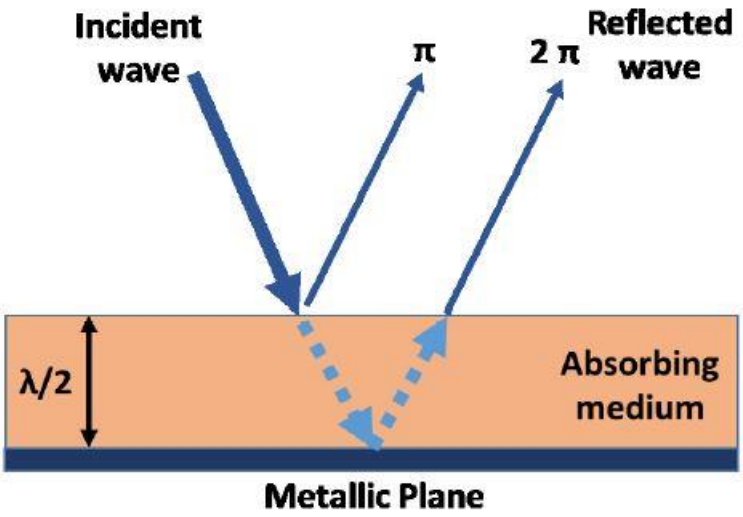

Figure 2.12. Destructive interference phenomenon in resonant absorbers [28].

There are mainly three types of resonant absorbers which are Dallenbach layers, Salisbury screens, and Jaumann layers.

2.5.1.2.1 Dallenbach Layers

The first type of resonant absorber is Dallenbach layer and it can be produced by placing a homogenous lossy material layer in front of the metal plate, and it is shown in Figure 2.13. This type of absorbers can be formed by using a single or multiple layers of lossy material layer, and they have good absorption properties even in low frequency working conditions. The absorption properties can be enhanced by changing thickness, permeability (μ_1), and permittivity (ε_1) of the lossy material layer. If the impedance of the lossy material layer (Z_M) is equal to the impedance of the incident wave (Z_0), minimum reflectivity can be obtained [29].

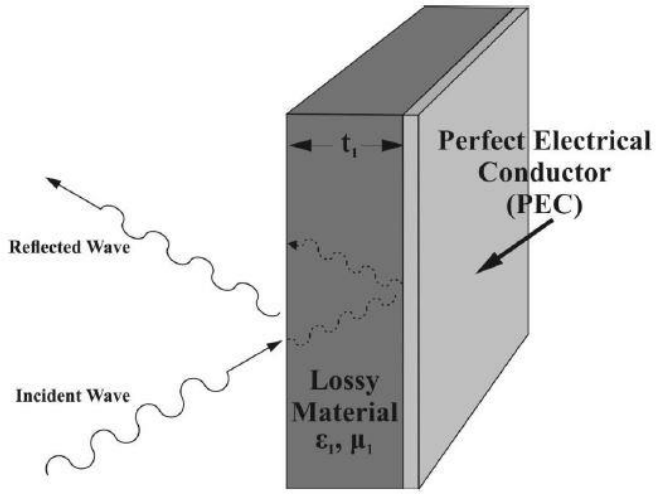

Figure 2.13. Dallenbach layer [30].

2.5.1.2.2 Salisbury Screen

The second type of resonant absorber is the Salisbury screen. It is the simplest and common absorber that is used among the other absorbers. As shown in Figure 2.14, the resistive sheet is put at a quarter wavelength distance from the metal surface. When an incident wave encounters the system, some of the waves will be reflected from the resistive sheet and the rest will be transmitted through the gap to reach the metal surface. Since there is a quarter wavelength space between resistive sheet and

the metal surface, the wave that is reflected from the metal surface will have same amplitude with the first reflected wave but there will be $\lambda/2$ phase difference between them. This will cause a destructive interface, and these two waves will cancel each other. The gap between the resistive sheet and the metal surface can be filled with air or lossy material with higher permittivity than air. In the case of using lossy material to filled the gap, thickness of the band gap should be decreased to obtain phase cancelation.

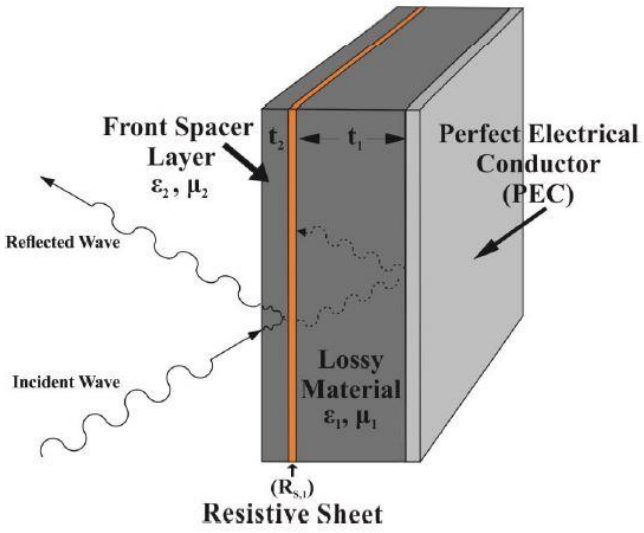

Figure 2.14. Salisbury screen [30].

2.5.1.2.3 Jaumann Layers

The third type of resonant absorber is Jaumann layers (Figure 2.15) and it is the improved version of Salisbury screen. Even though, Salisbury screen is the common and simplest form of the resonant absorbers, the bandwidth of these types of absorbers is very narrow and they can only be matched to a single frequency. So Jaumann absorber may be the best way to increase bandwidth of the absorber and to get minimum reflectivity over a wide range frequency. Jaumann absorber is made by placing multiple layers of Salisbury resistive sheets in front of the metal plate and space between the sheets is filled with lossy material. Since the number of resistive

sheets increases, the number of minima in reflectivity can be increased, and in this way, the bandwidth of the absorber can be increased [31].

The placement of the resistive sheets also has great importance in the construction of Jaumann type absorbers. The sheet having the lowest conductivity must be placed on the frontmost layer, and conductivity of sheets must be increased toward to metal back.

Besides the many advantages, Jaumann absorbers have some disadvantages from time to time. For instance, as the number of sheets increase, the thickness and weight of the absorber also increases. So, this situation must be considered during the production of this type of absorber.

In this thesis study, electromagnetic absorption characteristic of ITO coated glass fiber woven fabric in 8-12 GHz frequency range is investigated. Since the wide frequency range is used to characterized the absorption properties of the material, the best way is fabricating combination of Jaumann and graded type absorber with ITO coated fabrics to get broad bandwidth.

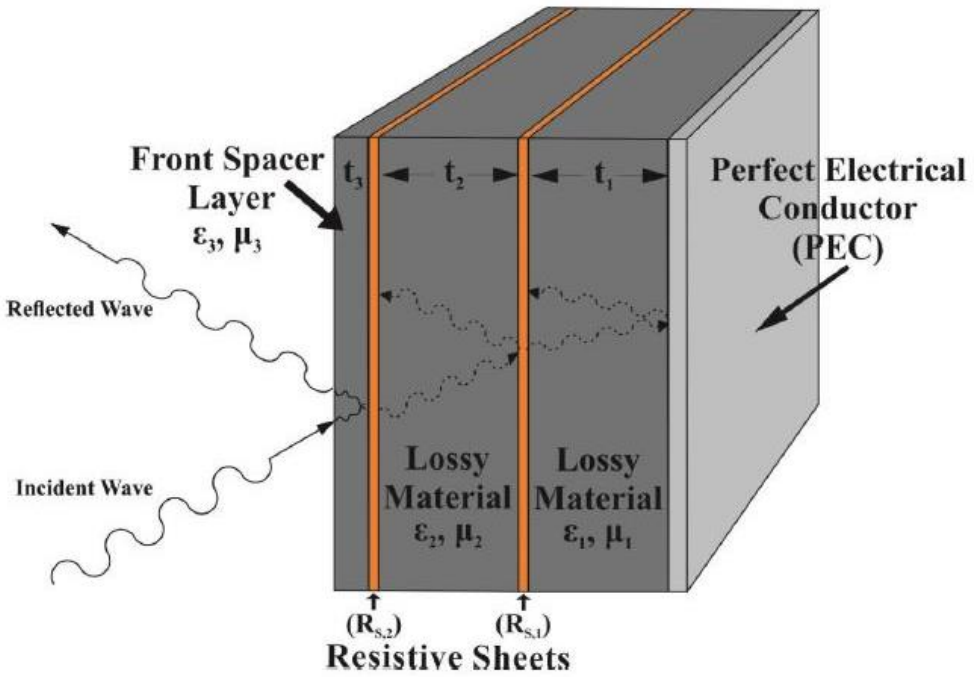

Figure 2.15. Jaumann absorber [30].

2.5.2 Electromagnetic Interference (EMI) Shielding and Absorbing Materials

Today's technological developments have increased the need for electromagnetic shielding materials and accelerated research on this topic. In the previous section, the classification of electromagnetic wave absorbers is explained, and in this section, the materials that are used in these absorbers will be discussed.

Electromagnetic wave absorbing materials are used in variety of applications and there are many different types of materials used in EM wave absorbing applications. These materials should have some basic properties to satisfy the requirements of the application and material selection should be made according to the usage conditions. The first and the foremost property that EM wave absorbing material should have is maximum absorption of the incoming wave. The frequency range of absorption should be broad. The thickness of the absorber should be optimum for application and the weight of the absorber should not be high. The material used should be durable to environmental and operating conditions such as moisture, heat, etc. If the absorber works in mechanical loading conditions, the material should have mechanical stability, and it should not degrade chemically or physically. Last but not least, materials should be feasible in terms of cost [32],[33].

The first class of materials used for electromagnetic shielding is metals. Due to their electrical properties and ability to conduct electricity with the help of free electrons, they can reflect, absorb and transmit electromagnetic interference. This is why metals are so commonly used in EM wave shielding applications. Copper (Cu), Aluminum (Al), stainless steel, silver (Ag), nickel (Ni) are the most preferred metals because they have high reflection loss due to their high conductivity. Another popular metallic material is an alloy called mumetal, which consists of nickel, iron, chromium and copper. It is generally used for shielding sensitive devices from the low frequency magnetic waves. In addition to these bulk metals, metal foams, metal sheets, and metal coatings on insulators are also used for electromagnetic shielding purposes[34].

Materials with magnetic or electrical dipoles in their structure are another class of electromagnetic absorber material. The previous sections explain the effects of electrical end magnetic properties on electromagnetic loss mechanisms. It can be said that material with high electrical conductivity or high magnetic permeability increases the amount of absorption loss. So, barium titanate ($BaTiO_3$) and magnetite (Fe_3O_4) are the most common examples of these types of materials.

Polymeric materials are also gained attention due to their lightweight and non-corrosive structure. Intrinsically conducting polymers that gain their conductive by doping or partial oxidation is one of the most preferred types of polymers in absorber applications. Polyaniline (Pan) and polypyrene (PPY) can be given as an example of these kinds of polymeric materials.

Composite materials constitute a large part of electromagnetic absorber materials. Dispersing metallic particles such as silver, copper, ferrite, or nonmetallic particles such as carbon, carbon black into polymeric resins is one way to produce composite material for shielding applications. The other way to fabricate EM wave shielding composite is to use conducting fibers such as aluminum fiber, carbon fiber, nickel-coated graphite fibers, or carbon nanotubes as a reinforcement material. Using composite materials as a shielding and/or absorbing material creates many advantages. They provide shielding of waves in a wide frequency range, using particles like nickel, ferrite in composite increases the magnetic loss, using metallic particles in composite increases the wave matter interaction due to their free electrons. Besides these advantages, each material has some restraints; for example, aluminum fibers have low impact resistance, metals are sensitive to a corrosive environment, carbon and graphite are brittle [34, 35].

The other class of materials used for electromagnetic absorbing are transparent conductive oxides (TCOs), which can be defined as doped metal oxides. According to the dopant type, they can be either n-type or p-type semiconductors. Aluminum-doped zinc oxide (AZO), fluorine-doped tin oxide (FTO), antimony-doped zinc oxide (ATO), and indium-doped tin oxide (ITO) can be given as an example of

transparent conductive oxide materials. Due to their unique electrical and optical properties, bendable characteristics, lightweight structure, and ability to resist environmental effects, they gain attention in electromagnetic applications. As mentioned before, since insulating material can be gained certain electrical conductivity by coating transparent conductive oxide, these materials are great candidates for EM shielding and/or absorbing.

In this thesis study, ITO coated glass fiber woven fabric was chosen as electromagnetic absorber material and characterization of electromagnetic shielding and absorption properties of this material were investigated in 8-12 GHz frequency range. Since ITO is a semiconductor and has certain electrical conductivity, various ITO coated glass fiber woven fabrics with different film thicknesses were prepared and combination of Jaumann and graded type composite were fabricated to increase the shielding effectiveness.

2.6 Electromagnetic Characterization Methods of EM Wave Absorbing Materials

There are various methods to investigate materials' electromagnetic properties, such as shielding effectiveness and absorption characteristic. According to the important parameters of the material such as shape, thickness, and form, the most suitable characterization method should be chosen. Material can be either in the form of panel, thin sheet or bulk. Coaxial probe method, parallel plate method, transmission line method, surface waveguide method, shielded box method and free space method can be given as some of the important electromagnetic characterization methods. In Figure 2.16, EM characterization methods are positioned according to the loss characteristic of the material and the frequency range used [7].

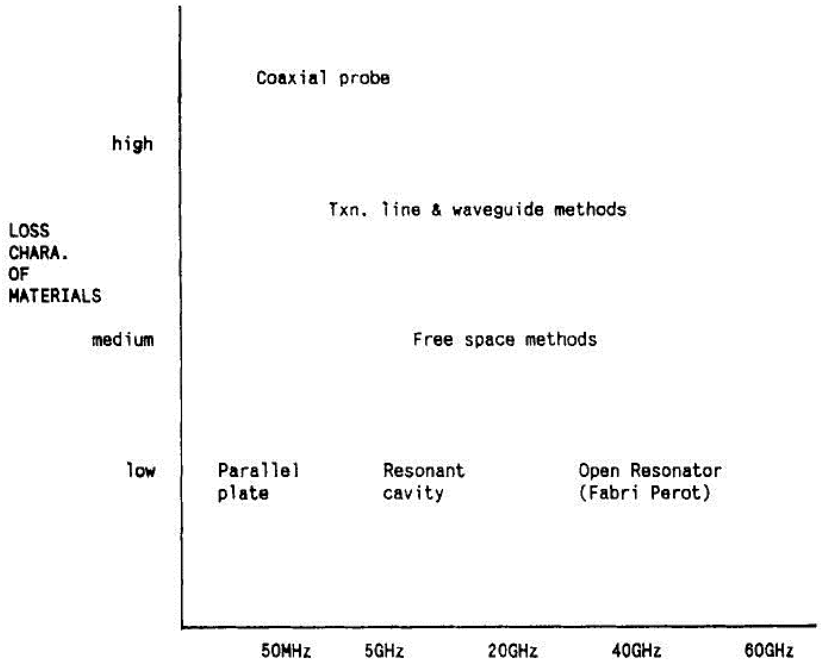

Figure 2.16. The Proper EM characterization method selection [7].

The free space method was chosen as the most suitable method to characterize EM properties of ITO coated glass fiber woven fabric in this study since this method is used to characterize the reflection transmission behavior of the material. This method also allows to characterize the electromagnetic properties of inhomogeneous materials. In addition to these, according to Figure 2.16, the free space method is suitable for the frequency range and the loss characteristic of the material used in this study.

2.6.1 Characterization by Free Space Method

The free space method is one of the commonly used non-destructive technique and working principle based on the reflection and transmission behavior of the media. The free space measurement set-up consists of two horn antennas that are aligned facing one another and power generated by the vector network analyzer is transmitted thorough the antennas with the help of coaxial cables. Then

electromagnetic wave comes from the horn antennas focus on the specimen surface via lenses. The schematic drawing of the free space set-up is shown in Figure 2.17 [36].

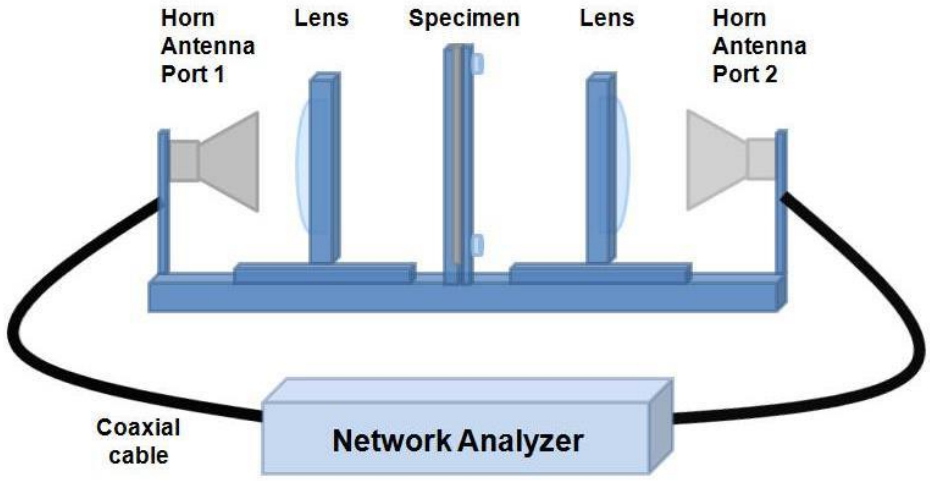

Figure 2.17. Free space measurement set-up.

In the previous sections, the main EM wave matter interaction mechanisms are defined as reflection loss and absorption loss. The free space method measures the reflection and transmission coefficient as the phase (dB) and magnitude (θ) and gives the output in the form of four S parameters which are S_{11}, S_{12}, S_{22} and S_{21}. The first number in the s parameter indicates the port that receives the EM wave and the second number in the S parameter indicates the port that transmits the EM wave. So, when the incident wave comes from antenna 1 is reflected from the sample and comes to the antenna 1, it can be indicated by the reflection coefficient as S_{11}. When the incident wave comes from the antenna 1 is transmitted to antenna 2, it is indicated by the transmission coefficient as S_{12}. The opposite situation can be named as S_{22} and S_{12} [37].

Reflection (R) and transmission (T) loss in decibel can be expressed as the logarithm of the ratio of reflected and transmitted power to the incident power. When the

network vector analyzer gives the outputs in the form of power, multiplication factor becomes 10. However, when it gives the outputs in the form of voltage, the multiplication factor becomes 20. Equation 2.8 and 2.9 show reflection and transmission loss formulation in both voltage and power form [38].

$$R(S_{22}) = 10\log\frac{P_R}{P_0} \qquad R(S_{22}) = 20\log\frac{V_R}{V_0} \qquad \text{(Equation 2.8)}$$

$$T(S_{12}) = 10\log\frac{P_T}{P_0} \qquad T(S_{12}) = 20\log\frac{V_T}{V_0} \qquad \text{(Equation 2.9)}$$

The percent absorption value can be defined as ratio of the power neither reflected nor transmitted. Percent absorption of EM wave can be found by using Equation 2.10 and 2.11 according to the power and voltage form respectively.

$$\%\, Em\ Wave\ Absorption = 100 \times (1 - |S_{22}| - S_{12}|) \qquad \text{(Equation 2.10)}$$

$$\%\, Em\ Wave\ Absorption = 100 \times (1 - |{S_{22}}^2| - |{S_{12}}^2|) \qquad \text{(Equation 2.11)}$$

In order to get accurate measurements, free space setup needs to decent calibration steps. In order to minimize the environmental factors and measurement inaccuracies thru-reflect-line (TRL) calibration should be done.

2.6.1.1 Thru-Reflect-Line (TRL) Calibration

TRL calibration technique is used for de-embedding of S-parameters, i.e. measurement reference planes are carried to faces of the samples to be measured. There are different types of calibrations such as thru-reflect-match (TRM), line-reflect-match (LRM) and so on. However, TRL calibration is the most suitable one for the analysis of multilayered samples and composites. TRL calibration can be performed using VNA's calibration wizards. At the beginning of the calibration, the distance between antennas should be adjusted to twice of the focal distance to achieve the THRU standard. Calibration of THRU is done to enable the direct

passage of electromagnetic waves, i.e. zero length line. After that, LINE calibration is done by moving one of the antennas backwards by the quarter wavelength of center frequency of the test range. For wide band measurements multiple LINE standards can be used. Finally, REFLECT calibration is done for two ports by placing a metal plate on the locations of two faces of the sample and by moving the antennas backwards according to the thickness of the calibration sample. After the calibrations, both phase and magnitude measurements of reflection and transmission losses can be evaluated with the help of VNA.

2.7 Indium Tin Oxide (ITO) in Electromagnetic Applications as an Absorber

Today, using semiconductor materials in the many applications is the most important contributor to the technological advancement. Because of their excellent optical transmittance in the visible range and high electrical conductivity, transparent conductive oxides (TCOs) thin films produced using semiconductor technology have been intensively studied in recent years. In order to achieve these two properties at the same time, transparent conductive oxides are produced as a non-stoichiometric and appropriately doped structure with broad bandwidth. They are used in a wide range of applications, mainly in optoelectronic and electromagnetic applications such as touch screens, solar cells, electrochromic devices, data transfer systems and electromagnetic shielding devices [39]– [41].

The first study of a transparent conductive oxide (TCO) material took place in the early 1900s. It is realized that when a coating of cadmium metal was heated, the metal oxidized and became conductive. Although the invention of these materials dates back to the 1900s, the usage of transparent conductive oxide increases day by day. According to the global transparent conductive films market, the demand for TCO was nearly 2 billion US dollars in 2012, and it reaches almost 20 billion Us dollars in 2020 [42].

There are almost 20 distinct types of doped binary oxide as a transparent conductive oxide such as indium doped cadmium oxide, fluorine doped tin oxide (FTO), antimony doped zinc oxide (ATO), aluminum doped zinc oxide (AZO), tin doped indium oxide (ITO) etc. According to the application and its parameters and requirements, the chosen TCO changes. Figure 2.18 shows the properties necessary for specific applications and selection criteria for each application.

Applications	Sheet Resistance	Transparency	Thermal Stability	Chemical Stability	Mechanic Stability	Deposition Temperature	Cost
Flat Panel Displays	Low	High	-	Good	Good	Low	-
Solar Cells	Low	High	Good	-	-	Low < (200° C)	Low
Smart Windows	-	High	Good	Good	Good	-	Low
EMI shielding	Low	-	-	-	Good	Low	-
Touch Screens	Low	High	-	-	Good	-	Low

Figure 2.18. Selection criteria of TCOs for certain application [43].

Indium tin oxide (ITO) belongs to the class of transparent conductive oxides in materials science because of its structure, properties, and chemistry. The invention of the ITO dates back to 1954, and it was proposed first by G. Rupprecht. Tin-doped indium oxide (ITO) has the same cubic structure as indium oxide, called bixbyite structure. Bixbyite structure has 40 atoms in a unit cell. Indium atoms lie at the six and four-fold interstitial sites and each indium atom is closely packed with six-fold oxygen atoms. The bandgap of ITO is between 3.5 Ev and 4.3 Ev [44].

The structure of ITO is obtained by substitutional doping of Sn^{+4} ions to the lattice. After the doping, In^{+3} ions replace with the Sn^{+4} ions and form electron vacancy in the lattice. By this way n-type semiconductor is formed. Another thing about ITO is that there is some change in the lattice parameter after doping. The lattice parameter of indium oxide is about 1.012 nm however, after doping lattice parameter changes by about 0.05% because of the size difference between host and doping atoms.

Nowadays, ITO dominates the transparent conductive oxide market and is the most commonly used one in both optoelectronic applications and electromagnetic shielding purposes among all the other TCOs. Besides the conductivity and transparency, indium tin oxide is preferred since it has good substrate adherence and wetting, it does not require high temperature during coating, it is chemically and mechanically stable in acidic and basic environments, resistive to corrosion, it is not toxic, and it can absorb wave in the ultraviolet and infrared region [45].

2.8 Microstructural, Electrical and Electromagnetic Properties of ITO Thin Films

In this part of the study, important process parameters (starting chemicals, the molarity of the solution, doping concentration, heat treatment temperature, spray coating parameters, the thickness of the coating) were examined and optimized according to the results found in the literature. Then the effect of these parameters on microstructural, electrical, and electromagnetic properties of ITO coatings were explained.

2.8.1 Effect of Starting Precursors and Solvents

It is important to determine appropriate precursors and solvents combination in this study, because each and every precursor and solvent have various features and impact on the quality of the resulting ITO thin film.

Basically, there are three types of starting precursors to prepare indium tin oxide, which are organic metal alkoxides ($M(OR)_n$), inorganic salts (M_mX_n) and crystallized ITO nanoparticles. They all have pros and cons when the effects of precursors on properties of the thin film were considered.

The first group, which is metal alkoxides, have advantage of high purity. However, due to the disadvantages like high cost, low reachability, high sensitivity to temperature and humidity, they have limited usage in the studies [46], [47].

The second group which is crystallized nanoparticles also commonly used precursors to get ITO thin films. J. Ederth et al. prepared ITO thin films onto glass substrate by using chemically produced nanoparticles and the resulting films have a porous structure [48]. So even though, using crystallized nanoparticles have advantages like deposition at low temperature, the final structure will be porous and hence electron transportation will be low [49].

The final group of precursors which are metal inorganic salts draws more attention among the others due to their cost-effective structure, availability and easy deposition. T. F. Stoica et al., M.J. Alam et al. and many other researchers used indium chloride ($InCl_3$), indium chloride tetrahydrate ($InCl_3 \cdot 4H_2O$), tin chloride ($SnCl_4$) and tin chloride pentahydrate ($SnCl_4 \cdot 5H_2O$) in their research [50-52]. Besides, like in this thesis study, many researchers also used indium nitrate (In (NO_3)) and indium nitrate hydrate (In (NO_3)$_3 \cdot xH_2O$) as a starting precursor [53,54].

There are different types of solvents for the sol preparation such as isopropanol, acetylacetone, ethanol, methanol and so on [55,56]. According to the selected precursors, one of these solvents will be appropriate for the sol preparation.

2.8.2 Effect of Dopant Concentration

Dopant concentration is another important parameter that affects the electrical properties and the quality of the indium oxide thin film. There are various types of dopants used for indium oxide thin films such as fluorine, titanium, molybdenum and so on. In this thesis study, one of the commonly used doping element which is tin (Sn) was used to improve the electrical properties of the film.

As it was mentioned before, the structure of ITO is formed by doping Sn to indium oxide. After the doping, In^{+3} ions replace with the Sn^{+4} ions and form unpaired

electrons in the structure due to the mismatch of a number of electrons. By this way n-type semiconductor is formed. These free electrons act as a carrier and influence the electrical conductivity of the film.

Among the many researchers working on this subject, the studies done by Zhang et al. and S. M. Kim et al. can be given as an example [57,58,46]. The results of studies show (Figure 2.19) that optimum Sn concentration should be between 8 and 10 mol%. When the Sn concentration increases from 5 to 10 mol%, sheet resistance and resistivity of the start to decrease and show minima at 10 mol%. However, after that point, resistivity starts to increase again because after exceeding critical concentration, dopant Sn ions segregate at grain boundaries. Therefore, Sn concentration was decided as 10 mol% for this thesis study.

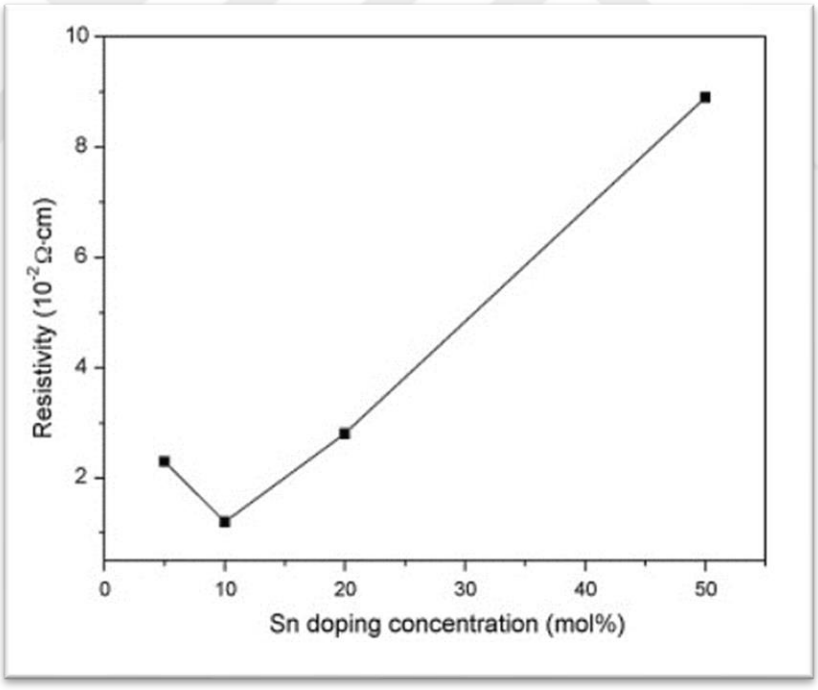

Figure 2.19. Effect of Sn doping concentration on electrical resistivity of ITO thin films [57].

2.8.3 Effect of Annealing Temperature

The post coating annealing temperature or heat treatment has a significant impact on the structural and electrical properties of sol gel based thin films. The final annealing heat treatment can promote crystallization, create an oxygen vacancy, or remove excess oxygen from the film structure [59]. At temperatures above the deposition temperature, if there is a lack of oxygen in the film, it supplies oxygen to the ITO, and if there is excess oxygen, it decreases. If the film is deposited under ideal conditions, heat treatment can also improve the characteristic of the film. In addition to all these, heat treatment ensures the densification of the films. Annealing also improves grain size while also optimizes structure by removing structural flaws.

Takahashi et al. and Nishio et al. found that increase in the heat treatment temperature results in a decrease electrical resistivity of the film [60,61]. According to their studies, the reason for this situation is that when the temperature increases from 400 °C to 700 °C, the mobility of the carriers increases from 1.3 cm^2/V_s to 14 cm^2/V_s.

TG-DTA study conducted by H. Cho et al. shows that there is a peak between 200 and 350 °C and this peak corresponds to weight loss due to the burning of organic compounds. Another peak observed at 450 °C indicates the starting crystallization of ITO film (Figure 2.20) [62].

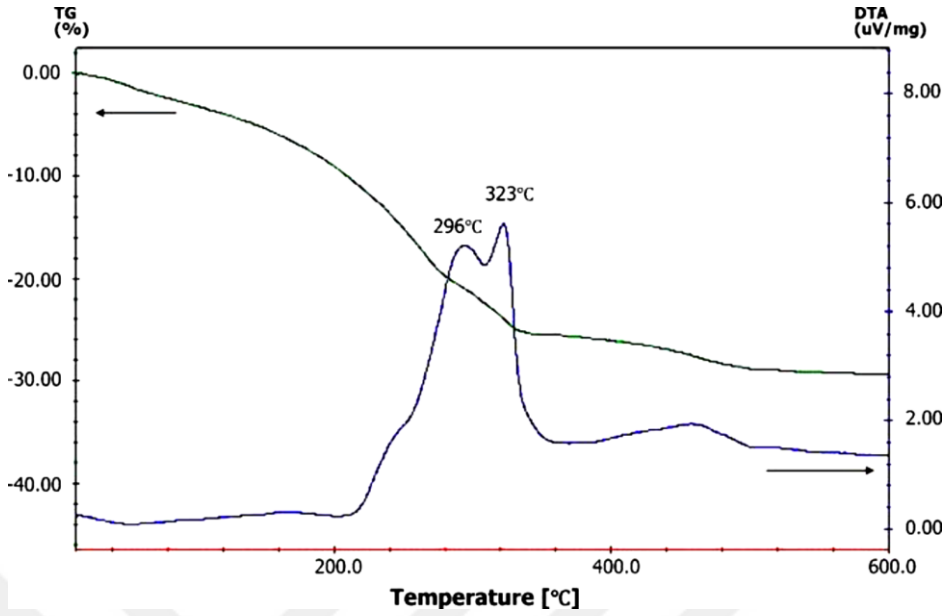

Figure 2.20. TG-DTA graph of an ITO thin film [62].

M. Toki et al. also confirm that the crystallization of ITO film starts at around 400 to 450 °C by XRD analysis. There is no peak belongs to ITO below 400 °C, and all the pattern shows amorphous nature (Figure 2.21). In addition, they observed that when the temperature increases, the peaks belong to ITO film increase in terms of intensity and get sharper due to increase in crystallization behavior [63].

As a result of many studies conducted by different researchers concluded that crystallization of ITO thin films starts at around 400 °C, and resistivity of the films decreases when temperatures increase from 400 to 600 °C. Figure 2.22 also shows that after exceeding 600 °C, the resistivity of films starts to fall again since, at high temperatures, reduction of SnO_2 to SnO may causes decrease in ionic conductivity [51]. So, at high temperatures, oxygen removal from the system starts to slow down and decrease in the formation of oxygen vacancies causes decrease in the charge carrier concentration [62].

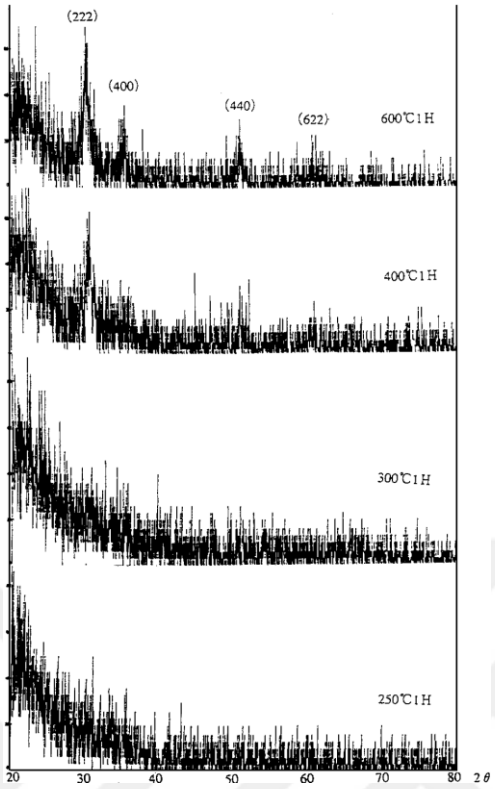

Figure 2.21. XRD pattern of ITO thin films with respect to annealing temperature.

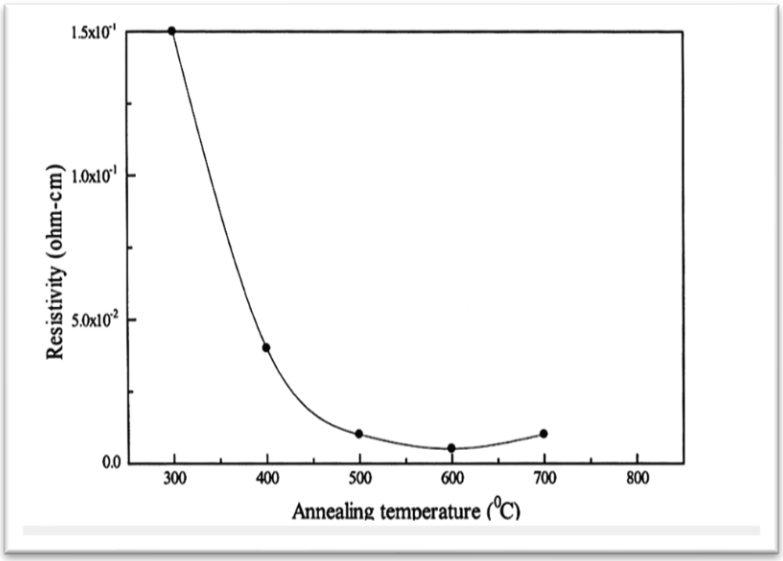

Figure 2.22. Resistivity change of ITO thin films with respect to temperature [51].

2.8.4 Effect of Film Thickness

Film thickness is another important parameter that affects the electrical and electromagnetic properties of the ITO thin film. In brief explanation, when the thickness of film increases, the number of charge carriers also increases. The number of charge carriers can be correlated with the resistivity of the film. The more charge carrier means higher conductivity. There are a lot of parameters that affect the thickness of the film such as spray coating parameters (spray distance, pressure applied to airbrush), but most importantly, film thickness is directly related with the molarity and the amount of solution that is deposited.

The first parameter that affects film thickness is molarity, and if the molarity of solution increases, it favors the formation of thicker film since higher molarity means a higher number of In^{+3} and Sn^{+4} ions in the solution and higher molecular interactions between atoms. In addition to these, changes in the molarity and hence the change in the thickness of the coatings explains the changes in the grain sizes and morphologies of the grains. This situation confirms by M. Dutta et al., and they show that when the molarity of solution increases from 0.03 molar to 0.1 molar, the thickness of the film rises from 36 to 247 nm and grain size increase from 25 to 55 nm (Figure 2.23) [64].

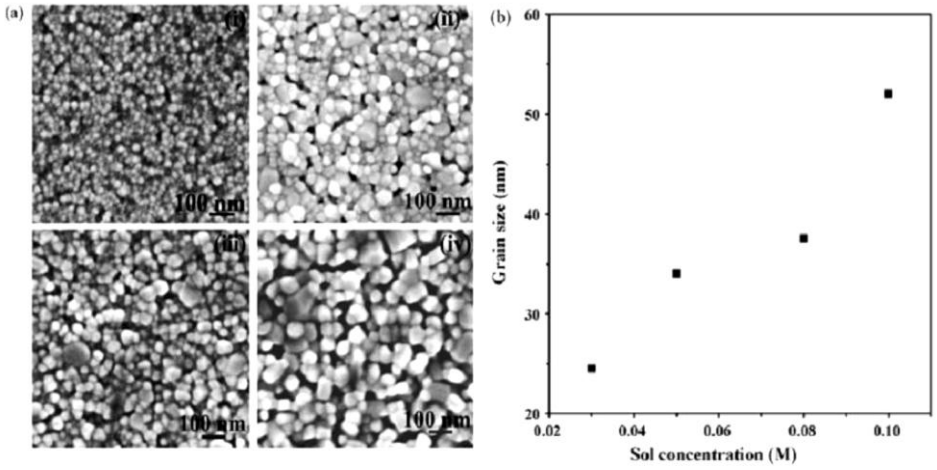

Figure 2.23. Change in the grain size with respect to molarity of the sol [64].

The active diffusion mechanism changes with the changing molarity. At lower molarities and hence lower thicknesses, the diffusion mechanism is bulk diffusion, so the nuclei formed during coating were homogenous and small. At higher molarity, the diffusion mechanism changes to surface diffusion, and some of the nuclei grow to larger grain sizes with tetragonal shapes [46]. In conclusion, all parameters are related to each other. Higher molarity means higher thickness and thicker films mean lower resistivity. According to the study conducted by Beaurain et al. for ITO thin film prepared with 0.1 mol/L sol, the sheet resistance value is equal to 2350 Ω/sq and thin films prepared with 0.2 mol/L sol, sheet resistance equals to 1420 Ω/sq [65].

The second parameter that affects the film thickness is the amount of sol. As suggested by many researchers, for the constant molarity condition, the thickness of the coatings increases with the increasing sol amount. This is because the wetting ability of the coating layers increases with the increasing amount of solution [66]. Besides the increase in thickness, for the high amount of ITO sol deposition, the crystallite size of the film also increases. Consequently, it causes a reduction in grain boundary scattering and an increase in the mobility of carriers.

2.8.5 Effect of Conductivity

The behavior of materials against electromagnetic waves is related to the electrical resistivity or conductivity of the material. Sheet resistance can be defined as the resistance of a unit square thin sheet. It is an important material property that determines whether electromagnetic waves pass through or are reflected at the interface. The sheet resistance of the material can be correlated with the conductivity of the sample by multiplying the sheet resistance with the thickness of the sample and taking reciprocal of this calculation. There are a lot of factors that affect the surface resistivity of the sample, as they were mentioned in previous parts of the study.

As a summary of the previous parts, when the molarity and amount of deposited sol increases, the conductivity of the film also increases due to the rise in the number of charge carriers. When the Sn doping concentration increases from 5 to 10 mol%, the sheet resistance of the film decreases and shows minima at 10 mol%. This means that conductivity of the same sample shows maxima at 10 mol% Sn doping. At high annealing temperatures until 550 to 600 °C, resistivity of the thin film is low. Hence, the conductivity of the sample is high since at high temperatures, mobility of the charge carriers increases. Finally, thickness which is related to all parameters that were mentioned before, leads to change in conductivity of the film. Higher thickness means a higher number of Sn and In ions, leading to an increase in conductivity.

Reflection is the main mechanism for electromagnetic shielding. The impedance mismatching between the surface of the shielding material (ITO thin film in this case) and incident electromagnetic wave causes reflection loss. For the highly conductive material, reflection loss would be higher as seen from Equation 2.12 [67].

$$RL = 20\log\frac{Z_0}{4Z_{in}} = 39.5 + 10\log\frac{\sigma}{2f\pi\mu}\ \alpha\ \sigma/\mu \qquad \text{(Equation 2.12)}$$

The other mechanism for electromagnetic shielding is transmission loss, and it decreases when the conductivity of the film increases. Therefore, it can be said that conductivity is related to the film's thickness and conductivity increases with increasing film thickness. As seen from Equation 2.13, an increase in thickness decreases the transmission coefficient [68].

$$T = e^{-\gamma d} \qquad \text{(Equation 2.13)}$$

The important thing in a good absorber design is that the incoming wave should be less transmitted and less reflected. In other words, in a multilayered absorber design, the incident wave should enter into the absorber but should not go through the shielded material, so it should be reflected from the back of the absorber. In this way, the incident wave is absorbed efficiently inside the multilayered design.

2.9 Literature Studies about ITO Containing Absorber Designs

ITO coated substrates were studied in different kinds of absorber structures both conventional and metamaterial absorbers with different frequency range by many researchers. K. Chaudhary et al. examined the absorption characteristic of metamaterial absorber which is formed by single layer ITO coating on polyethylene terephthalate (PET) sheets, and the effect of polyvinyl butyral (PVB) surface treatment on ITO in the X-band frequency range (8.2-12.4 GHz). The results come from the free space measurement shows that ITO coatings without PVB layer have 95.94% and ITO coatings with PVB layer have 98.56% EM absorption in 4-16 GHz frequency range [69]. Mi Zhu et al. reported research about the EM shielding characteristic of single layer ITO coating on glass substrate and multilayer ITO coating combined with the antireflection layer in the 2-18 GHz frequency range. The best coating sample in the study has 220 nm coating thickness and 25.6 Ω/sq sheet resistance and shows higher than -1.5 dB reflection loss between the 2-18 GHz frequency range [70].

In the other study, S.S. Kim et al. used the ITO to improve the electromagnetic shielding properties of ferroelectric materials. Ferroelectric ceramic substrates were coated with the ITO film with a sheet resistance of 377 Ω/sq to obtain impedance matching with the free space and hence better absorption value. By controlling the thickness of the ferroelectric substrate and electrical properties of ITO films, reflection loss is decreased to -20 dB and 99% absorption power is achieved between 0.5-18 GHz frequency range [71].

M. Lin et al. also used ITO in their studies and prepared frequency-selective absorber (FSA) design using ITO film which acts as an absorbing layer (100 Ω/sq sheet resistance), substrate named Roger 5880 (Rogers Technologies Corporation, Ltd., Shanghai Branch) and metal back. The structure is designed by placing the ITO layer at the top of the Roger substrate and placing metal back at the bottom of the Roger substrate. In conclusion, the absorber structure shows 80% absorption between the 9.18-11.06 GHz frequency range. T. Li et al. used the ITO in their studies by making

the Salisbury screen as a part of the metamaterial absorber structure and compared the performance of this structure with conventional Salisbury screen. Results show that bandwidth performance and broadband absorption is significantly enhanced between 4.1-17.5 GHz frequency range [72,73].

Literature research shows that ITO is used in electromagnetic shielding structures such as Salisbury screen, Dallenbach layer, metamaterial absorbers. However, to the best of the author's knowledge, there is no work in the literature about cascading ITO resistive sheets to obtain hybrid type EM wave absorbing composite, a combination of Jaumann and graded type absorber. In this study, ITO sols were deposited onto glass fiber woven fabrics by spray pyrolysis technique. The electrical and electromagnetic properties of these resistive glass fiber sheets were controlled by adjusting the amount and molarity of the solutions. Then these surface functionalized fabrics were used as reinforcement in hybrid type EM wave absorbing composite by cascading resistive sheets in the order of increasing conductivity. EM wave absorbing characteristic of each resistive sheet was measured by free space technique which works frequency range of 2-18 GHz.

CHAPTER 3

EXPERIMENTAL PROCEDURE

3.1 Introduction

In this thesis study, indium tin oxide (ITO) coatings were deposited on glass fiber woven fabrics and the electrical conductivity of these conducting oxide coatings were controlled to incorporate electromagnetic (EM) wave absorbing characteristics. With the scope of this aim, ITO sols were prepared by the sol-gel route. After that, homogenous and electrically conductive ITO coatings were deposited on glass fiber woven fabric substrates using the spray pyrolysis method.

At the beginning of the study, preliminary experiments were done to optimize the process parameters such as molarity and the amount of sol, the concentration of dopant, pH, temperature, scanning speed, nozzle to substrate distance. According to the preliminary results, optimum coating parameters were applied to all substrates throughout the study. ITO sols were not only coated on glass fiber woven fabrics, but also coated on soda-lime glass substrates simultaneously using the same parameters to have witness sample for electrical and thickness measurements.

3.2 Materials

Indium (III) nitrate hydrate ($In(NO_3)_3 \cdot H_2O$, 99.9 % Sigma Aldrich) and tin (IV) chloride pentahydrate ($SnCl_4 \cdot 5H_2O$, 98 % Sigma Aldrich) starting chemicals were used as indium and tin sources of the ITO solutions. Acetylacetone ($C_5H_8O_2$, 99 % Sigma Aldrich) and 2-propanol (C_3H_8O, 99.5 % Sigma Aldrich) were selected as solvents for these two precursors, respectively. At the film deposition step, the prepared ITO sols were coated on glass fiber woven fabrics (0/90° oriented, cross plied-EC5/11x2 tex, 0.13 mm C type glass fiber woven fabrics with areal weight 105

g/m^2). In addition, soda-lime-silicate glass slides were also used as a substrate to obtain dummy ITO coatings accompanying the glass fiber woven fabrics coated with ITO where same coating protocols have been applied. The substrates were cleaned with the help of acetone (CH_3COCH_3, 99.5% Merck), ethanol (C_2H_5OH, 96% Sigma Aldrich) and distilled water (DI) during preparation stage prior to coatings. The detailed information about all the used chemicals is summarized in Table 3.1.

Table 3.1. Chemicals used in ITO coatings.

Name of the Chemicals	**Purity**	**Brand Name**	**Chemical Formula**
Indium (III) nitrate hydrate	99.9%	Sigma-Aldrich	$In(NO_3)_3 \cdot H_2O$
Tin (IV)chloride pentahydrate	98%	Sigma-Aldrich	$SnCl_4 \cdot 5H_2O$
Acetylacetone	99%	Sigma-Aldrich	$C_5H_8O_2$
2-Propanol	99.5%	Sigma-Aldrich	C_3H_8O

3.3 Preparation of ITO Coating Sols and Cleaning Procedure of Substrates

Glass fiber woven fabrics were cut as 10×10 cm sized sheets and ultrasonically cleaned with acetone and ethanol for 15 min and then washed with DI water. After each cleaning step, substrates were dried at 70 °C for 30 min in an open air-drying oven. Soda-lime-silicate glass slides (76×26 mm in size) precleaned at the production stage were then used to get witness samples. They were also cleaned according to the same procedure, additionally a pre-cleaning step was performed with a detergent solution.

In order to observe the effect of molarity on structural, electrical and electromagnetic properties, ITO coating sols with different molarity were prepared using the sol-gel technique. The formulations of the sols are listed in Table 3.2. The composition of the sols was adjusted such that In:Sn ratio was 9:1 at% for all sols which corresponds

to 10 mol% Sn. In order to prepare the coating sols, the necessary amount of indium (III) nitrate hydrate ($In(NO_3)_3 \cdot H_2O$) was dissolved in acetylacetone at room temperature (25 °C) and then refluxed at 85 °C for 3 h. In another beaker, proper amount of tin (IV) chloride pentahydrate ($SnCl_4 \cdot H2O$) was dissolved in 2-propanol at room temperature and mixed for 3 h using a magnetic stirrer. After 3 h, tin (Sn) containing solution was added to indium (In) solution under continuous stirring at room temperature and mixed for 30 min. Then, final solution was aged at room temperature for 4 days in open atmosphere within a closed beaker. Figure 3.1 demonstrates the process route of the sol preparation.

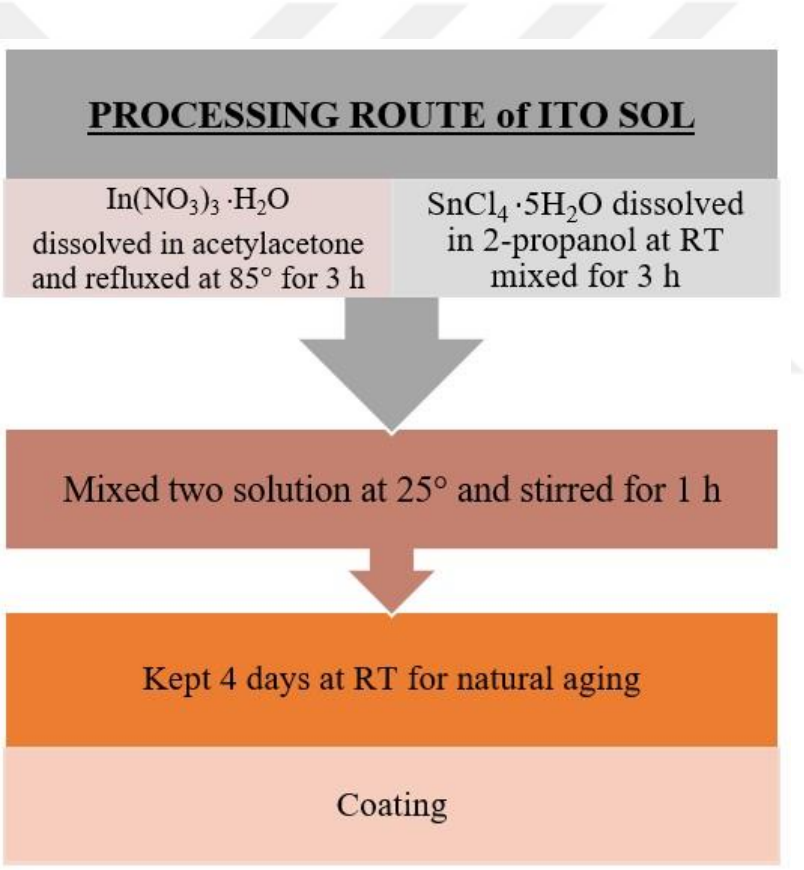

Figure 3.1. Process route of ITO sol preparation.

Table 3.2. Composition of ITO forming sol in terms of amount of precursors used to achieve desired molarity.

Solution Molarity	$In(NO_3)_3 \cdot H_2O$ (g)	Acetylacetone (mL)	$SnCl_4 \cdot 5H_2O$ (g)	2-propanol (mL)
0.1	3	100	0.35	10
0.2	6	100	0.7	10
0.3	9	100	1.05	10

3.4 Deposition of ITO Coating Sols on Glass Fiber Woven Fabric Substrates

ITO sols prepared in different molarities and quantities were deposited on glass fiber woven fabric substrates using the spray pyrolysis technique. All of the coating operations were carried out within the week the sols were prepared since ITO has a shelf life of about a month. Figure 3.2 shows the prepared sols and aged for 4 days, 2 weeks, 1 month and more than 2 months.

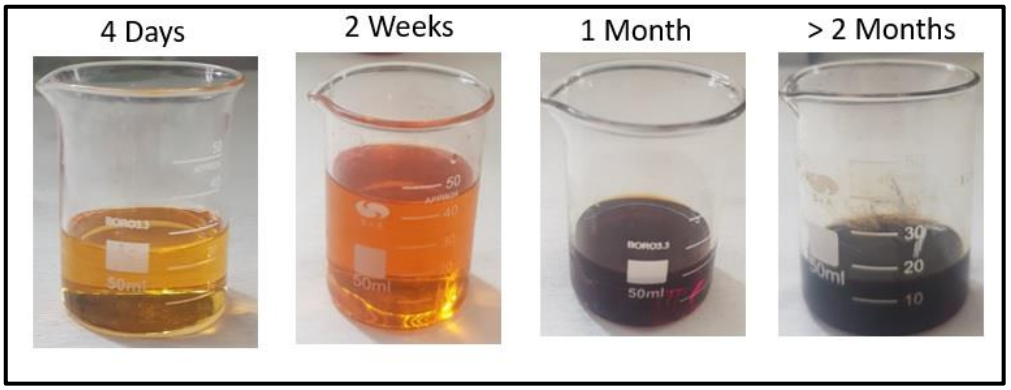

Figure 3.2. ITO sols aged for 4 days, 2 weeks, 1 month and more than 2 months.

Coating operations were done by using Magic brush Airbrush AB-119A with a 0.5 mm tip. Cleaned glass fiber woven fabric and a small piece of the glass substrate as a witness were placed on the hot plate and surface of the substrates heated to 300 °C. Nozzle to substrate distance was adjusted as 8 cm, and spray pressure of the sol was 1.5 bar. Sol was manually sprayed to the substrates, by scanning from left to right to cover the whole sample surface. Then the same procedure was repeated by rotating the substrate by 90° and alternating layers were deposited until the whole coating sol was consumed. Between each subsequent coating operations, there was 2 min waiting period to dry the coating layer on the substrate in the open air. At the end of the coating procedure, a post-heat treatment operation was carried out at 500 °C for 1 h in open air using a chamber furnace (Protherm PLF series 140-160). Figure 3.3 shows an uncoated glass fiber woven fabric along with one coated using 0.2 molar 50 mL and another one coated using 0.2 molar 100 mL ITO sols.

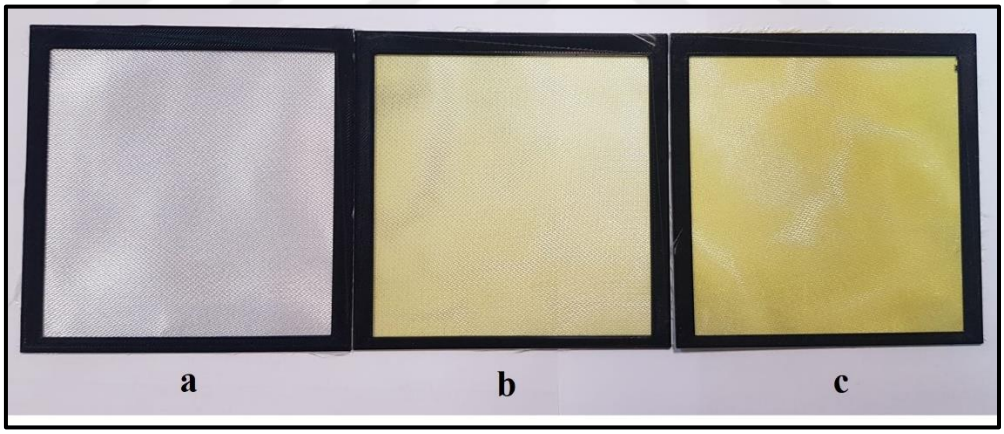

Figure 3.3. Representative image of a) uncoated fabric b) coated fabric with 0.2 M 50 mL ITO sol and c) coated fabric with 0.2 M 100 mL ITO sol.

3.5 Characterization Methods

Characterization of the ITO coating layer on soda-lime glass substrates and glass fiber woven fabrics were conducted in detail in order to evaluate and improve the properties of the processed materials. Scanning electron microscopy or field

emission scanning electron microscopy (SEM or FESEM) is one of the major characterization techniques and it was used to get information about microstructure, morphology, surface topography, chemical composition and thickness of the ITO coatings obtained. X-ray diffraction (XRD) technique was used for phase analysis and to get information about whether the coating layer crystallized or not by the heat treatment applied. In addition to that diffraction pattern of the coatings was used to determine crystallite size and lattice parameter change due to the doping procedure. Together with the two major characterization techniques, to investigate electrical properties of the coating, 4-point probe electrical resistivity set-up was used and sheet resistance values of the deposited ITO coating layers were gauged. Finally, electromagnetic interference (EMI) properties of the ITO coated glass fiber woven fabrics were measured in X-band frequency range using free space set-up which was integrated to vector network analyzer (VNA, Anritsu 37269E).

3.5.1 Scanning Electron Microscopy (SEM)

It is important to get information about morphological and structural feature of the materials processed. For this purpose, ITO coated soda-lime glass slides, and glass fiber woven fabrics were examined using Nova 430 NanoSEM model field emission scanning electron microscope (FESEM). Since substrates are insulators and the ITO coating is semiconductor, to prevent charge buildup, samples were coated with a gold layer about 3 min before the examination. Besides the gold coating, a small amount of silver paste was put at the edge of the samples to get better contact. Then the images were taken at an accelerating voltage of 20 kV and spot size of 3.5 in a high vacuum environment.

SEM images were taken from different areas with varying magnifications according to the purpose of the examination. SEM micrographs can be divided into two major categories: surface and cross-section of the ITO deposited glass substrate and glass fiber woven fabrics. Surface images were taken to examine the morphology of the coating layer as well as, distribution, size and shape of the particles forming the

coating. Cross-sectional images were taken to measure the thickness of the coatings which was then correlated with other properties obtained.

3.5.2 X-Ray Diffraction (XRD)

X-ray diffraction is a non-destructive and very efficient method to identify the characteristic of the materials. This method allows researchers to have information about the state of the material whether it is amorphous or crystalline. In addition, it is possible to determine the phases present in the material, the ratio of these phases, crystallite size, lattice parameters, texture by using the XRD technique.

In this thesis study, the X-ray diffraction technique was used to determine the stable phases present in the material, crystallite sizes and the transition temperature from the amorphous to the crystalline state. Bruker D8 Advance model diffractometer with Cu Kα radiation with a wavelength of 1.54056 Å was used for the analysis. All of the ITO coatings were scanned between 20-70° diffraction angles (2θ) with a scanning rate of 1°/min and a step size of 0.02°. Data obtained from the measurement were analyzed.

3.5.3 Four-Point Probe Resistivity Measurement

The four-point probe is one of the primary techniques to measure the surface resistance of the semiconductor materials. It is a simple setup consisting of 4 thin probes with tungsten tips placed sequentially on the surface at the same distance. Then current is applied through the outer probes and resulting voltage is measured by the inner probes. By this way surface resistivity or sheet resistance (R_s) of the sample can get in the unit of ohm/sq (Ω/□).

Four-point probe was used to get sheet resistance of the ITO coated glass fiber woven substrates. For this purpose, PRO4-4G00 model Signatone brand four-point probe device, Keithley 2100 source meter and SP4-62085TFY model tip were used.

Measurements were taken from 10 different positions of the sample; the average and standard deviation values were calculated accordingly. Finally, average values were used to determine the resistivity of the ITO coatings by multiplying the sheet resistance with the thickness of the coatings measured using SEM.

3.5.4 Electromagnetic Characterization by Free Space Method

Electromagnetic behavior (reflection and transmission) and hereby the absorption characteristics were identified using the home-designed and built free space set-up which is connected to Anritsu 37269E model vector network analyzer (VNA) via coaxial cables. The free space set-up was custom designed and built using fused deposition modelling (FDM) 3D printers, and it is operative in 2-18 GHz frequency range. The network analyzer generates power which is transmitted through coaxial cables and this power waves are transmitted to the surface of the specimen via condensing lenses. At the beginning of the measurements, all critical parameters (focus distance, diameter of the lenses, focal planes) were optimized to produce excellent quality and precise results. Then, reflection and transmission coefficient were taken from VNA in the form of S parameters where S_{11} and S_{22} correspond to reflection coefficients, while S_{12} and S_{21} correspond to transmission coefficients. In this thesis study, even though the results taken from both ports were same, reflection and transmission coefficients were taken from the only port 2, since only one side of the substrate was coated with ITO sol. In addition, geometry of the frames to which coated substrates were attached is more convenient for port 2 measurement. Subsequently, the absorption characteristic of the samples in the X-band frequencies (8-12 GHz) was examined by means of these coefficients. VNA and free space set-up used in this study are shown in Figure 3.4.

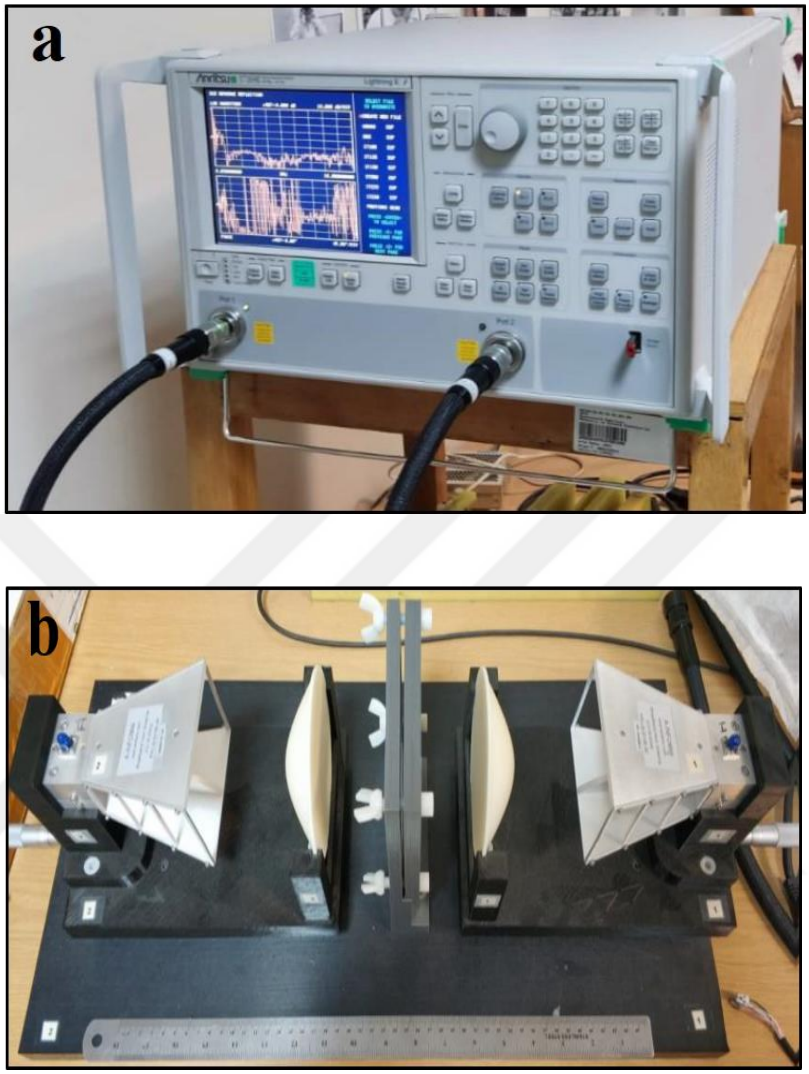

Figure 3.4. a) Custom designed and 3D printed free space set-up b) Anritsu 37269E model VNA.

3.6 Mathematical Simulation for Multilayer EM Wave Absorber Design

In the previous part of the study, glass fiber woven fabrics were functionalized by coating ITO sols onto their surfaces. These surface functionalized fabrics were used as reinforcement of multilayered hybrid version of Jaumann type EM wave absorber, where they have been cascaded within the composite in increasing order of surface conductivity. The single and multilayer structures were examined using free space method to analyze their electromagnetic behavior in 8-12 GHz frequency.

In this part of the study, in order to overcome the difficulties and time-consuming production steps, simulation studies were carried out to determine the best combination of the surface functionalized glass fabric stacking and to develop efficient multilayered hybrid EM wave absorber composite. For this specific purpose, AWR Microwave Office software (AWR Corporation, CA, USA) was used for mathematical simulations. Scattering parameters of single layers of functionalized glass fiber woven fabrics measured by free space method were introduced into the software database, and various combinations of multilayer structure was created by cascading. Finally, multilayer structures simulated to have relatively high EM wave absorption values were built, and their EM characteristics were tested experimentally in 8-12 GHz frequency range.

CHAPTER 4

RESULTS AND DISCUSSION

As mentioned previously, glass fiber woven fabrics were functionalized with varying amounts and concentration of ITO sols by spray pyrolysis technique. ITO coated single layer fabrics were characterized to investigate their microstructural, electrical and electromagnetic properties. In the later stage of the study, these surface functionalized fabrics were used as a reinforcement of multilayered EM wave absorber composite which is a combination of hybrid and graded type absorber approaches (Figure 4.1). In order to avoid the time-consuming step of composite preparation, scattering parameters of single layer structures were measured and introduced to AWR software, and different composite designs with varying surface conductivity and gradients were cascaded by using this program. At the final stage of the study, simulation results were correlated with the experimentally measured properties of the multilayered structures to create guidelines for preparing tailored composite design according to the needs of specific applications.

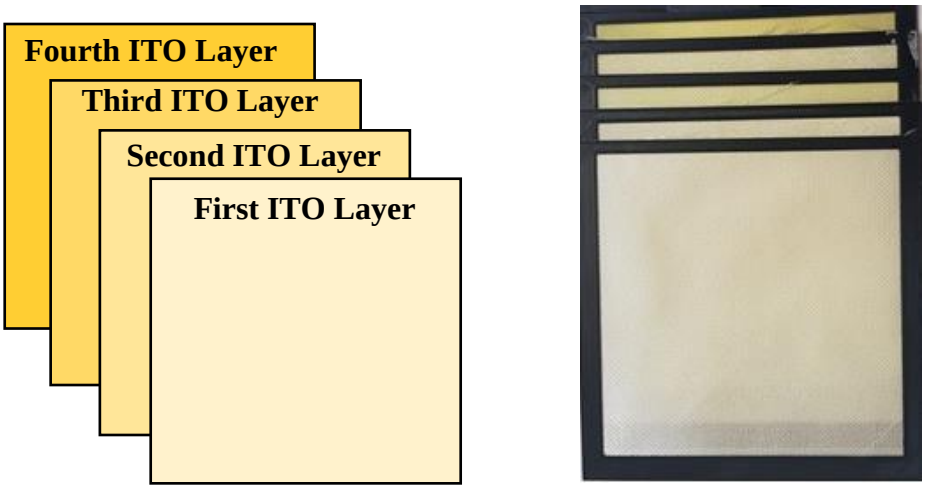

Figure 4.1 Schematic and real image of multilayered EM wave absorber composite representing the design approach of the current study.

4.1 SEM Characterization of the Coatings

Microstructural characterization was carried out on all ITO coated glass fiber woven fabrics by scanning electron microscopy. Since all of the coatings are semiconductors and have medium electrical conductivity, gold plating was applied to the ITO coated surfaces by sputtering technique. In order to observe the change in the grain size and surface morphology, surface examination was carried out. Cross-sectional examination was carried out to investigate the thickness of the coatings. In addition to these, EDS analys were conducted to check the successful doping along with surface mapping to check the homogeneity of the coatings.

4.1.1 Surface Analysis

Surface characterization of ITO coated single layer glass fiber woven fabrics was done using FESEM to observe microstructural properties. Before going into details (grain size and morphology, film thickness), it is important to observe surface of the fabrics globally after deposition of the sols. Figure 4.2 (a) and (b) show the surface images of fiber woven fabrics which have the thinnest and thickest ITO coatings applied, respectively.

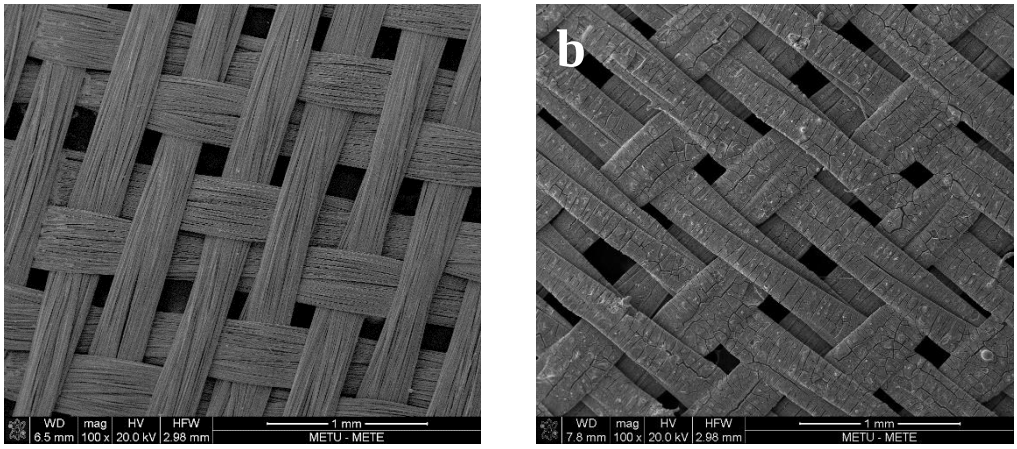

Figure 4.2. SEM images of thinnest and thickest ITO coated fabrics using a) 0.1 Molar 25 mL and b) 0.3 Molar 50 mL sols.

As shown in Figure 4.2, for the thin coating, fiber structure can clearly be seen and ITO coating on the fabric surface is uniform without crack formation. However, for the thicker coatings, the crack formation can be observed and beyond a critical thickness, determined to be ~1.5 μm, ITO coatings partially detach from the surface.

9 different coatings were prepared by two experimental routes: constant molarity with varying amounts of sol (25, 50, 100 mL) and constant amount with varying molarity of sol (0.1, 0.2, 0.3 molar). SEM images were taken to investigate the microstructure and morphology of the films shown in Figure 4.3.

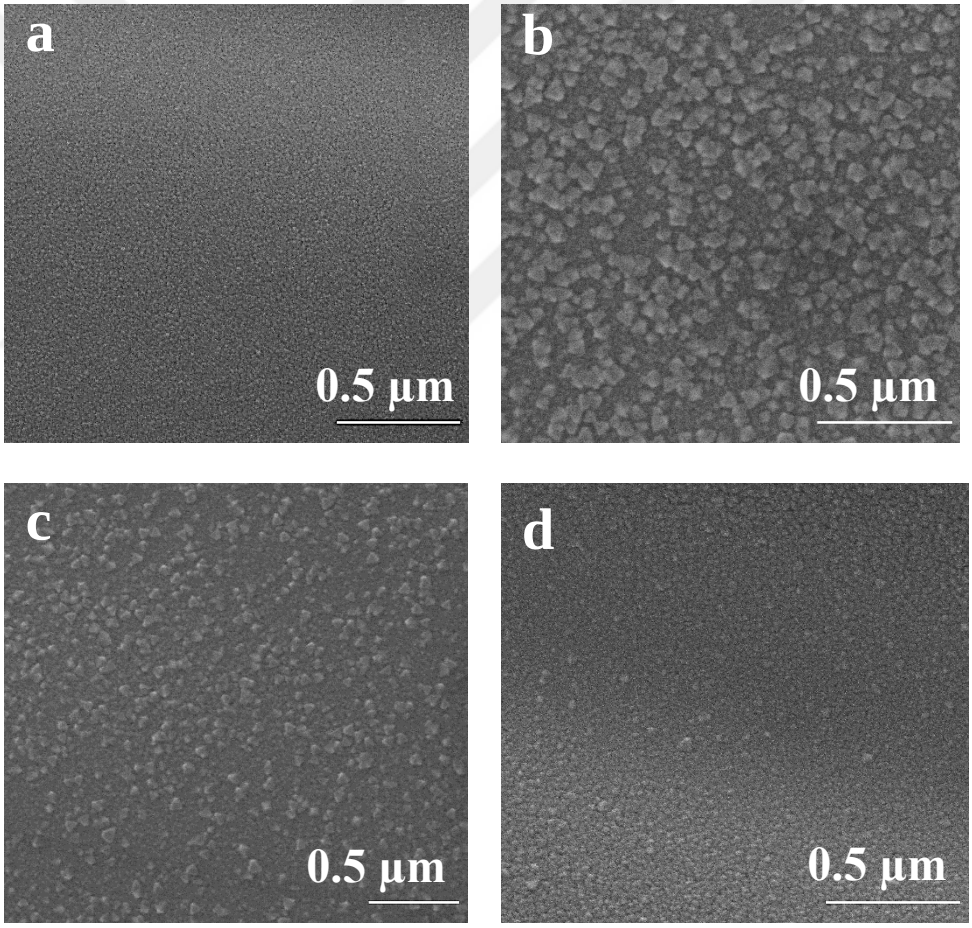

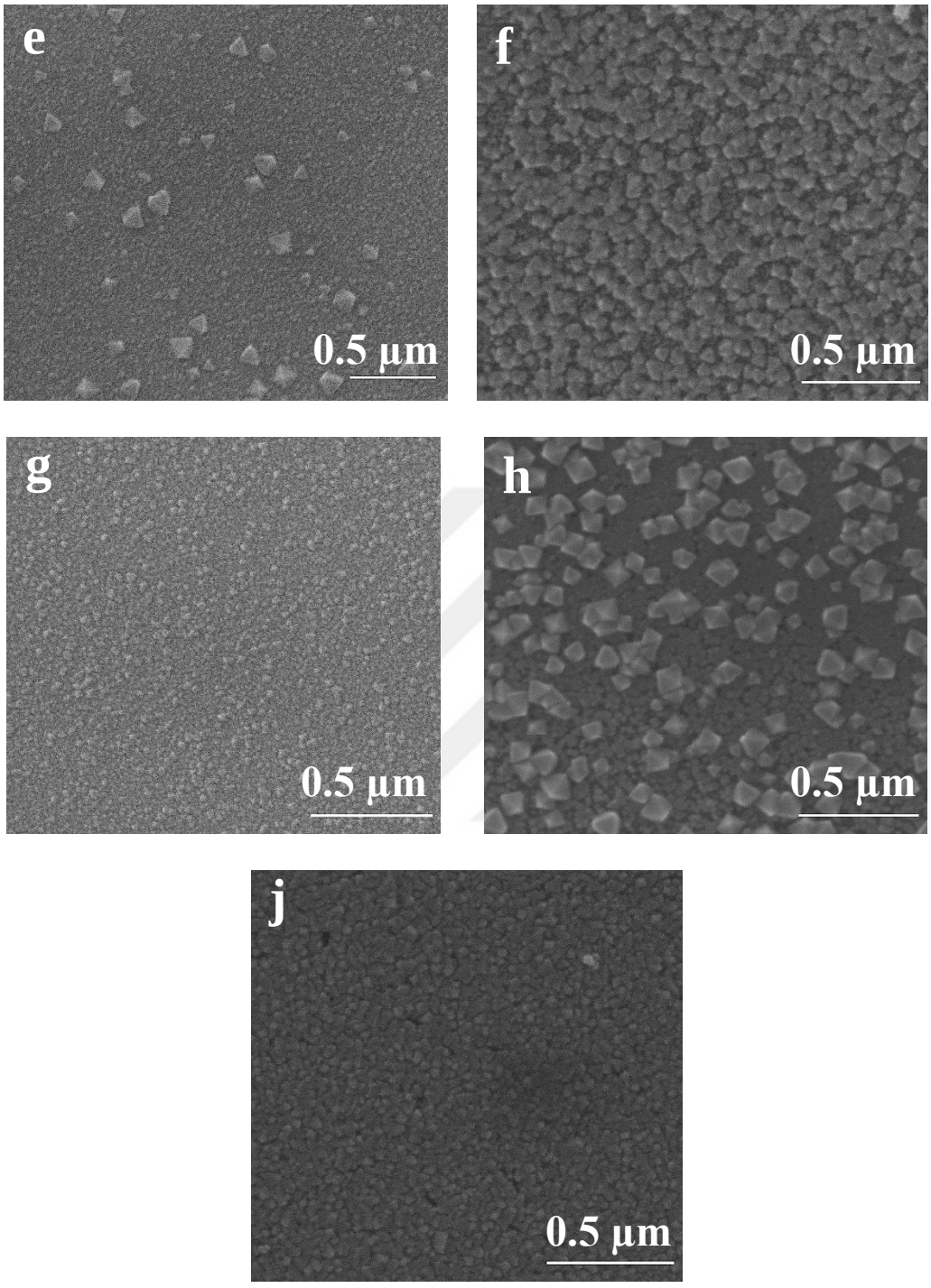

Figure 4.3. SEM images of ITO coated glass fiber fabric surfaces deposited using a), b), c) 0.1 molar 25, 50, 100 mL sol d), e), f) 0.2 molar 25, 50, 100 mL g-j)0.3 molar 25, 50, 100 mL sol respectively.

Microstructural, electrical and electromagnetic properties are directly related with the sol molarity and amount deposited to the substrate since both parameters change the charge carrier concentration on the surface. For both cases, when the amount and concentration of the sol increases, the number of In^{+3} and Sn^{+4} ions also increases in the coating, leading to higher molecular interactions between the atoms.

Variation in the grain size and morphology can be explained by the variation of sol molarity and hence thickness of coatings. As mentioned in Section 2.8.4, active diffusion mechanism changes from bulk to surface diffusion with changing molarity. At lower molarities, nuclei form during coating were homogenous and small. At higher molarity, nuclei grow to bigger sizes with a tetragonal shape [46], which has been confirmed by the SEM images shown in Figure 4.3. When the molarity increases from 0.1 molar to 0.3 molar, for constant amount of sol (for example 50 mL), grain size changes from ~40 nm to ~90 nm (Figure 4.3 (b), (e) and (h)), and grain morphologies change to tetragonal shape. For constant molarity, size of the grains increases with increasing sol amount. As seen from Figure 4.3 (a), (b) and (c), when the amount of sol deposited on the surface increases from 25 to 100 mL at constant molarity, grain size also increases from ~15 nm to ~64 nm. The variation of grain size with respect to these parameters were given in Table 4.1 as a summary of the experimental results regarding the coating microstructure.

Table 4.1. Variation of grain size with respect to molarity and amount of ITO sol.

	0.1 M	**0.2 M**	**0.3 M**
25 mL	14.8 ± 2.9 nm	15.0 ± 4.3 nm	22.5 ± 6.2 nm
50 mL	41.0 ± 25.6 nm	57.3 ± 26.3 nm	89.8 ± 27.5 nm
100 mL	64.0 ± 22.6 nm	81.1 ± 38.9 nm	61.2 ± 21.3 nm

Even though surface images give quite good information about the microstructure, morphology and homogeneity of the films, to be sure about the distribution of In and Sn elements, EDS mapping was carried out on the surface of the thin films. EDS mapping of thin film coated with 0.1 molar 25 mL ITO sol is given as an example in Figure 4.4. The figure shows that film formation is homogenous and the distribution of elements are quite uniform.

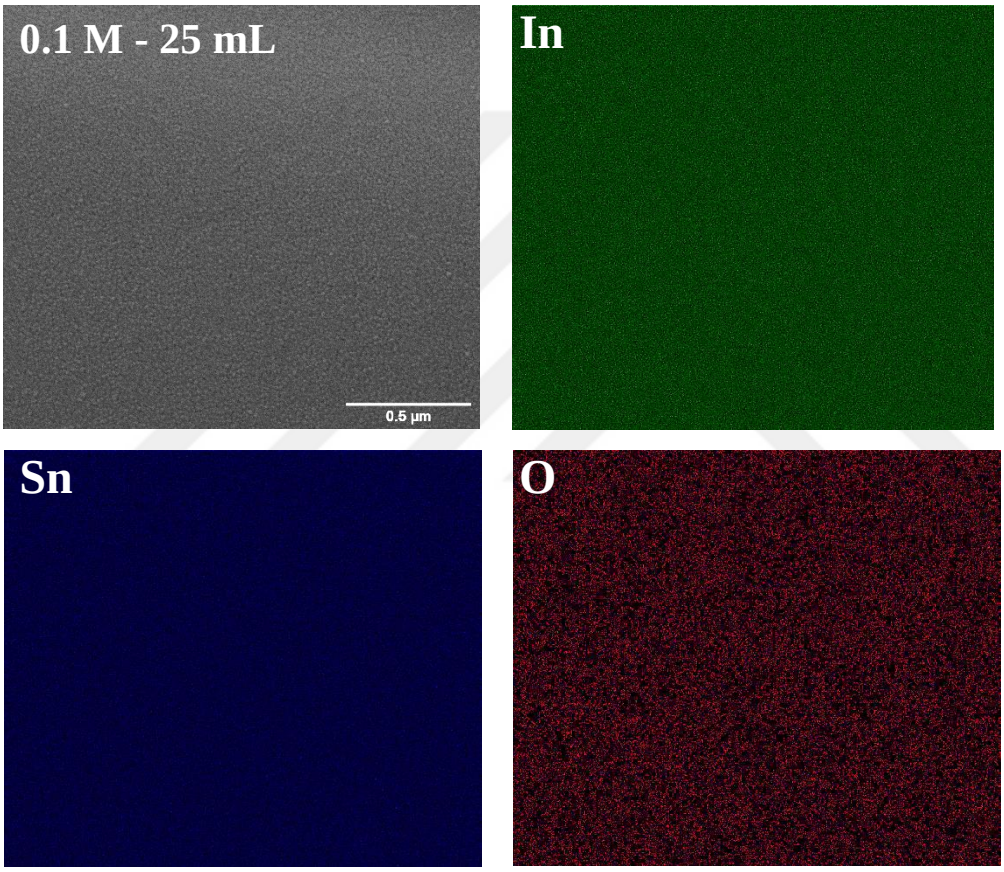

Figure 4.4 EDS mapping of glass fiber woven fabric coated with 0.1 Molar 25 mL ITO sol.

Subsequently, to ensure success of the doping, elemental analysis is carried out by energy-dispersive X-ray spectroscopy (EDS) point analysis on the coatings. The analysis was carried out for each coating at 5 different points, and average values

were taken with standard deviation. Table 4.2 presents the EDS analysis results, where results confirm that doping was successful with In:Sn ratio 9:1 at%.

Table 4.2. EDS analysis results of ITO coated glass fiber woven fabric surfaces.

Point Label	In (at%)	Sn (at%)	In: Sn
1st Point	91.04	8.96	10.16
2nd Point	88.38	11.62	7.61
3rd Point	88.86	11.14	7.97
4th Point	91.1	8.9	10.23
5th Point	90.01	9.99	9.01
Average	89.88 ± 1.11	10.12 ± 1.11	8.99 ± 1.08

4.1.2 Cross Sectional Characterization

Thickness analysis of the coatings were carried out from the cross-section of the witness samples using FESEM. Figure 4.5 indicates change in the coating thickness with respect to molarity and amount of the sol deposited.

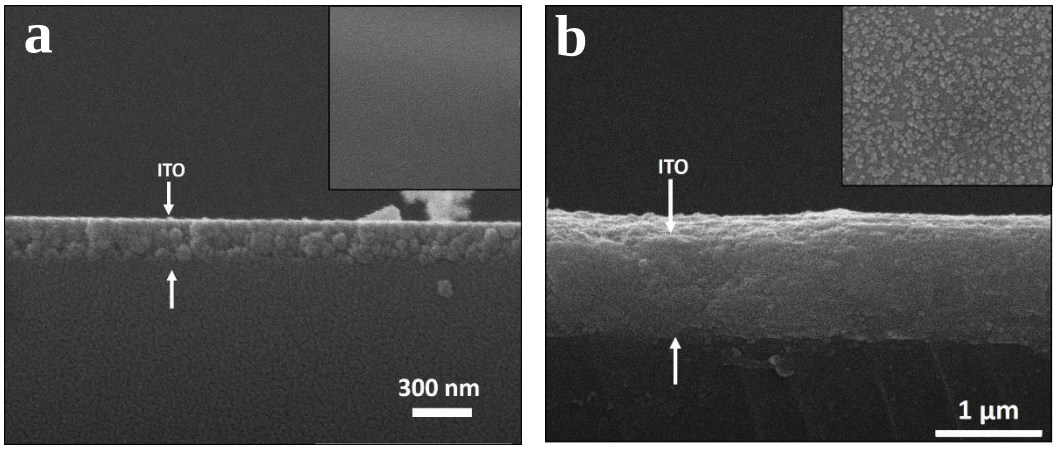

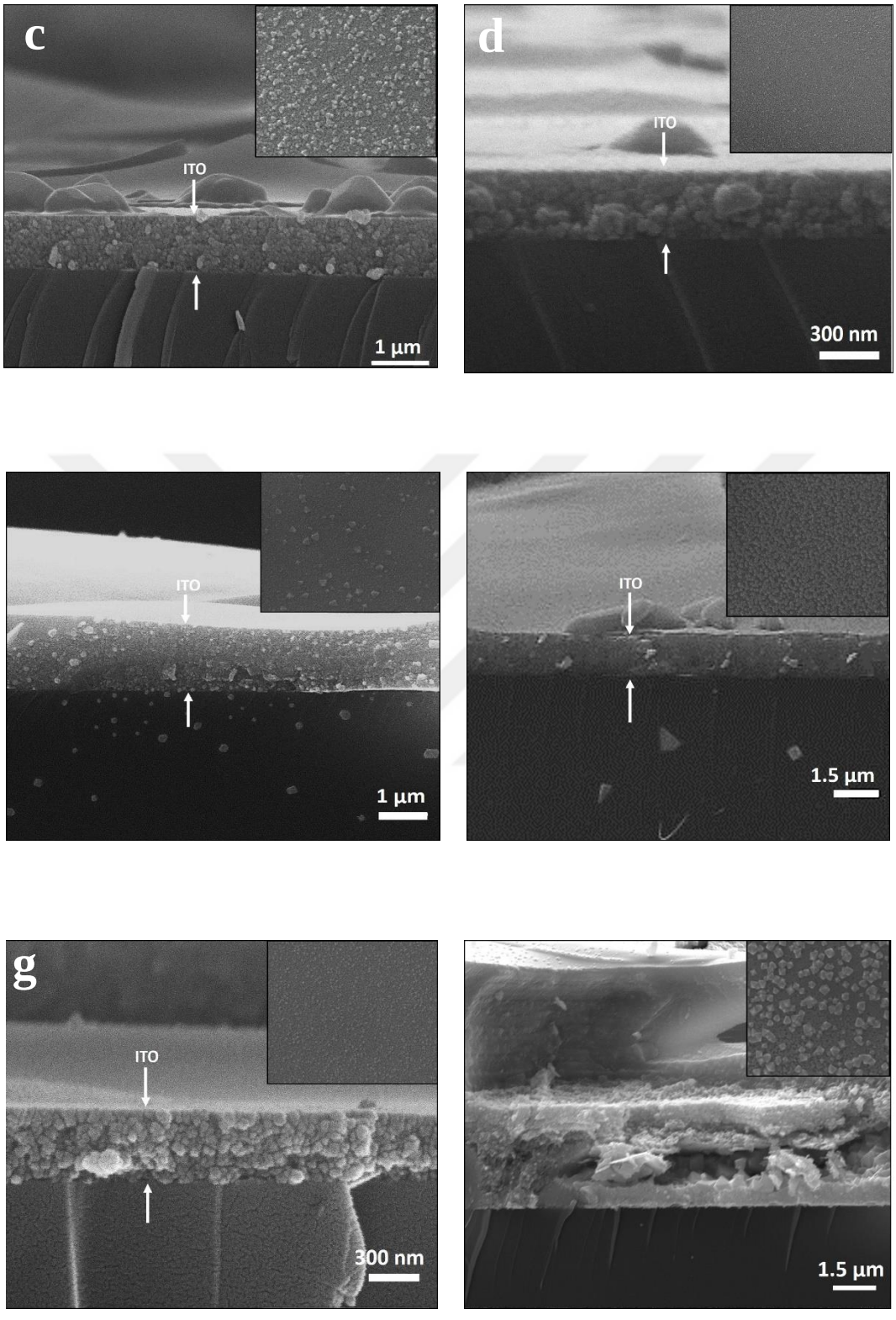
c
ITO
1 µm
d
ITO
300 nm
ITO
1 µm
ITO
1.5 µm
g
ITO
300 nm
1.5 µm

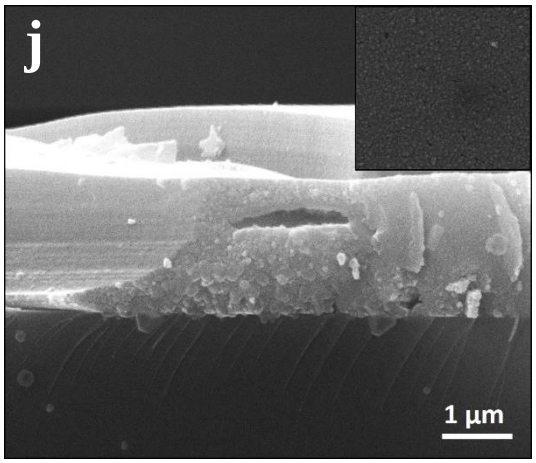

Figure 4.5. Cross sectional SEM images of ITO coatings deposited using a), b), c) 0.1 molar 25, 50, 100 mL d), e), f) 0.2 molar 25, 50, 100 mL g), h), j) 0.3 molar 25, 50, 100 mL sol, respectively.

Figure 4.5 shows that an increase in the molarity and amount of sol deposited on the surfaces, results in an increase in the thickness of the coating. This is because the wetting ability of the coating layer will be higher when the molarity and amount of the sol are higher. A higher number of charge carriers at high molarity and amount is also responsible for this situation.

As seen from Figure 4.5, there is a critical thickness for homogenous and continuous film formation (~1.5 μm) and beyond this thickness, film starts to peel off and detach from the surface. Therefore, even though the thickness of some coatings was measured to be higher than ~1.5 μm locally, the average thicknesses of last two samples (0.3 molar 50 mL and 0.3 molar 100 mL) were taken as 1.5 μm. This situation is not complicating for the electromagnetic measurement part, since chosen measurement method (free space method) is the most proper method for inhomogeneous materials and EM measurements were done on a relatively large sampling area on the material surfaces under consideration. The average thickness values of each coating are summarized in Table 4.3 as an experimental matrix.

Table 4.3. Variation of thickness of the coatings with respect to molarity and amount of ITO sol.

	0.1 M	**0.2 M**	**0.3 M**
25 mL	198 ± 6.5 nm	319 ± 25.2 nm	427 ± 22 nm
50 mL	1230 ± 65.8 nm	1400 ± 89.8 nm	1500 ± 70.2 nm
100 mL	1020 ± 7.07 nm	1550 ± 21.6 nm	1500 ± 23.1 nm

In the study, SEM analyses were carried out to examine microstructural features and to measure the thickness of the ITO coatings applied on glass fiber woven fabrics. SEM results show that grain size changes from ~15 to ~90 nm (Table 4.1), and the thickness of the coatings changes from ~200 nm to ~1.5 μm (Table 4.3) for the thinnest and thickest coatings, respectively. In order to observe a considerable effect of surface and internal features on the electromagnetic properties, the wavelength of the incident wave should be close to surface roughness and grain size of the coatings. In this study, EM properties of the coatings were characterized in 8-12 GHz frequency range which corresponds to wavelengths between 2.49 and 3.74 cm. According to the results obtained, it can be said that surface roughness and grain size have no significant effect on electromagnetic properties of the coatings. This is because the maximum electromagnetic interaction can be observed when the wavelength of the incident wave and the surface or internal features of the material are comparable in size. In this case, interaction between the coatings and the incident waves was not on a topographic or microstructural scale, yet it was in the form of electrical coupling interaction.

4.2 XRD Analyses of the Coatings

The selection of process parameters in the fabrication of ITO coatings is very important to obtain functionalized surfaces with better quality. The effects of some important parameters on the quality of the coatings were mentioned in Section 2.8. Within the scope of this aim, final annealing temperature of the coatings was decided by conducting X-ray diffraction analysis on coatings that were prepared with the same parameters yet annealed at various temperatures. 0.1 molar 100 mL ITO sol coated glass fiber fabrics were annealed at 300, 400, 500 and 600 °C and XRD results of the coatings are shown in Figure 4.6.

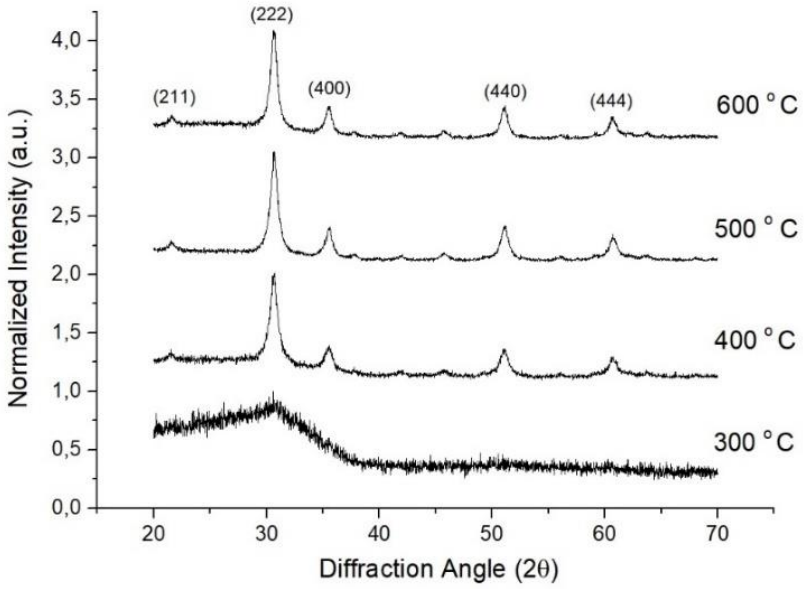

Figure 4.6. XRD pattern of 0.1 molar 100 mL ITO coated glass fiber woven fabrics annealed at various temperature.

The X-ray diffraction analysis results (Figure 4.6) are in accordance with the results found in the literature (Section 2.8.3). At 300 °C, the film remains amorphous, and there was no peak belonging to ITO. Crystallization and densification behavior of the film starts at about 400 °C. However, 400 °C was not enough to complete crystallization of the film and burnout of carbonic compounds were not fully

completed. The optimum firing temperature was decided as 500 °C since at that temperature, burnout of carbonyl compounds complete and densification of the film took place. In addition to that, the peaks belonging to ITO can be clearly observed without noisy background. These situations are also valid for 600 °C, nevertheless, it is not the most proper choice because further increase in annealing temperature results in surface oxidation of grain surfaces and increase in the number of defects in the structure. Besides, at high temperatures, the reduction of SnO_2 to SnO is favorable, which can lead to reduction in the conductivity of the coatings. This conclusion will also be supported by four-point probe analysis results in the following sections. The effect of molarity and amount of sol deposited on the crystallinity of the coatings has been shown with XRD analysis. XRD analyses results of coatings prepared by changing sol amount with constant molarity are given in Figure 4.7, while those of prepared by changing molarity at constant amount of sol are shown in Figure 4.8.

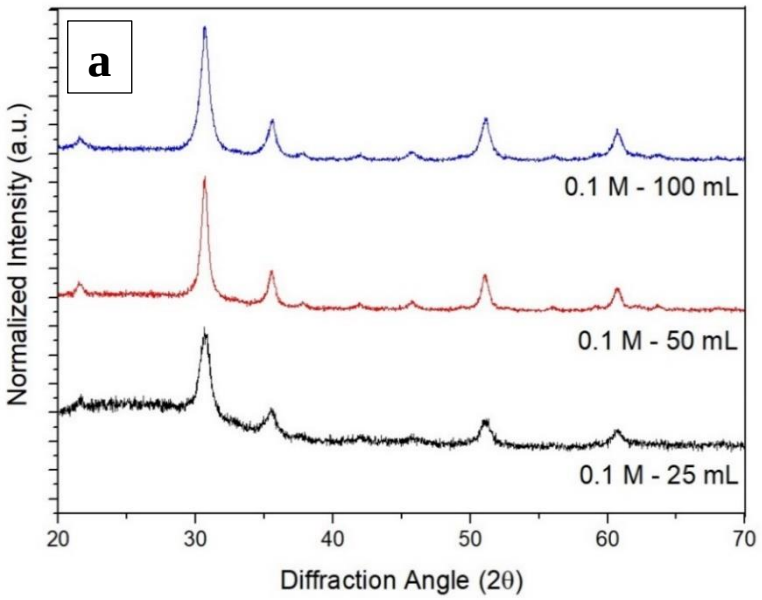

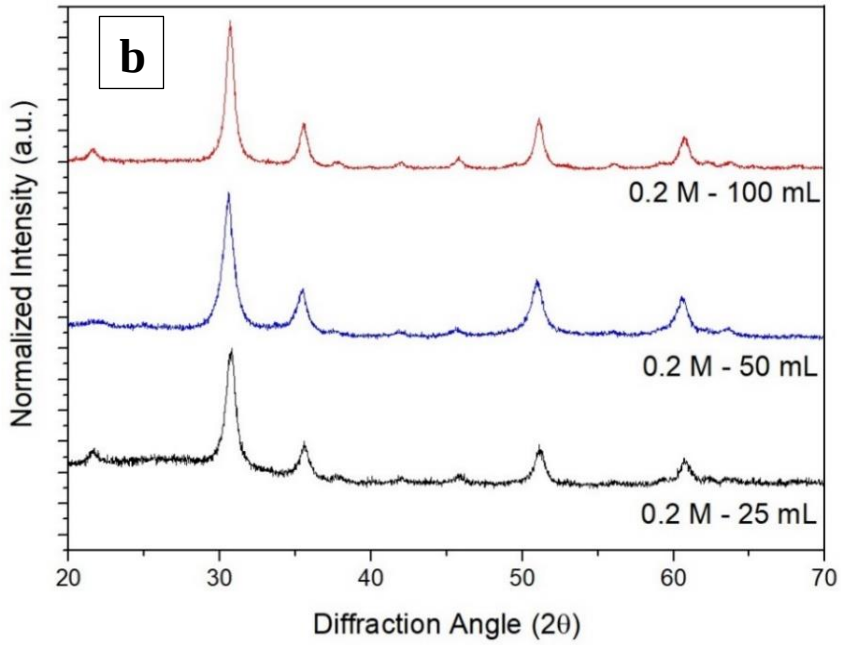

Figure 4.7. XRD patterns of glass fiber woven fabrics ITO coated with varying sol amounts at constant molarity a) 0.1 molar 25, 50, 100 mL ITO sol and b) 0.2 molar 25, 50, 100 mL ITO sol.

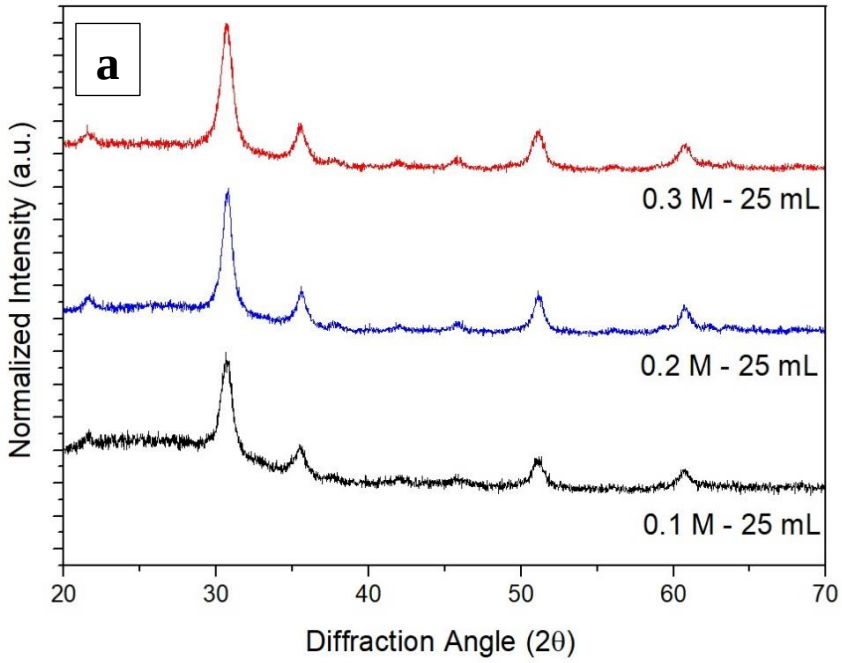

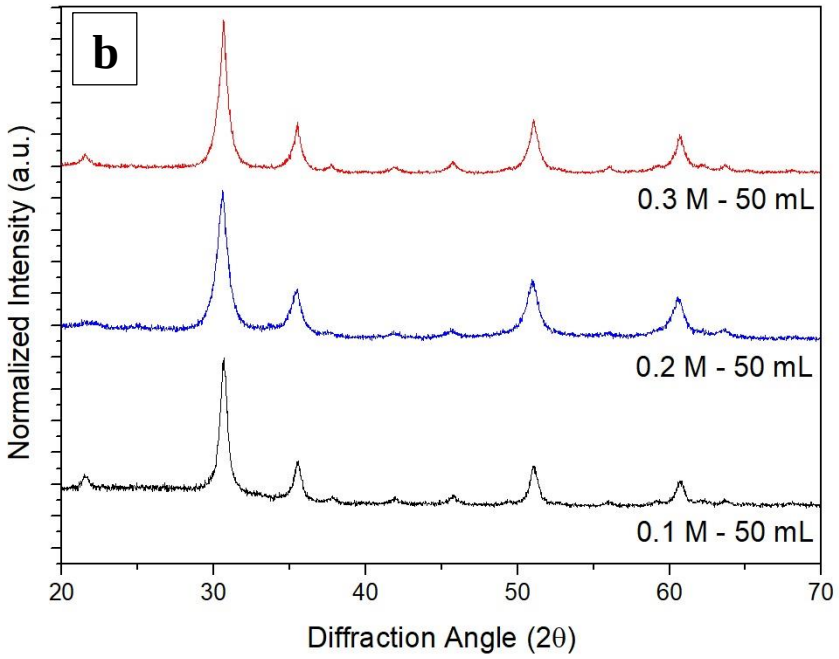

Figure 4.8. Diffraction patterns of glass fiber woven fabrics ITO coated with constant amount of sol having varying molarity a) 25 mL 0.1, 0.2, 0.3 molar ITO sol and b) 50 mL 0.1, 0.2, 0.3 molar ITO sol.

XRD patterns of the fabrics coated by ITO sol show that all coatings have the same cubic bixbyite structure with indium oxide (In_2O_3), which matches with the standard ITO pattern found in the literature. It can be said that there is no other phases and no peaks belonging to tin oxide. With this result the success in the Sn doping has been demonstrated. However, there is a slight difference between peak positions to pure indium oxide. This is due to the atomic size difference of host and doping atoms, where it causes very little change in lattice parameter.

The other point that can be observed from Figure 4.7 is that when the molarity of sol increases, the intensity of the peaks also increases due to the formation of the thicker coatings. For the coating with lower thickness (Figure 4.8 (a)), XRD data are noisy and peaks are broadened, while XRD data of the coating with a higher thickness are smooth, free of noise and sharp (Figure 4.8 (b)). This is always the case when the molarity is kept constant but amount of sol deposited is increased. Besides, when the

amount of sol rises, the number of intermittent drying heat treatments also increases since coating operations were carried out on the hot plate with a few minutes of waiting for drying between each spraying operation.

4.3 Four-Point Probe Analysis of the Coatings

The sheet resistance of the coatings (R_s) was measured using the four-point probe technique. At first, four-point probe analysis was carried out to find out the optimum annealing temperature of the coatings and correlate the results with the X-ray diffraction analysis. For this purpose, sheet resistance of the coated fabric surfaces which were deposited with 0.1 molar 100 mL ITO sol annealed at different temperatures were measured at 5 different points to determine the relationship between the sheet resistance and the annealing temperature. The average values of these measurements are shown in the Figure 4.9.

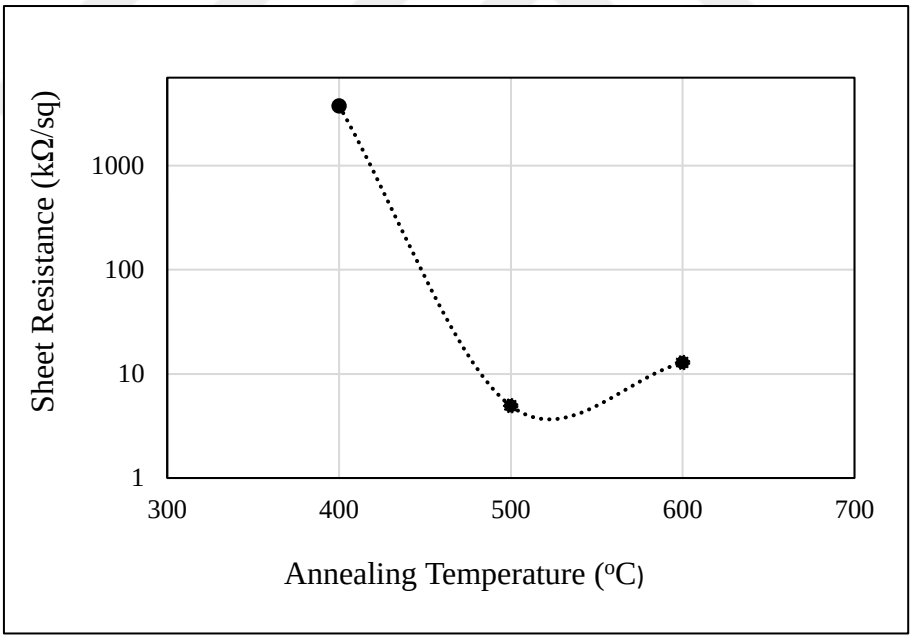

Figure 4.9. Sheet resistance of the ITO coatings with respect to annealing temperature.

Sheet resistance of the coating decreases from ~3000 kΩ/ sq to ~5 kΩ/ sq when annealing temperature increases from 400 °C to 500 °C. Sheet resistance of the

coatings show higher value at lower firing temperatures since their densification and crystallization process is not completed at lower temperatures. On the contrary, at higher temperatures, surface oxidation and hence the number of defects in the structure increases, leading to higher sheet resistance [74]. Consequently, the optimum annealing temperature has been chosen as 500 °C in the current study to obtain minimum sheet resistance with proper grain size.

After determining the optimum annealing temperature, the sheet resistance of 9 ITO coated glass fiber woven fabrics deposited using sols with varying amounts and molarity were measured using the four-point probe technique. 10 measurements were taken at different points on the surface of the coatings and the average and standard deviation of the data were calculated. Obtained average values were multiplied with the thickness of each coating measured using FESEM to determine the resistivity of the coatings. Finally, the electrical conductivity of the coatings was found by taking reciprocal of the resistivity. Table 4.4 shows the average values of the sheet resistance, thicknesses and electrical conductivity of each coating. In Table 4.4, coatings were ordered with increasing conductivity and they were designated with the numbers for easy understanding in the following sections.

Table 4.4. Sheet resistance, thickness and electrical conductivity of ITO coatings on glass fiber woven fabric surfaces.

Sample Designation (#)	Sheet Resistance (kΩ/sq)	Thickness (nm)	Conductivity (S/m)
Uncoated Subs. (# 1)	-	-	0
0.1 M- 25 ml (# 2)	829.10 ± 110.42	198 ± 6.48	6.06
0.2 M- 25 ml (# 3)	59.16 ± 31.94	319 ± 25.2	53.07
0.3 M- 25 ml (# 4)	30.42 ± 17.10	427 ± 22	77.01
0.1 M- 50 ml (# 5)	8.26 ± 1.48	1230 ± 65.8	98.50
0.2 M- 50 ml (# 6)	1.39 ± 0.25	1400 ± 89.8	511.20
0.1 M- 100 ml (# 7)	1.29 ± 0.45	1020 ± 7.07	758.11
0.2 M- 100 ml (# 8)	0.73 ± 0.11	1550 ± 21.6	883.78
0.3 M- 100 ml (# 9)	0.66 ± 0.20	1500 ± 231	1010.1
0.3 M- 50 ml (# 10)	0.63 ± 0.16	1500 ± 70.2	1058.2

The sheet resistance of the coatings is inversely proportional with their thickness, where the thickness of the coatings is directly related with the amount and the molarity of the sol used during their deposition. As seen from the Table 4.4, the sheet resistance of the coatings decreases from ~829 kΩ/sq to ~0.63 kΩ/sq with the thickness increasing from ~200 nm to ~1.5 μm. Conductivity values increase from ~6 S/m to ~1050 S/m with the increasing thickness as expected. However, due to the aforementioned diffusion mechanisms, the relationship between the sheet resistance (conductivity) and the thickness of the coating is not linear [66]. This can clearly be seen from Figure 4.10, where the change in the surface conductivity is shown from that of uncoated fabric (#1) to the one with the thickest coating (#10). In both higher molarity and higher amount of sol conditions, an increase in the number of charge carriers with the increasing thickness is responsible for a decrease in the sheet resistance. In addition, higher thickness corresponds to larger crystallite size and higher density. Due to this phenomenon, electron scattering is lower at the larger crystallite size, and higher mobility of the electrons leads to higher conductivity [75].

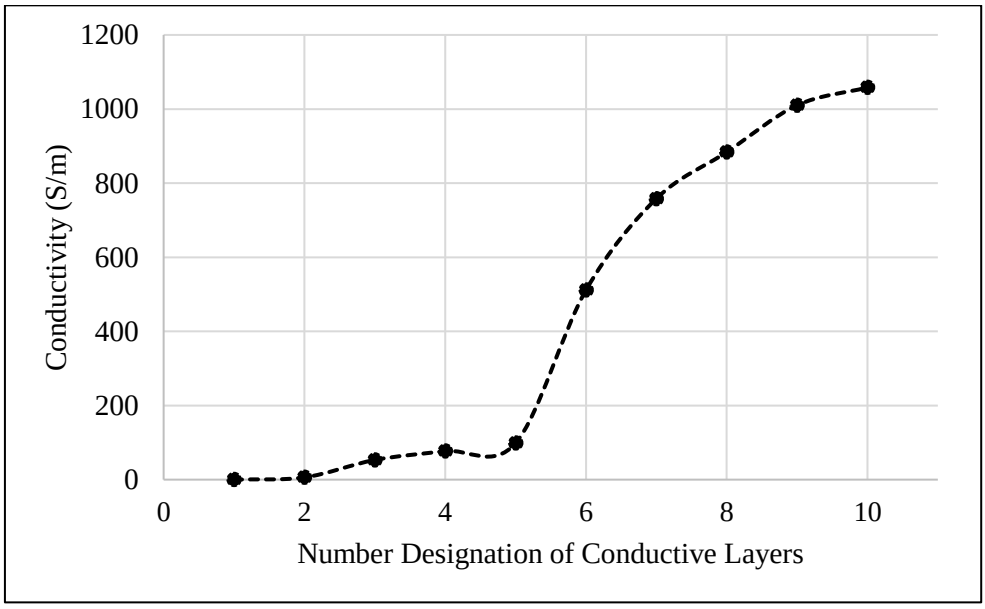

Figure 4.10. Change in conductivity of the coatings with increasing thickness.

4.4 Electromagnetic Characteristic of ITO Surface Functionalized Single Layer Glass Fiber Woven Fabrics

Electromagnetic analysis was conducted on all of the ITO surface functionalized single layer glass fiber woven fabric samples to observe their reflection, transmission, and absorption behavior in the X-band frequency range (8-12 GHz) using a free space set-up that works in 2-18 GHz frequency range. Electromagnetic properties were correlated with the electrical properties of the ITO coatings. Free space set-up measures the reflection and transmission coefficient of the surface conductive sheets in the form of S parameters which are S_{22} and S_{12}, respectively, with the unit of decibel (dB). Reflection (R) and transmission (T) loss in the unit of dB can be expressed as the logarithm of the ratio of reflected power and transmitted power to the incident power, respectively. The multiplication factor of logarithm in the equation becomes 20 since VNA gives the output as voltage not power in this study. Equation 4.1 and 4.2 show reflection (S_{22}) and transmission (S_{12}) loss formulation based on voltage [76,77]. The percent absorption can be defined as the portion of the EM energy neither being reflected nor transmitted as shown in Equation 4.3.

$$R\ (S_{22}) = 20log\frac{V_R}{V_0} \quad \text{(Equation 4.1)}$$

$$T\ (S_{12}) = 20log\frac{V_T}{V_0} \quad \text{(Equation 4.2)}$$

$$\%\ EM\ Wave\ Absorption = 100\ \times\ (1 - \left|{S_{22}}^2\right| - \left|{S_{12}}^2\right|) \quad \text{(Equation 4.3)}$$

One uncoated sheet and 9 ITO coated surface conductive sheets were measured by the free space set-up. Measured reflection and transmission loss values exported from the VNA and absorption percentage calculated using Equations 4.1, 4.2, and

4.3 of the surface functionalized single layer glass fiber woven fabrics with increasing ITO coating thickness from #1 to #10 are presented in Figure 4.11.

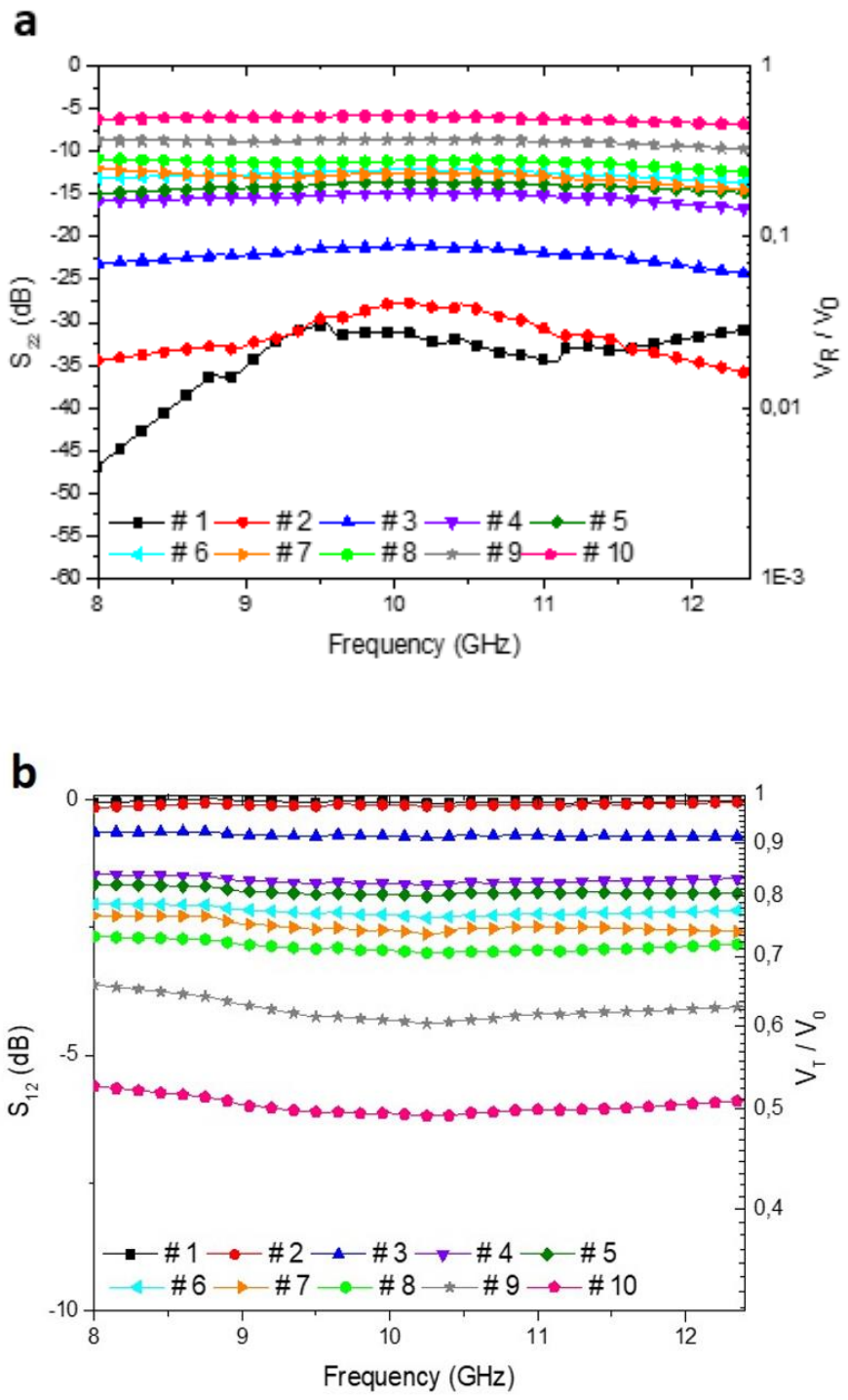

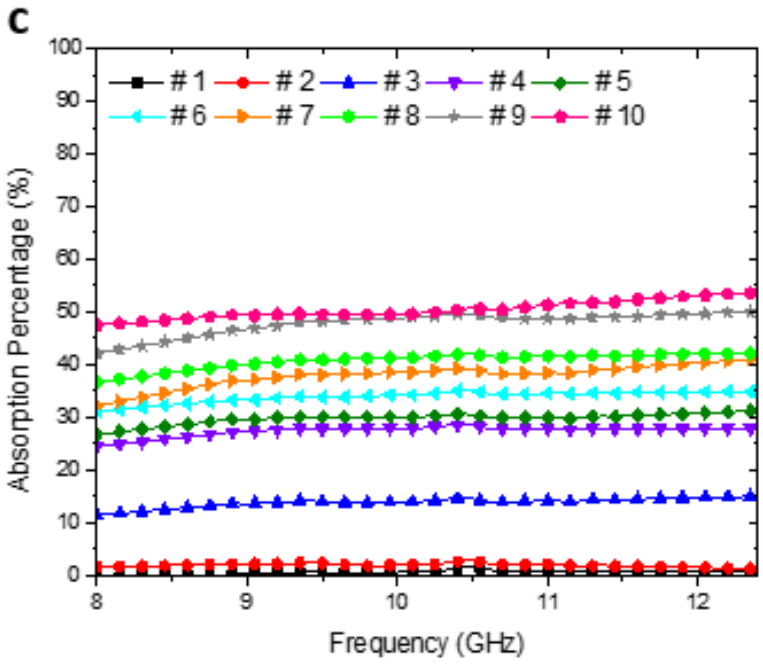

Figure 4.11. EM wave a) Reflection loss, S_{22} b) Transmission loss, S_{12} c) Absorption percentage of uncoated and ITO coated single layer glass fiber woven fabrics in X-band frequency range.

As seen from Figure 4.11, reflection and transmission losses are related to the coating thickness and conductivity. Reflection loss results from the impedance matching between the surface of the shielding material and incident electromagnetic wave. Impedance mismatch would be higher for the fabrics with highly conductive surface leading to higher reflection, and hence higher S_{22} values (closer to 0 dB). Figure 4.11 (a) confirms this situation, where measured reflection loss of the single layer glass fiber woven fabrics changes between ~-7 dB for the fabric with the highest conductivity (# 10) and ~-35 dB for the uncoated fabric (# 1).

Increasing the coating thickness, and hence conductivity, resulted in a reduction in transmission loss, indicating that the conductive coating application suppresses the glass fiber woven fabrics transmissive nature. This is an expected outcome since impedance drop is observed when the film thickness increases. Figure 4.11 (b) shows the transmission loss of ITO coated single layer glass fiber woven fabrics. Measured

transmission loss values change between ~-5 dB for the fabric with the highest surface conductivity (#10) and ~0 dB (almost complete transmission) for the uncoated fabric (#1).

As a consequence of the observed reflection and transmission behavior of the ITO surface modified single layer, fabric with the highest coating thickness corresponding to the highest number of charge carriers and conductivity shows the highest absorption percentages of ~50%. On the contrary, glass fiber woven fabric without coating shows almost no absorption of incident wave.

4.5 Electromagnetic Analysis of the Multilayered Structures by Simulation

At this stage of the study, multilayered and graded EM wave absorbers, which are in a sense hybrid version of Jaumann absorbers were designed by cascading ITO coated glass fiber woven fabrics with increasing order of surface conductivity. In order to overcome the difficulties and time-consuming composite production steps, simulation study was carried out to examine the EM behavior of the multilayered structure as fast as possible by AWR microwave office software. For this purpose, ITO coated glass fiber woven fabrics mentioned before were used as reinforcement of multilayered and graded type EM wave absorber composite.

The aim of the simulation studies is not just to find out the best combination of the conductive sheets by cascading them in increasing order of conductivity but also to make a guideline for specific applications which works in the X-band frequency range according to the EM behavior of the multilayered structures.

In order to simulate EM characteristics of multilayered structures, reflection and transmission properties of each ITO coated fabric has been measured experimentally. These experimentally determined reflection and transmission loss values of the ITO coated single layers taken from the VNA as a scattering parameter (S parameters), were inputted to the AWR software. Then desired multilayered structures were prepared by cascading surface modified single layers with increasing surface

conductivity like a series electrical circuit. The incident electromagnetic wave between 8-12 GHz was sent to the circuit from the initial port and collected from the second port. Finally, reflection and transmission losses of the multilayered structures were taken as an outcome with the dB unit.

Before building desired structure, the consistency of the simulation with the experimental results has been tested by preparing a preliminary multilayer structure by cascading surface conductive fabrics. For this purpose, 4 layered multilayered structure was formed using one uncoated and three coated sheets with 0.1 M 25 mL ITO sol, 0.1 M 50 mL ITO sol and 0.2 M 100 mL ITO sol. Reflection and transmission loss values taken from both simulation and experiment were compared to check the accuracy of the simulation results. It can be seen from Figure 4.12, there is no significant difference between results of experiment and the simulations. Even though, the experimental reflection behavior is a slightly different from the simulated one, the transmission behavior is almost the same for both. So, simulation would be a convenient, easy, and less time-consuming way to test a high number of structures to find the best composite design.

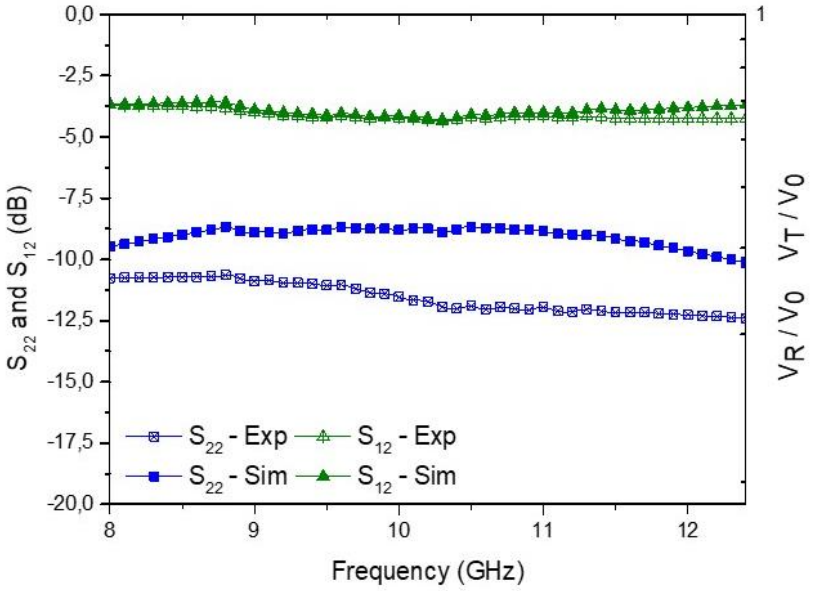

Figure 4.12. Comparison of the experimentally determined and simulated reflection (S_{22}) and transmission (S_{12}) loss data of the preliminary multilayered structure.

After confirming that simulation studies provide similar results to the experimental studies, various multilayered absorber structures were designed and simulated between 8-12 GHz frequency range by cascading 4 and 6 surface conductive glass fiber woven fabrics with different conductivity gradient (rate of change) through the material.

Reflection and transmission response of 3 different multilayered structure composed of 4 ITO coated fabric layers with varying conductivity gradients were simulated between 8-12 GHz. Figure 4.13 (a) presents the conductivity gradient (rate of change) in these multilayered structures through their thickness while Figure 4.13 (b)-(d) shows their simulated EM behavior in the X-band frequency range.

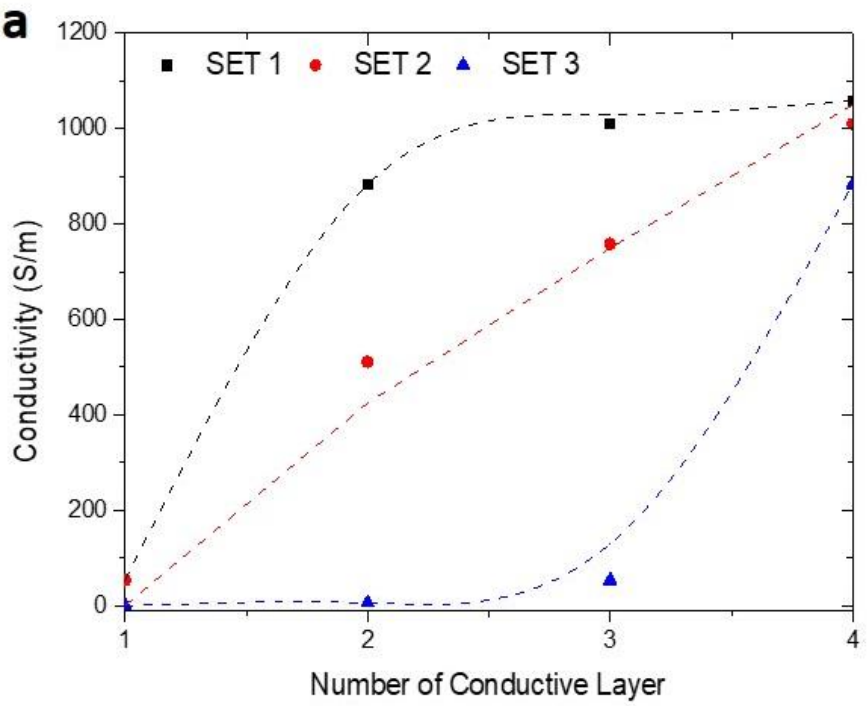

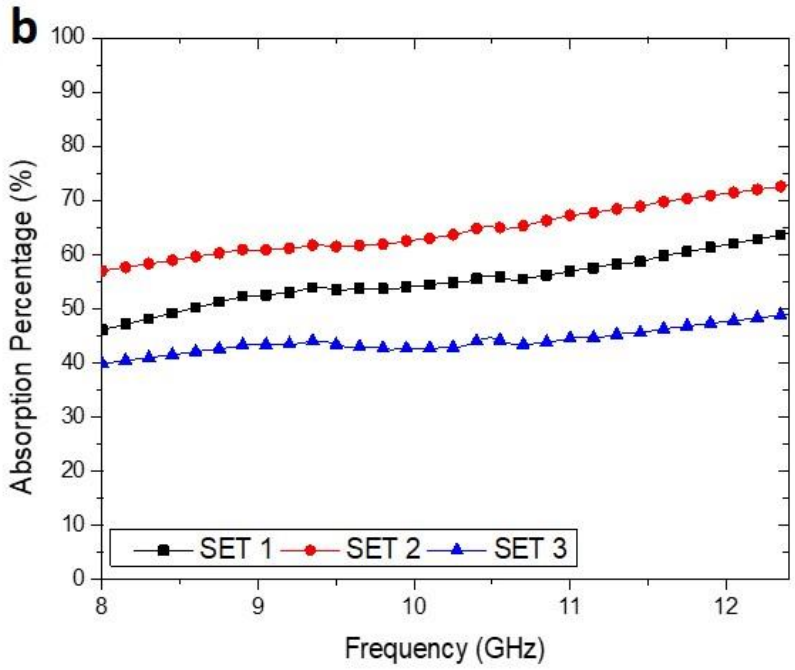
b
Absorption Percentage (%)
100
90
80
70
60
50
40
30
20
10
0
8
9
10
11
12
Frequency (GHz)
SET 1
SET 2
SET 3

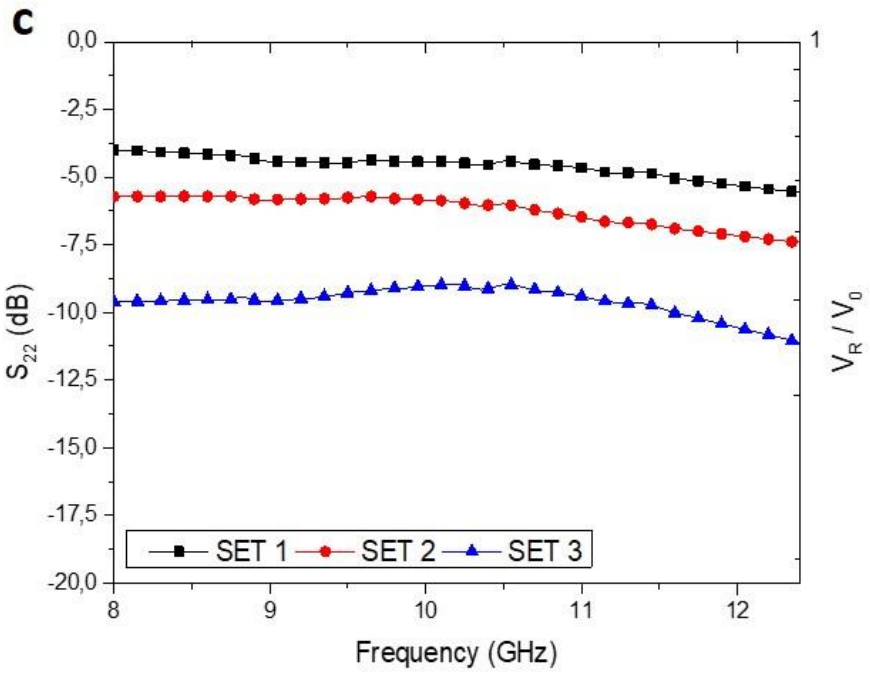
c
0,0
-2,5
-5,0
-7,5
-10,0
-12,5
-15,0
-17,5
-20,0
S22 (dB)
1
VR / V0
8
9
10
11
12
Frequency (GHz)
SET 1
SET 2
SET 3

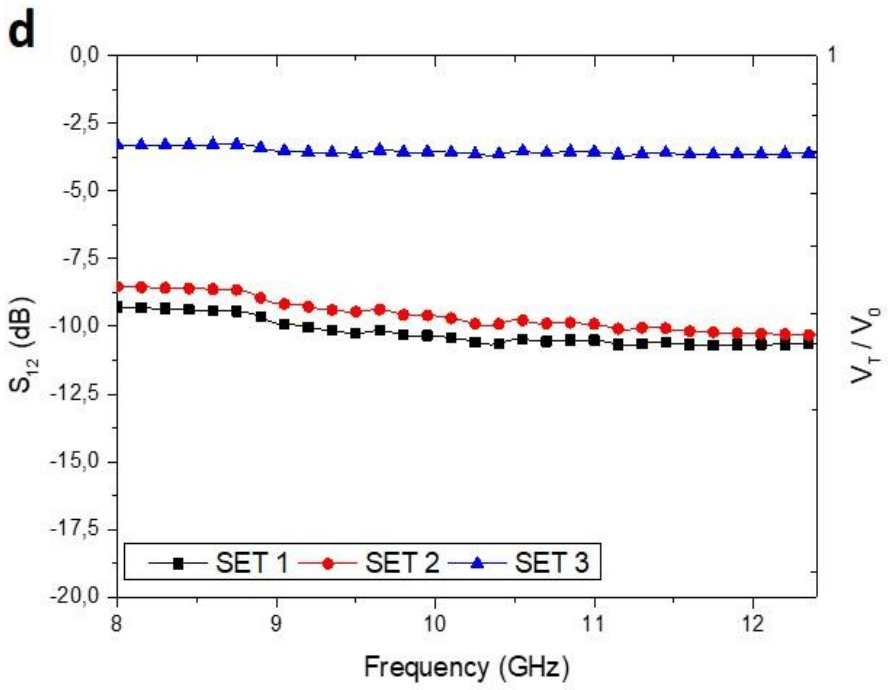

Figure 4.13. (a) Conductivity gradient and (b)-(d) EM characteristics of 4 layered graded type EM wave absorber composites.

The first of these 3 composite combinations, set 1, was designed by placing one low conductivity layer at the front surface and three highly conductive layers at the back with increasing conductivity (Figure 4.13 (a)). On the contrary to set 1, set 3 was designed by placing three low conductivity layers at the front and one higher conductivity layer at the back. Finally, set 2 was designed by placing surface modified layers by a gradually increasing conductivity order from front to back.

Conductivity of the layers and their grading in the structure which forms the composite is an important factor for the EM wave absorption capability. Lower conductivity corresponds to low absorption, while reflection is minimum, and most of the EM wave is transmitted through the material. Set 3 starts and finishes with the layers having lower conductivity value than the others. This is why set 3 has lowest reflection and highest transmission and hence lowest absorption value of ~45%.

The conductivity of the layers that are used in preparation of composite absorbers is not the only factor that affects the EM characteristic, where the structure of the array and the gradient of the conductivities of the layers are also important factors in absorber design. Set 1 and 2 start and finish with surface modified fabrics which have almost same conductivity values. In set 1, highly conductive layers are arranged in back rows while in set 3, low conductivity layers are lined up in the front rows. As a result, set 1 shows the highest reflection loss due to the highly conductive layers and set 3 shows the highest transmission due to low conductivity layers. On the contrary to set 1 and 3, in set 2, two low conductivity layers were placed in the front and two high conductivity layers were placed at the back. The first two layers prevent the reflection of incident the wave and the last two layers prevent the transmission of the wave through the multilayered structure. This type of conductivity gradient makes the multilayered structure keep the wave inside the absorber and ensures absorption. It can be observed from Figure 4.13 (b)-(d) that, the reflection loss and transmission loss of set 2 are in the intermediate level among the other sets, where their balance provides the highest absorption percentage with an average of ~65% in the X-band.

After simulation of 4 layered composite absorber design, 6 layered structures with a similar conductivity gradient were also simulated in the X-band frequency range. Figure 4.14 (a) shows the sets with different conductivity gradients (rate of change) and (b)-(d) shows EM characteristics of these sets.

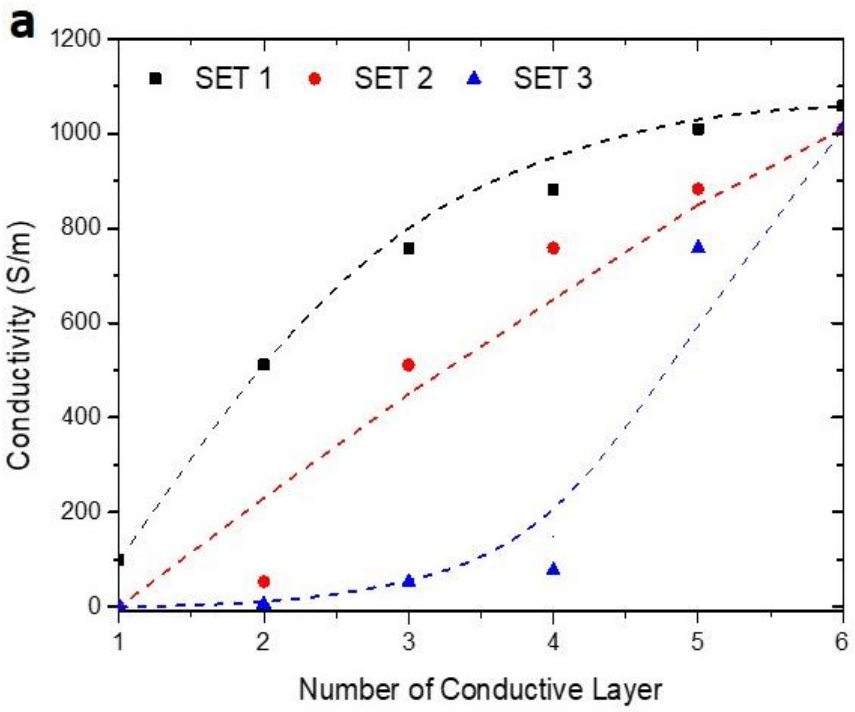
a
SET 1
SET 2
SET 3
Conductivity (S/m)
Number of Conductive Layer
0
200
400
600
800
1000
1200
1
2
3
4
5
6

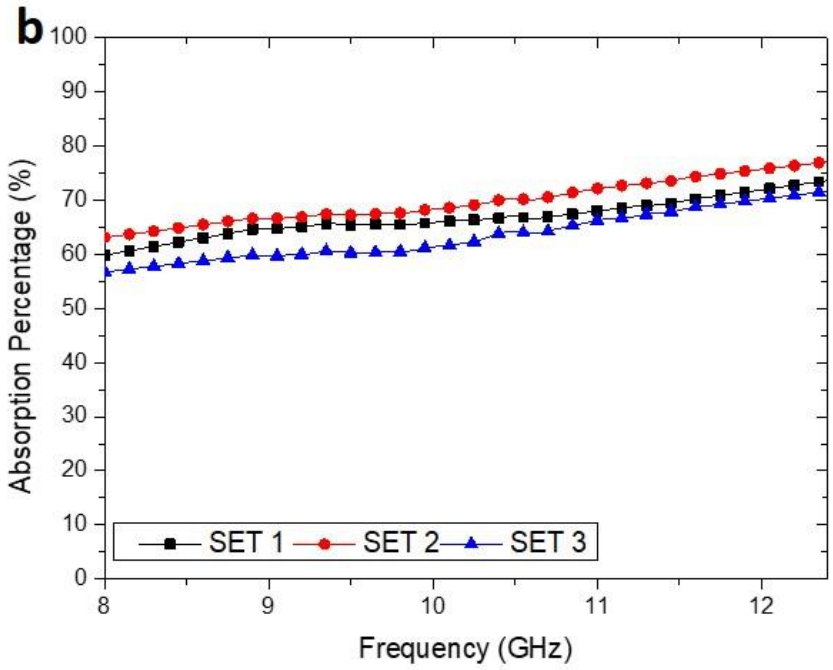
b
Absorption Percentage (%)
Frequency (GHz)
SET 1
SET 2
SET 3
0
10
20
30
40
50
60
70
80
90
100
8
9
10
11
12

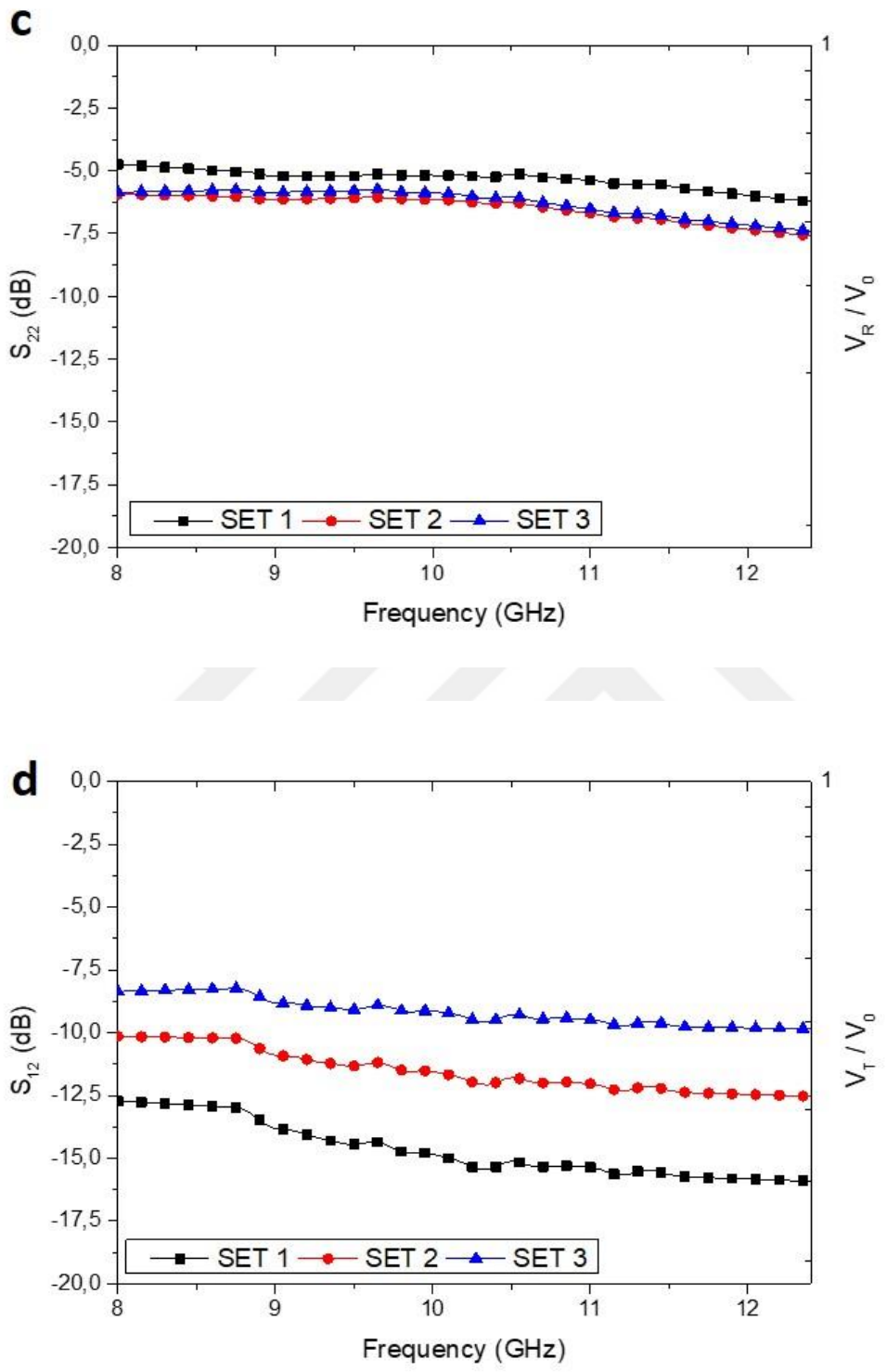

Figure 4.14. (a) Conductivity gradient and (b)-(d) EM wave characteristic of 6 layered graded type EM wave absorber composites.

As seen from Figure 4.14 (a) and (c), reflection loss is directly related to the conductivity of front layer. The reflection loss of set 1 and set 2 is almost the same and lower than that of set 3, since set 3 has a front layer higher in conductivity compared to the other two sets. The change in the transmission loss of sets is consistent with the variation in the conductivity, where higher conductivity layers in a set results in lower transmission loss in the structure. Average transmission loss changes between ~-8 and ~-12.5 dB from set 1 to set 3, respectively. Finally, even though set 3 has layers with the highest conductivity at all positions in the structure, set 2 shows the highest absorption behavior since the lowest conductivity layers at the front provide good impedance matching with the air and transmits the wave to the interior for absorption. Furthermore, highly conductive layers placed at the back provide more internal reflection of the EM wave and block transmittance of the wave through the protected material.

Figure 4.14 (b) shows that 6 layered structures with different conductivity gradients have similar absorption percentages changing between ~55 and 70%, although their reflection and transmission loss values are different from each other. Therefore, according to the need of a specific application, if reflection loss is important and should be high, slowly increasing conductivity gradient similar to that of set 3 will be the appropriate choice. On the other hand, if the transmission loss of the multilayered structure should be minimized with a certain amount of absorption, then a multilayered structure design with a rapidly increasing conductivity gradient similar to that of set 1 should be selected. For applications where the thickness of the structure is a limitation, 4 layered graded absorber design with a gradually increasing conductivity, similar to that of set 2 in Figure 4.13 (a), could be selected for balanced reflection and transmission loss along with a high level of absorption.

4.6 Comparison of the Experimentally Measured Electromagnetic Properties of Multilayered Structures by Simulation Results

In this part of the study, 4 and 6 layered graded type absorber designs revealing the highest simulated absorption values were constructed experimentally, and their EM characteristics have been measured and compared with the simulation results. Best composite designs were compared for the validation of the study. For this comparison set 2 of both 4 and 6 layered structures (Figure 4.13 (a) and Figure 4.14 (a), respectively) having a gradually increasing conductivity gradient were used. The electromagnetic characterization results 4 layered set 2 (Figure 4.15 (a) and (b)) and 6 layered set 2 (Figure 4.15 (c) and (d)) are presented in Figure 4.15 as a function of frequency in terms of reflection loss, transmission loss and absorption percentage.

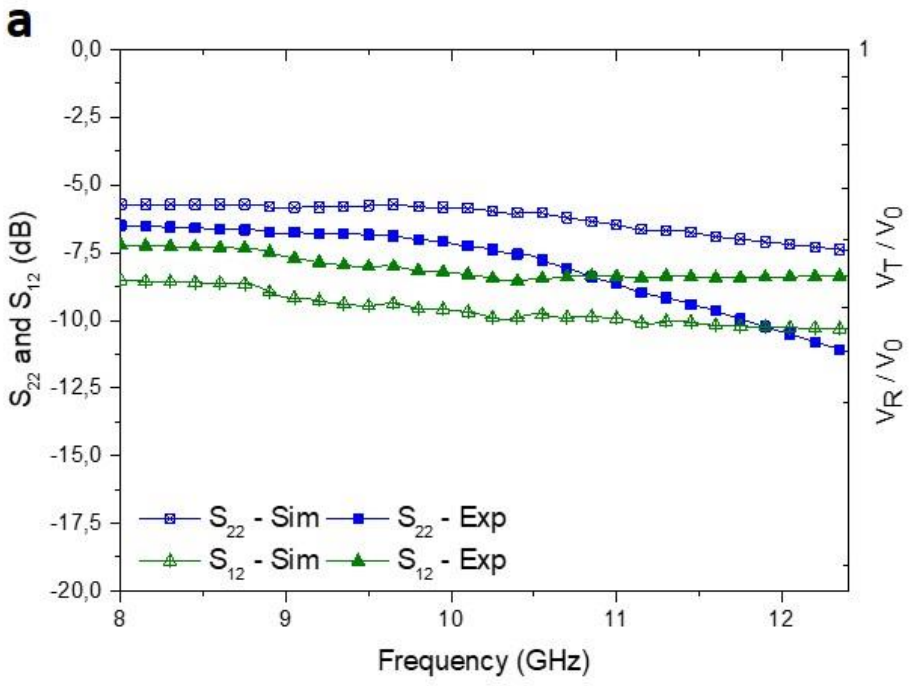

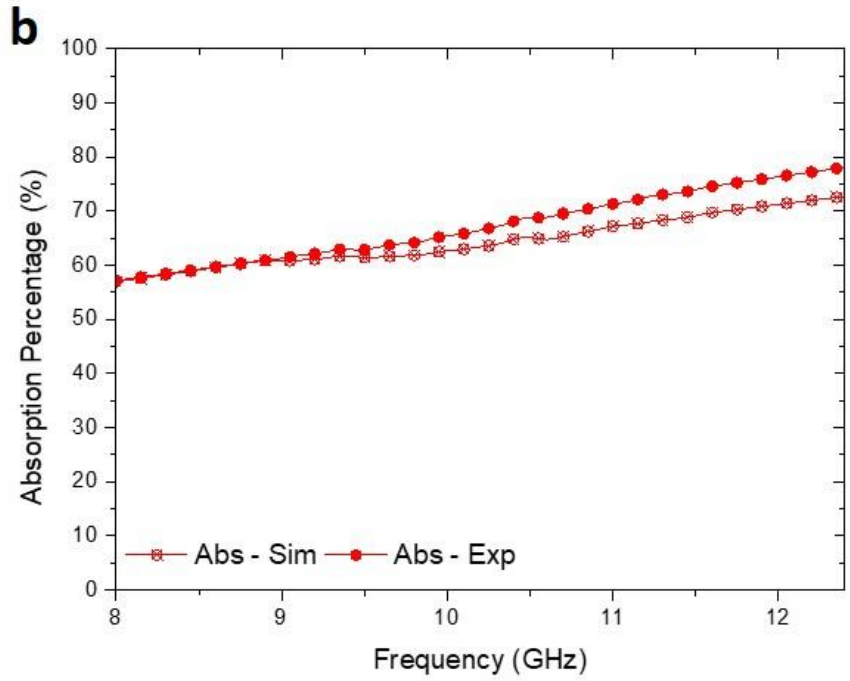
b
Absorption Percentage (%)
Frequency (GHz)
Abs - Sim
Abs - Exp

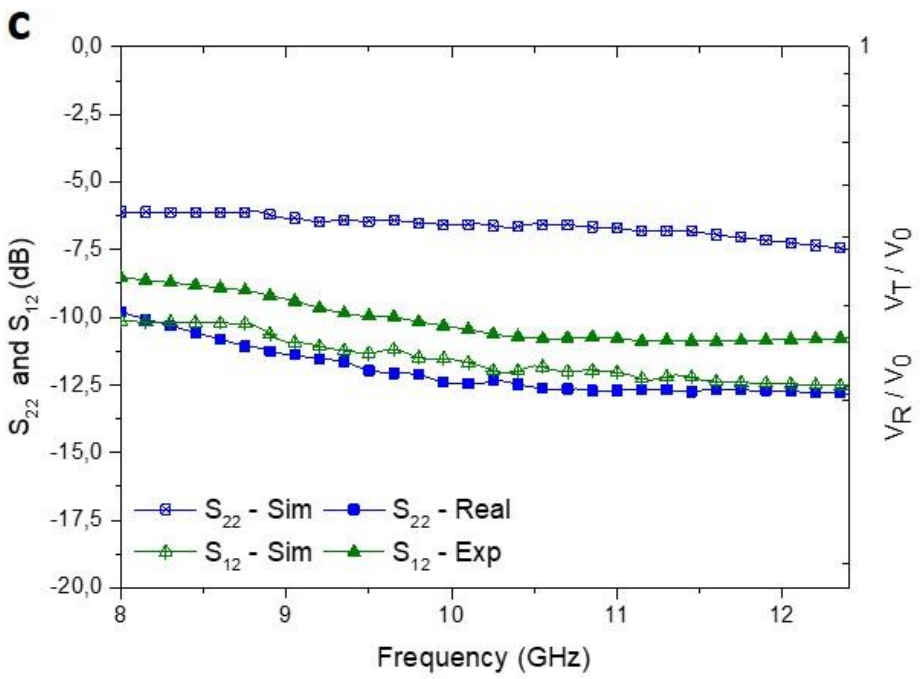
c
S22 and S12 (dB)
VR / V0
VT / V0
Frequency (GHz)
S22 - Sim
S22 - Real
S12 - Sim
S12 - Exp

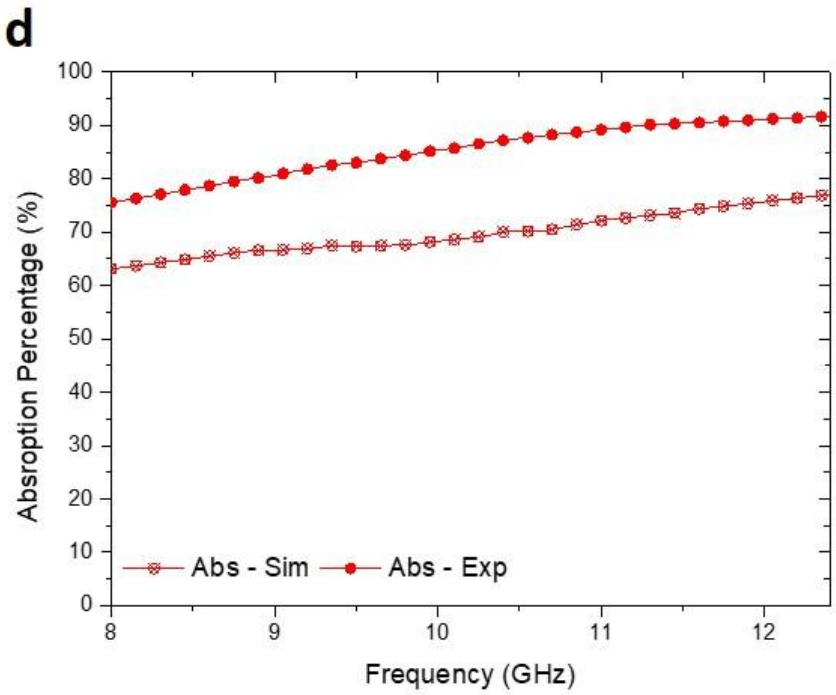

Figure 4.15. Comparison of the experimentally measured and simulated electromagnetic behavior of a), b) set 2 of 4 layered structure and c), d) set 2 of 6 layered structure.

It can be seen from the Figure 4.15, that transmission loss values measured experimentally and simulated by the AWR software are very close to each other for both composite designs. The amount of transmission of the incident wave through the 4 layered composite design is slightly higher than that of the 6 layered one due to the lower number of conductive layers used in the design. Measured and simulated transmission loss values of the 4 layered composite design similar at lower frequencies in the X-band. Average measured and simulated transmission loss of the 4 layered composite design is ~-7.5 dB and by simulation is ~-8.5 dB in the X-band range, respectively. Similar tendency is also valid for the transmission loss of the 6 layered composite design, where average measured and simulated transmission loss of the 6 layered composite design is ~-8.5 dB and ~-10 dB in the X-band range, respectively.

In addition, there is a slight difference between the measured and simulated reflection loss values. The difference is higher when the number of layers in the multilayered design is higher. In the simulation set-up, multilayer structures only composed of modified fabrics were designed and measured for ideal conditions, and the air gaps sandwiched between the layers were not considered. However, during the experimental measurement, the multilayer structure is composed of the surface modified fabrics and air gaps in between them. In addition to this, in the AWR simulations, multilayer structure is constructed in the form of an electrical circuit composed of properly arranged surface modified single layers, where multiple reflections were not considered by the simulation set-up. In addition, the software was not considering the human related experimental errors, geometrical errors and errors caused by the nature of the free space set-up. Slightly different configurations of layers with millimetric deviations are possible sources of the experimental error which may have resulted in unanticipated destructive or constructive interferences of the EM waves. However, these type of potential errors in the simulation results are not problematic for this study, since simulation studies were carried out preliminarily to guide experimental studies in order to avoid time consuming composite production in selecting the most appropriate cascading combinations. At the end of the simulation studies, it was also observed that experimental and simulated results follow same trends, and there were no irrational results.

The complication explained above also results in a difference between the experimentally determined and simulated absorption percentages. Experimental and simulated absorption percentages follow a similar trend with matching values for the 4 layered structure from 8 to 12 GHz. As seen from Figure 4.15 (b), for four layered design, the absorption percentage is changing between ~55% and ~75% in the x-band. In the case of 6 layered structures (Figure 4.15 (d)), ~10-15% difference is present between the experimentally determined and simulated absorption percentages. Experimental absorption percentage is ~75% at lower frequencies and more than 90% at higher frequencies, while the simulated one changes between ~65% and ~75% in the X-band.

4.7 Electromagnetic Properties of the Multilayered Structures with Metal Backing

In actual case, Jaumann type composite is formed by cascading resistive layers with increasing order of resistivity on a perfectly conductive metal sheet. In order to see the effect of metallic backing on EM wave absorbing characteristic of the designed multilayered structure similar to the Jaumann configuration, a perfectly conductive metallic sheet was placed at the back of the 4 composite designs discussed in previous sections and electromagnetic properties of this construction has been measured by the free space set-up in 8-12 GHz frequency range. Since there is no transmission of the incident wave through the measured material, Figure 4.16 present the reflection loss and corresponding absorption percentage of 4 layered structure with metallic back in X-band frequency range.

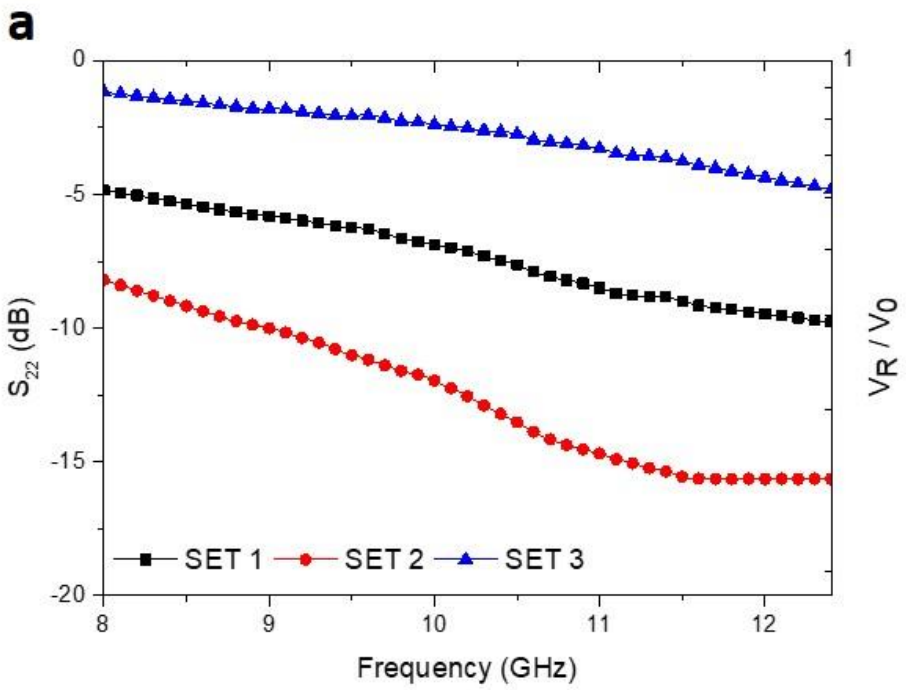

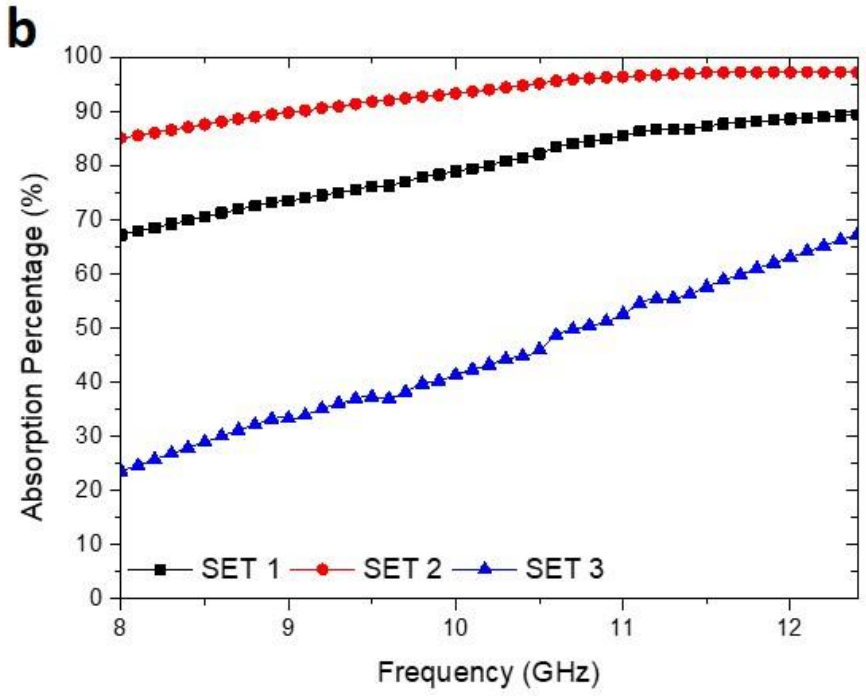

Figure 4.16. EM wave characteristic of the 4 layered graded structure with metallic backing similar to the Jaumann configuration; a) Reflection loss (S_{22}) and b) Absorption percentage

In the previous case (multilayered structure without metallic back), set 1 has the highest reflection loss (S_{22}) due to the highly conductive layer at the front of the structure. However, in this case, set 3 shows the highest reflection loss value since it is composed of low conductivity layers placed frontmost. This means that, set 3 composite design accepts higher amount of the incident waves coming from the input port and transmits into the structure. The incident wave transmitted through the multilayered structure is reflected back from the metallic backing and collected by the same port again. During this process, waves which are reflected from the metallic plate interact with the incident waves destructively and constructively and remaining amount of the EM waves are collected back. Consequently, set 3 has the highest reflection loss, and hence lowest the absorption percentage due to low conductivity layers in its structure. The absorption percentage starts at about 25% at low frequencies and increases with the frequency reaching to ~65% at 12 GHz.

As determined in the previous section, set 2 is again the most promising structure with respect to reflection loss and absorption percentage values among the multilayered structures with a metallic backing. Set 2 shows the lowest reflection loss and highest absorption percentage. The reflection loss value of the 4 layered structure starts ~-7.5 dB at 8 GHz and decreases with increasing frequency. Finally, it reaches to approximately – 17 dB when the frequency is 12 GHz. Due to the decrease in the reflection loss at higher frequencies, absorption percentage would be higher at higher frequencies. As seen from Figure 4.16 (b), the absorption percentage of set 2 changes between ~85% and ~98% in the X-band.

After 4 layered composite designs, EM properties of the metallic backing containing 6 layered structures were also characterized in the X-band frequencies by free space measurement set-up, and Figure 4.17 shows the results of the measurements.

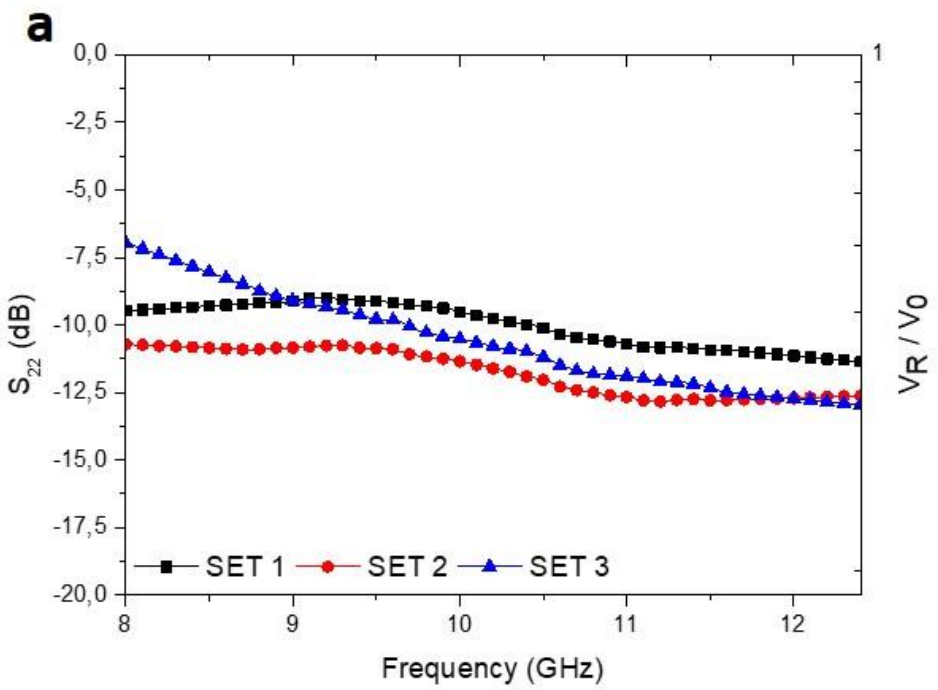

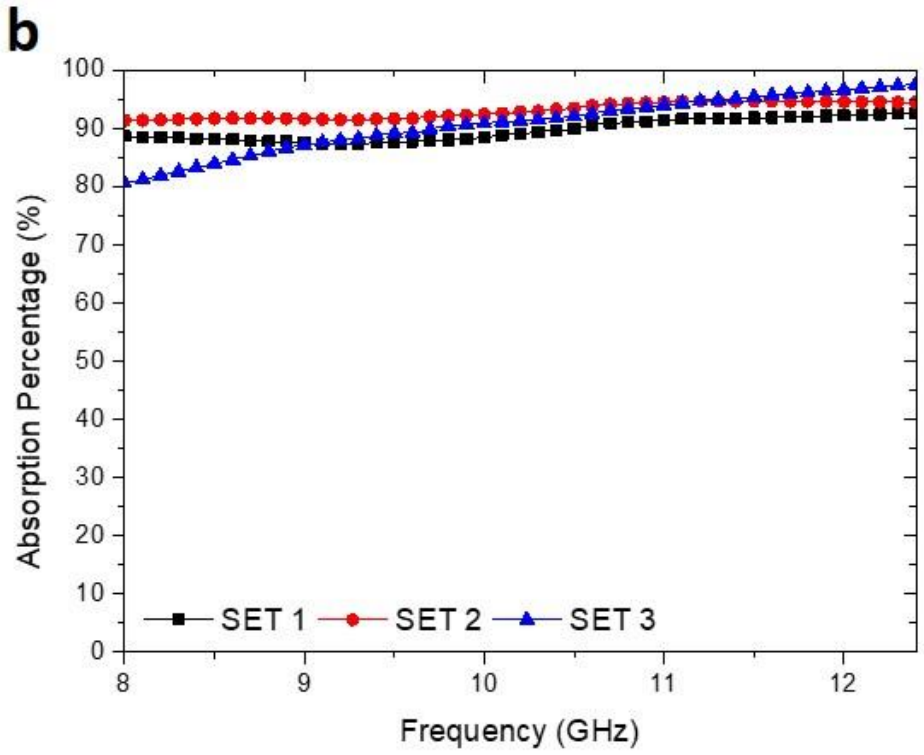

Figure 4.17. EM wave characteristic of the 6 layered graded structure with metallic backing similar to the Jaumann configuration; a) Reflection loss (S_{22}) and b) Absorption percentage

In 6 layered composite designs, reflection loss values are lower than those of the 4 layered ones. It is a reasonable result, since when the number of layers in the multilayered structure increases, more waves will be absorbed due to the intensified interaction between incoming and outgoing waves. Consequently, due to more multiple reflections, the intensity of waves returning back to the collection port would be lower.

As seen from Figure 4.17 (b), all of the 3 sets tested show more than ~90% absorption, especially at higher frequencies. In addition to that, a multilayered structure composed of 6 surface conductive layers shows a higher absorption percentage when a metallic plate is placed to the back of the composite design.

In conclusion, it is seen that among all of the designs, the multilayered structure which is prepared by cascading conductive layers with gradually increasing surface

conductivity (set 2) shows the highest absorption of the incident wave with and without metallic backing.

CHAPTER 5

CONCLUSION

In the current study, glass fiber woven fabrics were functionalized with ITO coating using the spray pyrolysis technique. The electrical properties of these substrates were controlled by depositing ITO sols with different molarity and amount. Electromagnetic properties of single layer surface functionalized glass fiber woven fabrics, and composite designs, which were formed by cascading surface conductive layers with different order were measured in 8-12 GHz frequency range by free space measurement technique**.**

The effects of starting chemicals, doping concentration, annealing temperature, molarity and coating thickness on microstructural, electrical, and electromagnetic properties were discussed. SEM and EDS analyses were carried out to examine microstructural features, to determine the thickness and analyze the elemental composition to check success of doping. XRD analyses were carried out to investigate the phases present in the material as well as, their ratio and the texture to determine whether the material is amorphous or crystalline. After structural characterization, four-point probe measurement technique was used to determine the electrical properties of the coatings. Electromagnetic properties, which are reflection loss, transmission loss, and absorption characteristic of the ITO surface functionalized single layer woven fabrics were measured by free space method in the X-band frequency range.

Using the information collected on the surface functionalized single layer, their electromagnetic properties were introduced to the AWR microwave software, and multilayered structure designs were formed by cascading single surface conductive fabrics with different conductivity gradients (rate of change). Electromagnetic

behavior of these multilayered composite designs was measured simulated and then measured with and without metallic backing in 8-12 GHz. Finally, based on the obtained results, a guideline was proposed for the design of multilayered EM wave absorbing composites according to the needs of a specific application.

In summary, following conclusions have been drawn from this thesis study:

- The surface conductivity of the ITO modified glass fiber woven fabrics can be controlled by controlling the thickness. Higher molarity and amount of sol leads to higher thickness and hence surface conductivity. It is observed that beyond a critical thickness value (~1.5 μm), ITO coatings start to crack and partially detach from the surface.
- Free space set-up measurements in the X-band frequency range (8-12 GHz) show that reflection loss of single fabrics with different surface conductivity changes between -7 and -35 dB, while transmission loss changes between 0 and -5 dB corresponding to absorption percentage between 0 and 50%.
- Experimental results of single layers have been used in the AWR software to estimate the EM characteristics of different multilayer combinations. The good correspondence of the simulation results with the experimental results has been tested by preparing a preliminary multilayered structure by cascading surface conductive fabrics. It was observed that there is no significant difference between the experimental and simulated results.
- It was observed that the best design was achieved when cascading surface modified layers with gradually increasing surface conductivity. By this way, the front layer provided impedance matching between air and the receiving surface of the composite which minimizes the surface reflection. The highly conductive layers at the back prevented the transmission of incident wave through the protected material. These two effects, led to high overall EM wave absorption.
- The highest absorbing composite design has been formed by cascading six ITO coated fabrics both with and without metal sheet placed at the back of

the composite. This composite has ~-11 dB reflection loss and ~-9 dB transmission loss which corresponds to ~85% absorption without metallic sheet, while its reflection loss and absorption values are ~-10.5 dB and ~93%, respectively, in the X-band with metallic backing.

- Therefore, according to the need of a specific application, if reflection loss is important and should be high, slowly increasing conductivity gradient will be the appropriate choice. On the other hand, if the transmission loss of the multilayered structure should be minimized with a certain amount of absorption, then a multilayered structure design with a rapidly increasing conductivity gradient should be selected. For applications where the thickness of the structure is a limitation, 4 layered graded absorber design with a gradually increasing conductivity could be selected for a balanced reflection and transmission loss along with a high level of absorption.

REFERENCES

[1] D. C. T. F. S. Geetha, K. K. Satheesh Kumar, Chepuri R. K. Rao, M. Vijayan, "EMI Shielding: Methods and Materials—A Review," J. Appl. Polym. Sci., vol. 116, 2010.

[2] W. S. Chin and D. G. Lee, "Development of the composite RAS (radar absorbing structure) for the X-band frequency range," Compos. Struct., vol. 77, no. 4, pp. 457–465, 2007.

[3] Erokhin, Victor, Ozlem Yavuz, and Manoj Kumar Ram. The New Frontiers of Organic and Composite Nanotechnology. Elsevier, 2008.

[4] C. F. Del Pozo, "Electromagnetic fields," Encycl. Toxicol., no. June, pp. 155–158, 2005.

[5] Z. Yang, H. Peng, W. Wang, and T. Liu, "Crystallization behavior of poly(ε-caprolactone)/layered double hydroxide nanocomposites," J. Appl. Polym. Sci., vol. 116, no. 5, pp. 2658–2667, 2010.

[6] P. Saville, "Review of Radar Absorbing Materials Defence R & D Canada – Atlantic," Def. Res. Dev. Canada, no. January, p. 62, 2005.

[7] K. J. Vinoy and R. M. Jha, "Trends in radar absorbing materials technology," Sadhana, vol. 20, no. 5, pp. 815–850, 1995.

[8] R. W. Wright, O. Halpern, and P. Palisades, "by 22.2%," pp. 2–5, 1960.

[9] O. Halpern, "Method and means for minimizing refelction of high-frequency radio waves," 1960.

[10] F. Che Seman, R. Cahill, V. F. Fusco, and G. Goussetis, "Design of a Salisbury screen absorber using frequency selective surfaces to improve bandwidth and angular stability performance," IET Microwaves, Antennas Propag., vol. 5, no. 2, pp. 149–156, 2011.

[11] J. B. Kim and J. H. Byun, "Salisbury screen absorbers of dielectric lossy sheets of carbon nanocomposite laminates," IEEE Trans. Electromagn. Compat., vol. 54, no. 1, pp. 37–42, 2012.

[12] F. Costa, A. Monorchio, and G. Manara, “Theory, design and perspectives of electromagnetic wave absorbers,” IEEE Electromagn. Compat. Mag., vol. 5, no. 2, pp. 67–74, 2016.

[13] W. H. Emerson, “Electromagnetic Wave Absorbers and Anechoic Chambers Through the Years,” IEEE Trans. Antennas Propag., vol. 21, no. 4, pp. 484–490, 1973.

[14] R. A. Serway and J. W. Jewett, Physics by serway. 2004.

[15] J. Coffman, Scientists vs. engineers, vol. 24, no. 9. 2010.

[16] A. Binjola, “Interaction of radiation with matter,” Pract. Radiat. Oncol., pp. 3–11, 2019.

[17] O. Karabayır, (2016), Investigation of Wind Turbune Effects on Radar Performance [Ph.D Thesis],Istanbul Technical University

[18] M. Gupta and W. W. L. Eugene, Microwaves and Metals. 2011.

[19] L. Duband, “Space cryocooler developments,” Phys. Procedia, vol. 67, pp. 1–10, 2015.

[20] Ismail, N., Surya Gunawan, T., Kartika S, S., Praludi, T. and A.Z. Hamidi, E., 2019. Design of microstrip hairpin bandpass filter for 2.9 GHz – 3.1 GHz s-band radar with defected ground structure. Malaysian Journal of Fundamental and Applied Sciences, 14(4), pp.448-455. 04.

[21] Mulders, Michel Adrianus. Remote Sensing in Soil Science. Amsterdam: Elsevier, 1987.

[22] S. Celozzi, R. Araneo, and G. Lovat, “Electromagnetic Shielding,” Electromagn. Shield., no. December, pp. 1–358, 2008.

[23] F. Wu, Z. Xu, Y. Wang, and M. Wang, “Electromagnetic interference shielding properties of solid-state polymerization conducting polymer,” RSC Adv., vol. 4, no. 73, pp. 38797–38803, 2014.

[24] P. Steffan, J. Stehlik, and R. Vrba, “Composite materials for electromagnetic interference shielding,” IFIP Int. Fed. Inf. Process., vol. 245, no. October 1999, pp. 649–652, 2007.

[25] M. Jalali, S. Dauterstedt, A. Michaud, and R. Wuthrich, “Electromagnetic shielding of polymer-matrix composites with metallic nanoparticles,” Compos. Part B Eng., vol. 42, no. 6, pp. 1420–1426, 2011.

[26] Yohandri and Z. Affandi, “Optimization of pyramidal radar absorber for anechoic chamber application,” J. Phys. Conf. Ser., vol. 1116, no. 3, 2018.

[27] Tong, X. C. (2016). Advanced Materials and Design for Electromagnetic Interference Shielding. Amsterdam University Press.

[28] C. M. Watts, X. Liu, and W. J. Padilla, “Metamaterial electromagnetic wave absorbers,” Adv. Mater., vol. 24, no. 23, 2012.

[29] F. Li, P. Chen, Y. Poo, and R. X. Wu, “Achieving perfect absorption by the combination of dallenbach layer and salisbury screen,” Asia-Pacific Microw. Conf. Proceedings, APMC, vol. 2018-Novem, no. 2, pp. 1507–1509, 2019.

[30] M. D. Yaman, “Thin film coating of glass fabrics for radar absorbing composites,” no. February, 2015.

[31] K. Li, X. Zhang, X. Hou, and P. Zhang, “Analysis and design of multilayer Jaumann absorbers,” ICMTCE2011 - Proc. 2011 IEEE Int. Conf. Microw. Technol. Comput. Electromagn., pp. 81–84, 2011.

[32] A. I. R. Force and S. Command, “FOREIGN TECHNOLOGY DIVISION Available Copy.”

[33] V. Zhurbenko, (2011). Electromagnetic Waves. Intechopen. Edited by Vitaliy Zhurbenko.

[34] S. Geetha, K. K. S. Kumar, C. R. K. Rao, M. Vijayan, and D. C. Trivedi, “EMI Shielding : Methods and Materials — A Review,” vol. 112, no. 1, pp. 2073–2086, 2009.

[35] I. Balan, C. Morari, and A. E. Patroi, “Composite materials for electromagnetic shielding,” UPB Sci. Bull. Ser. B Chem. Mater. Sci., vol. 78, no. 2, pp. 233–238, 2016.

[36] S. E. Lee, J. H. Kang, and C. G. Kim, “Fabrication and design of multi-layered radar absorbing structures of MWNT-filled glass/epoxy plain-weave composites,” Compos. Struct., vol. 76, no. 4, pp. 397–405, 2006.

[37] A. Fallis, “Network Analyzer Basics,” J. Chem. Inf. Model., vol. 53, no. 9, pp. 1689–1699, 2013.

[38] G. Ghione and M. Pirola, Microwave electronics. 2017.

[39] T. Minami, “Transparent conducting oxide semiconductors for transparent electrodes,” Semicond. Sci. Technol., vol. 20, no. 4, 2005.

[40] R. G. Gordon, “Criteria for choosing transparent conductors,” MRS Bull., vol. 25, no. 8, pp. 52–57, 2000.

[41] C. G. Granqvist, “Transparent conductors as solar energy materials: A panoramic review,” Sol. Energy Mater. Sol. Cells, vol. 91, no. 17, pp. 1529–1598, 2007.

[42] Ginley, D., Hosono, H., & Paine, D. C. (2010). Handbook of Transparent Conductors. Springer Publishing.

[43] Y. Wang, X. Chen, Y. Zhong, F. Zhu, and K. P. Loh, “Large area, continuous, few-layered graphene as anodes in organic photovoltaic devices,” Appl. Phys. Lett., vol. 95, no. 6, 2009.

[44] Ma, Z., Li, Z., Liu, K., Ye, C., & Sorger, V. J. (2015). Indium-Tin-Oxide for High-performance Electro-optic Modulation. Nanophotonics, 4(1), 198–213. https://doi.org/10.1515/nanoph-2015-0006

[45] C. G. Granqvist and A. Hultåker, “Transparent and conducting ITO films: New developments and applications,” Thin Solid Films, vol. 411, no. 1, pp. 1–5, 2002.

[46] Ramanan, S. R. (2001). Dip coated ITO thin-films through sol–gel process using metal salts. Thin Solid Films, 389(1–2), 207–212. https://doi.org/10.1016/s0040-6090(01)00825-2

[47] Kim, S. S., Choi, S. Y., Park, C. G., & Jin, H. W. (1999). Transparent conductive ITO thin films through the sol-gel process using metal salts. Thin Solid Films, 347(1–2), 155–160. https://doi.org/10.1016/s0040-6090(98)01748-9

[48] Ederth, J., Heszler, P., Hultåker, A., Niklasson, G., & Granqvist, C. (2003). Indium tin oxide films made from nanoparticles: models for the optical and electrical properties. Thin Solid Films, 445(2), 199–206. https://doi.org/10.1016/s0040-6090(03)01164-7

[49] Aegerter M.A., Al-Dahoudi N., (2002). Wet-chemical processing of transparent and antiglare conducting ITO coating on plastic substrates. Journal of Sol-Gel Science and Technology.

[50] Stoica, T. F., Stoica, T., Vanca, V., Lakatos, E., & Zaharescu, M. (1999). Colloidal sol-gel ITO films on tube grown silicon. Thin Solid Films, 348(1–2), 273–278. https://doi.org/10.1016/s0040-6090(99)00136-4

[51] Alam, M.J., and D.C. Cameron. "Characterization of Transparent Conductive Ito Thin Films Deposited on Titanium Dioxide Film by a Sol–Gel Process." Surface and Coatings Technology, vol. 142-144, 2001, pp. 776–780., https://doi.org/10.1016/s0257-8972(01)01183-5.

[52] Kobayashi, Y., Takahashi, N., Maeda, T., Yonezawa, T., & Yamasaki, K. (2015). Fabrication of ITO particles using a combination of a homogeneous precipitation method and a seeding technique and their electrical conductivity. Journal of Asian Ceramic Societies, 3(3), 266–270. https://doi.org/10.1016/j.jascer.2015.05.006

[53] Rajabi, N., Heshmatpour, F., Malekfar, R., Bahari-Poor, H. R., & Abyar, S. (2014). A comparative study of dip coating and spray pyrolysis methods for synthesizing ITO nanolayers by using Ag colloidal sol. Materials Science-Poland, 32(1), 102–106. https://doi.org/10.2478/s13536-013-0165-x

[54] Tsai, M. S., Wang, C. L., & Hon, M. H. (2003). The preparation of ITO films via a chemical solution deposition process. Surface and Coatings Technology, 172(1), 95–101. https://doi.org/10.1016/s0257-8972(03)00314-1

[55] Kuznetsova, S. A., Malinovskaya, T. D., Zaitseva, E. S., & Sachkov, V. I. (2004). Indium-Tin oxide films obtained from solutions based on acetylacetone. Russian Journal of Applied Chemistry, 77(10), 1609–1612. https://doi.org/10.1007/s11167-005-0081-x

[56] Djaoued, Y., Vu Hong Phong, Badilescu, S., Ashrit, P., Girouard, F. E., & Vo-Van Truong. (1997). Sol-gel-prepared ITO films for electrochromic systems. Thin Solid Films, 293(1–2), 108–112. https://doi.org/10.1016/s0040-6090(96)09060-8

[57] Zhang, X., Wu, W., Tian, T., Man, Y., & Wang, J. (2008). Deposition of transparent conductive mesoporous indium tin oxide thin films by a dip coating process. Materials Research Bulletin, 43(4), 1016–1022. https://doi.org/10.1016/j.materresbull.2007.04.021

[58] Kim, S. M., Seo, K. H., Lee, J. H., Kim, J. J., Lee, H. Y., & Lee, J. S. (2006). Preparation and sintering of nanocrystalline ITO powders with different SnO2 content. Journal of the European Ceramic Society, 26(1–2), 73–80. https://doi.org/10.1016/j.jeurceramsoc.2004.10.009

[59] Türküz S., (2010), İndiyum kalay oksit ince filmlerin optoelektronik özelliklerinin iyileştirilmesi, [Ph. D Thesis], Istanbul Technical University.

[60] K. Nishio, T. Sei, T. Tsuchiya, Journal of Materials Science. 31, 1761 (1996)

[61] Y. Takahashi, S. Okada, R.Tahar, K.Nakano, Journal of Non-Crystalline Solids 218, 129 (1997)

[62] Cho, H., & Yun, Y. H. (2011). Characterization of indium tin oxide (ITO) thin films prepared by a sol–gel spin coating process. Ceramics International, 37(2), 615–619. https://doi.org/10.1016/j.ceramint.2010.09.033

[63] Toki, M., & Aizawa, M. (1997). Sol-gel formation of ITO thin film from a sol including ITO powder. Journal of Sol-Gel Science and Technology, 8(1–3), 717–720. https://doi.org/10.1007/bf02436928

[64] M. Dutta, S. Mridha, D. Basak, Applied Surface Science, 254, 2743 (2008)

[65] Beaurain A, Dufour C, Koncar V, Capoen B, Bouazaoui M. Effects of annealing temperature and heat-treatment duration on electrical properties of sol–gel derived indium-tin-oxide thin films. Thin Solid Films 2008;516:4102.

[66] Z. H. Li and D. Y. Ren, "Preparation of ITO transparent conductive film by sol-gel method," Transactions of Nonferrous Metals Society of China (English Edition), vol. 16, no. 6, pp. 1358–1361, 2006, doi: 10.1016/S1003-6326(07)60020-X.

[67] Shukla, V. (2019). Review of electromagnetic interference shielding materials fabricated by iron ingredients. Nanoscale Advances, 1(5), 1640–1671. https://doi.org/10.1039/c9na00108e

[68] L. F. Chen, C. K. Ong, C. P. Neo, V. V. Varadan and V. K. Varadan,Microwave Electronics Measurement and Characterization (John Wiley & Sons Ltd., 2004).

[69] K. Chaudhary, G. Singh, J. Ramkumar, S. Anantha Ramakrishna, K. V. Srivastava, and P. C. Ramamurthy, "Optically Transparent Protective Coating for ITO-Coated PET-Based Microwave Metamaterial Absorbers," IEEE Transactions

on Components, Packaging and Manufacturing Technology, vol. 10, no. 3, pp. 378–388, 2020, doi: 10.1109/TCPMT.2020.2972911

[70] M. Zhu, C. Xiong, and Q. Lee, “Research on ITO transparent electromagnetic shielding coatings for E-O system,” 3rd International Symposium on Advanced Optical Manufacturing and Testing Technologies: Advanced Optical Manufacturing Technologies, vol. 6722, p. 67223Y, 2007, doi: 10.1117/12.783569.

[71] S. S. Kim, Y. C. Yoon, and K. H. Kim, “Electromagnetic Wave Absorbing Properties of High-Permittivity Ferroelectrics Coated with ITO Thin Films of 377 ω,” Journal of Electro ceramics, vol. 10, no. 2, pp. 95–101, 2003, doi: 10.1023/A:1025691621778.

[72] T. Li, K. Chen, G. Ding, J. Zhao, T. Jiang, and Y. Feng, “Optically transparent metasurface Salisbury screen with wideband microwave absorption,” Optics Express, vol. 26, no. 26, p. 34384, 2018, doi: 10.1364/oe.26.034384.

[73] M. Lin et al., “Compact multi-functional frequency-selective absorber based on customizable impedance films,” Optics Express, vol. 29, no. 10, p. 14974, 2021, doi: 10.1364/oe.422071.

[74] C. Su, T. K. Sheu, Y. T. Chang, M. A. Wan, M. C. Feng, and W. C. Hung, “Preparation of ITO thin films by sol-gel process and their characterizations,” Synthetic Metals, vol. 153, no. 1–3, pp. 9–12, 2005, doi: 10.1016/j.synthmet.2005.07.219

[75] H. Zhou, D. Yi, Z. Yu, L. Xiao, and J. Li, “Preparation of aluminum doped zinc oxide films and the study of their microstructure, electrical and optical properties,” vol. 515, pp. 6909–6914, 2007, doi: 10.1016/j.tsf.2007.01.041.

[76] W. Jiang et al., “Electromagnetic wave absorption and compressive behavior of a three-dimensional metamaterial absorber based on 3D printed honeycomb,” Scientific Reports, vol. 8, no. 1, pp. 1–7, 2018, doi: 10.1038/s41598-018-23286-6.

[77] J. Zhou, J. Yu, D. Bai, H. Liu, and L. Li, “Mechanically Robust Flexible Multilayer Aramid Nanofibers and MXene Film for High-Performance Electromagnetic Interference Shielding and Thermal Insulation,” 2021